EFFECT OF VARIOUS OPERATING CONDITIONS ON THE PERFORMANCE OF PHOTOVOLTAIC MODULE

MOHAMMAD MAFIZUR RAHMAN

DISSERTATION SUBMITTED IN FULFILMENT OF THE REQUIREMENTS FOR THE DEGREE OF MASTER OF PHILOSOPHY

INSTITUTE OF GRADUATE STUDIES
UNIVERSITY OF MALAYA
KUALA LUMPUR

2016

UNIVERSITI MALAYA

ORIGINAL LITERARY WORK DECLARATION

Name of Candidate: **Mohammad Mafizur Rahman**

Registration/Matric No: **HGF 120007**

Name of Degree: **Master of Philosophy**

Title of Thesis: **Effect of Various Operating Conditions on the Performance of Photovoltaic Module**

Field of Study: **Energy**

I do solemnly and sincerely declare that:

(1) I am the sole author/writer of this Work;
(2) This Work is original;
(3) Any use of any work in which copyright exists was done by way of fair dealing and for permitted purposes and any excerpt or extract from, or reference to or reproduction of any copyright work has been disclosed expressly and sufficiently and the title of the Work and its authorship have been acknowledged in this Work;
(4) I do not have any actual knowledge nor do I ought reasonably to know that the making of this work constitutes an infringement of any copyright work;
(5) I hereby assign all and every rights in the copyright to this Work to the University of Malaya ("UM"), who henceforth shall be owner of the copyright in this Work and that any reproduction or use in any form or by any means whatsoever is prohibited without the written consent of UM having been first had and obtained;
(6) I am fully aware that if in the course of making this Work I have infringed any copyright whether intentionally or otherwise, I may be subject to legal action or any other action as may be determined by UM.

Candidate's Signature Date

Subscribed and solemnly declared before,

Witness's Signature Date

Name:

Designation:

ABSTRACT

Photovoltaic (PV) modules are among the most effective, sustainable, and eco-friendly systems. A small portion of the incident solar radiation on a PV module is converted into electricity, whereas the remaining portion generates heat on the PV module layer, and consequently, decreases the output performance and efficiency of the module. Effective cooling systems can save energy and increase the performance of PV modules. In this study, various irradiation levels were applied to a PV module under indoor conditions to observe the temperature effects. A heat exchanger device was installed on the back of the module. Water flowed through the heat exchanger and radiator to cool the monocrystalline PV module. Results show that, under indoor conditions and without cooling, the total output power decreases by 20.47 W, and electrical efficiency decreases by 3.13% when solar temperature increases by 43.12 °C at 1000 W/m^2 irradiation level. This output performance is 41.03% lower than the initial output performance and equivalent to a decrease of approximately 0.47 W in output power and 0.07% in electrical efficiency per 1 °C increase in solar cell temperature. For every 100 W/m^2 increase in irradiation intensity, output power increases by 2.94 W with a 4.11 °C increase in solar cell temperature. Indoors, a 17.21 °C reduction in solar cell temperature increases output power by 8.04 W and electrical efficiency by 1.23%, thereby producing output power and efficiency that are 27.33% higher than those without cooling condition. The outdoor investigation shows that, without cooling, electrical efficiency decreases by 5.82% with a 26.10 °C increase in solar cell temperature during peak operating hours, thereby resulting in an output efficiency that is 43.83% lower than the initial output efficiency. Thus, electrical efficiency decreases by approximately 0.22% per 1 °C increase in solar cell temperature. For every 100 W/m^2 increase in irradiation intensity, output power increases by 3.14 W with a 3.82 °C increase in solar cell temperature. Outdoors, reducing solar cell temperature by 10.28 °C

increases output power by 7.64 W and electrical efficiency by 1.17%, thereby resulting in an increase of 15.72% in both performance parameters with respect to those without cooling condition. Output power decreases by approximately 3.16 W with an increase of 20% in relative humidity (RH), and is reduced by 7.70 W because of dust deposition on the surface of the indoor solar module. A decrease of approximately 1.6% in output efficiency occurs with an increase of 12.10% in RH, and this parameter decreases by 1.34% because of dust deposition on the surface of the outdoor solar module. Therefore, parameters such as solar cell temperature, irradiation intensity, cooling fluid mass flow rate, humidity, and dust influence PV module performance. Water cooling can be applied in large-capacity PV power generation plants located in tropical or hot-climate areas with exiguity of natural water resources. Different configurations of the heat exchanger device to cool PV modules, and consequently, improve performance can be considered in future studies.

ABSTRAK

Photovoltaic (PV) modul adalah salah satu sistem yang paling berkesan, lestari, dan mesra alam. Sebahagian kecil kejadian sinaran suria pada modul PV menghasilkan tenaga elektrik. Bahagian lain di penyinaran yang menjana haba pada lapisan modul PV menyebabkan pengurangan prestasi pengeluaran dan kecekapan. Sistem penyejukan yang sesuai boleh menjimatkan tenaga dan meningkatkan prestasi modul PV. Dalam penyiasatan semasa pelbagai penyinaran digunakan pada modul PV dalam keadaan tertutup untuk melihat kesan suhu. Peranti penukar haba telah digunakan pada permukaan belakang modul. Air mengalir melalui penukar haba dan radiator untuk tujuan penyejukan mono-kristal modul PV. Siasatan menunjukkan bahawa bagi ujikaji dalam makmal tanpa penyejukan jumlah kuasa keluaran berkurangan sebanyak 20.47 W dan kecekapan elektrik berkurangan sebanyak 3.13% dengan peningkatan suhu sel solar kepada 43.12° C di bawah 1000 W/m^2 penyinaran; iaitu 41,03% lebih rendah daripada prestasi pengeluaran awal. Kira-kira penurunan sebanyak 0.47 W dalam kuasa keluaran dan 0.07% penurunan dalam kecekapan elektrik untuk 1°C peningkatan suhu sel solar dicatatkan. Untuk setiap 100 W/m^2 peningkatan dalam keamatan sinaran, kuasa keluaran bertambah 2.94 W dengan peningkatan 4.11ºC suhu sel solar. Bagi ujikaji dalam makmal pengurangan 17.21ºC suhu sel solar, meningkatkan kuasa keluaran 8.04W dan kecekapan elektrik 1.23%, iaitu 27.33% lebih tinggi daripada kuasa keluaran dan kecekapan dihasilkan dalam tanpa penyejukan. Siasatan ujikaji luar makmal menunjukkan bahawa dalam keadaan tanpa penyejukan kecekapan elektrik berkurangan 5.82% dengan peningkatan suhu sel solar sebanyak 26.10°C pada waktu operasi puncak; iaitu 43.83% lebih rendah daripada kecekapan pengeluaran awal. Kira-kira 0.22% penurunan dalam kecekapan elektrik untuk 1°C peningkatan suhu sel solar dicatatkan. Untuk setiap 100 W/m^2 peningkatan dalam keamatan sinaran, kuasa keluaran meningkat 3.14 W dengan peningkatan suhu sel solar sebanyak 3.82ºC. Untuk

ujikaji luar makmal, pengurangan 10.28ºC suhu sel solar, meningkatkan kuasa keluaran 7.64 W pengeluaran dan kecekapan elektrik 1.17%, iaitu 15.72% lebih tinggi daripada kuasa keluaran dan kecekapan dihasilkan dalam tanpa penyejukan. Sejumlah 3.16 W kuasa keluaran berkurang dengan peningkatan 20% kelembapan relatif dan sebanyak 7.70 W kuasa keluaran berkurangan disebabkan jatuhan debu pada permukaan modul solar di ruang tertutup. Kira-kira 1.6% kecekapan keluaran menurun dengan peningkatan kelembapan relatif iaitu 12.10% dan sebanyak 1.34% kecekapan keluaran berkurangan akibat jatuhan debu pada permukaan modul solar di ruang terbuka. Ini menyimpulkan bahawa parameter suhu sel solar, keamatan sinaran, kadar aliran jisim cecair penyejukan, kelembapan, dan debu memberi kesan ke atas prestasi PV-modul. Penyejukan air boleh digunakan pada loji penjanaan kuasa dengan kapasiti PV yang besar dan terletak di kawasan iklim tropika atau panas di mana terdapat exiguity bagi air semula jadi. Konfigurasi berbeza peranti penukar haba boleh digunakan untuk menyejukkan modul PV bagi mendapatkan prestasi yang lebih baik dalam kajian masa depan.

ACKNOWLEDGEMENTS

In the name of Allah, the most beneficent, the most merciful, I would like to express my utmost gratitude and thanks to the Almighty Allah (s.w.t) for the help and guidance that He has given me through all these years. My deepest appreciation is to my father, mother, wife, brothers and sisters for their blessings and supports.

I would like to express my deepest appreciation and gratitude to my supervisor, Prof. Dr. Nasrudin Abd Rahim and Dr. Md. Hasanuzzaman for their brilliant supervision, guidance, encouragement and supports in carrying out this research work. I am deeply indebted to them. Special thanks to the UM Power Energy Dedicated Advanced Centre (UMPEDAC), University of Malaya for the financial supports.

Finally, thanks to all in UMPEDAC in helping me and for suggestion, ideas, discussions and advice in completing this research work.

TABLE OF CONTENT

LIST OF FIGURES

LIST OF TABLES

LIST OF SYMBOLS

A_c	Cross sectional area of fin (m^2)
A_{sc}	Area of solar cell (m^2)
C_f	Specific heat of water (J/kgK)
Dx	Elemental length
E_{ab}	Total energy (W) absorbed by module top surface
E_b	Total energy (W) transferred by conduction and convection from top surface to bottom surface
E_{ctop}	Total energy lost (W) by convection from top surface to ambient
E_e	Electrical energy (W) produced by module
G	Incident irradiation (W/m^2)
MPPT	Maximum power point tracker
PV	Photovoltaic
p	Perimeter (m) of fin
p_{sc}	Packing factor of solar module
T_a	Ambient temperature (°C)
T_b	Tedlar back surface temperature (°C)
T_{sc}	Solar module top surface temperature (°C)

U_{sca} Overall heat transfer coefficient through glass cover from module top surface to ambient (W/m^2K)

U_t Overall heat transfer coefficient from module top surface to tedlar back surface (W/m^2K)

W Width of the solar cell

Greek letter

τ_g Transmissivity of glass

α_{sc} absorptivity of solar module

η_{sc} Electrical efficiency of solar module

α_t Absorptivity of tedlar back sheet.

CHAPTER 1 : INTRODUCTION

1.1 Background

The use of renewable energy is currently promoted for the progress of modern civilization. Solar cells have a promising potential in the application of renewable energy because of their high efficiency and eco-friendliness. The use of photovoltaic (PV) modules in electricity generation has rapidly developed worldwide (Sahu, 2015). For the past two decades, using PV modules has been the most favorable and cost-effective option to supply electricity to rural areas. Modern PV arrays significantly contribute to the application of electrical grids (Spertino & Graditi, 2014). PV electricity is also encouraged because it minimizes the greenhouse effect created by the burning of fossil fuels (Hurng-Liahng et al., 2015). Seasonal environmental operating parameters have vital effects on the output performance of PV solar arrays. This output performance depends on the spectral response variation and the temperature coefficient of current and voltage (Otanicar et al., 2012). In general, the ratings of a PV module at standard test conditions (STC) are AM 1.5, 1000 W/m^2 irradiance, and 25 °C module temperature. In practice, PV cells are operated under different environmental conditions.

At present, consumers, installers, and designers of PV modules gather insufficient information about the performance and cost efficiency of PV modules under practical operations. Determining the optimal operating temperature and other parameters is essential to obtain maximum output from a PV module. An efficient design and optimum parameters facilitate the development and practical use of PV technology in the modern-day industrial revolution to satisfy desired environmental goals by mitigating the greenhouse effect.

1.2 Scope of the Study

PV cells generate electricity from incident sunlight, and they can be used in household and other applications. In practice, however, only 15%–20% of sunlight hitting a PV cell is converted into electrical energy, whereas the remaining portion generates heat on the cell body (Ceylan et al., 2014). The incident sunlight on a solar module increases module temperature, thereby causing the resultant performance drop (Sahay et al., 2015). To develop PV technology that can compete in the growing global market, considerable attention should be directed toward factors that vitally influence the output performance and efficiency of a PV module (Meral & Dinçer, 2011). Previous studies have proved that both efficiency and output power decrease with an increase in the surface temperature of a PV module (Moharram et al., 2013). Jong et al. (2011) found that output power decreases by approximately 0.5%, and electrical efficiency decreases by 0.05% with every 1 °C increase in ambient temperature. Malik et al. (2010) experimentally observed that an increase in the temperature of a polycrystalline solar module decreased both output power and efficiency, thereby reducing module output power by as much as 97%. Park et al. (2010) observed that output power decreased by 0.48% at STC under indoor operating conditions and by 0.52% under outdoor operating conditions at 500 W/m^2 solar irradiation level for every degree increment in cell temperature of the studied building-integrated PV (BIPV) arrays. Electrical efficiency and output power can be increased effectively by dropping the surface temperature of a PV module. Specific methods, such as water cooling and air cooling, are typically applied to reduce module temperature, and consequently, keep the surface operating temperature within a low range. In the study of Odeh and Behnia (2009), the efficiency of a PV module increased by 15% in a high-radiation environment by applying a water trickling arrangement on the top surface of the PV module. Teo et al. (2012) increased PV efficiency from 8%–9% to 12%–14% by inducing air flow through a parallel duct

attached to the back surface of a polycrystalline solar module. Ceylan et al. (2014) improved PV module efficiency from 10% to 13% by applying a temperature-controlled cooling water flow through a spiral tube cooling device connected to the bottom layer of a PV system (Ceylan et al., 2014). The temperature of a PV module was reduced by Alami (2014) by using an artificial mud film with water molecules on the bottom surface of the module, and heat was transferred from the module surface through evaporation. The resultant voltage of the module increased by 19.4%, and its output power increased by 19.1% (Alami, 2014).

Other operating parameters, such as dust and humidity, significantly decrease PV module power (Mekhilef et al., 2012; Panjwani & Narejo, 2014). The thickening of the accumulated dust layer on the PV module surface decreases the electrical efficiency of a PV system (Beattie et al., 2012). In general, the lower the ambient relative humidity (RH), the higher the efficiency of a PV module (Ettah et al., 2012).

The research scope to determine the effects of temperature and irradiation level on a PV module and improve PV module efficiency by applying different heat exchangers and cooling media is vast. In the current study, a heat exchanger tube with a finned plate is installed on the back surface of a PV module to decrease PV cell temperature. A finned tube-type heat exchanger is used to reduce PV module temperature. Water and air are used as cooling media. The use of these media is an effective cooling technique for both nonconventional and conventional PV modules to satisfy the competitive requirement for PV technology in the commercial market.

However, the effects of dust and humidity on PV module performance have been rarely studied. Thus, the current study also investigates the effects of both parameters on the output performance of the test PV module. Finally, the indoor and outdoor test performances of the PV module are also investigated.

1.3 Research Objectives

The objectives of this research are as follows:

1. To study the effect of temperature on the PV module
2. To investigate the effects of various operating conditions on PV module performance
3. To compare the indoor and outdoor test performances of the PV module.

1.4 Research Outline

In this study, the effects of various operating parameters on the performance of a monocrystalline PV module have been investigated. Water cooling and air cooling have been used to improve the performance of the PV module under both indoor and outdoor operating conditions. This research aims to improve the performance of PV modules and make a significant contribution to the promotion of renewable energy.

Chapter 2 provides an overview of the current global scenario of renewable energy and an introduction to solar energy. The different terms and parameters related to PV cells and modules, the historical development of PV cells, a short technical description of PV cells, and a review of the studies on the effects of various operating parameters on PV module performance are also presented in this chapter. As such, Chapter 2 can provide the necessary background to determine existing research gaps and accurately define the objectives of this study. The literature review is one of the vital research elements that provides a proper guide on how to conduct research.

Chapter 3 presents a short discussion of the methodology followed in conducting the experiment, including the experimental setup, data collection and processing techniques, and detailed mathematical modeling. Certain theoretical concepts of the heat transfer phenomena with regard to the heat exchanger used in the solar cell module are also

discussed in this chapter. Different equations and calculation methods related to PV technology are described. A brief description of the experimental setup and instruments is also provided in this chapter.

In Chapter 4, all the experimental results are presented in detail. Relevant graphs are plotted, and a short discussion of the experimental findings is provided.

In Chapter 5, the conclusions drawn from the research and several recommendations for further study are presented.

CHAPTER 2 : LITERATURE REVIEW

2.1 Introduction

This chapter provides an overview of the global energy scenario, solar energy, different terms and parameters related to PV cells and modules, and the historical development of PV cells. A brief technical description of PV cells and a review of studies on the effects of various operating parameters on different types of PV cells are also provided. Through this chapter, existing research gaps can be identified, and the objectives of this study can be defined. Thus, this literature review is an essential research component to properly guide the research project.

2.2 Global Energy Scenario

Considerable progress has occurred in the history of human civilization because of economic and industrial advancements that are strongly related to the journey of human society. These advancements are made possible by using natural energy sources. Two natural energy resources, namely, coal and petroleum, played a vital role in the Industrial Revolution during the 18th and 19th centuries, respectively. In the 20th century, energy from nuclear resources gained popularity because it was considered the best alternative to meet the increasing energy demand given the shortage of fossil fuels. Recently, however, harnessing nuclear resources has posed certain political and safety problems. Thus, satisfying the increasing energy demand for advanced sustainable globalization is the main challenge in the near future (Liserre et al., 2010). Fossil fuels and nuclear energy cannot be sustained for 200 more years (Roth, 1995).

Energy is a fundamental need of human society. The demand for energy increases gradually every day with population growth and global economic development.

However, natural sources of energy are limited and insufficient to fulfill future demand. A survey on future energy resources in the world was conducted, and its results are presented in Table 2.1.

Table 2.1: Summary of the current supply of energy resources in the world (Tomabechi, 2010)

Resources	**Ultimate resources**		**Recoverable resources**		**Consumption**
	(Tt)	**(ZJ)**	**(Tt)**	**(ZJ)**	**(ZJ/year)**
Solid fuels (Coal)	9.6	256.1	0.9	22.8	0.16
Oil	0.3	13.1	0.2	6.8	0.16
Natural gas	0.3	14.1	0.2	6.5	0.11
Oil shale	0.5	19.3	?	?	0.0000031
Peat	?	?	0.05	0.5	0.0000151
Natural gas hydrate	17.3#	712.2#	#	#	0.00
Maximum Usable Amount (ZJ/year)					
Solar energy		1.7		0.0000193*	
Hydropower*		0.06		0.010	
Tidal and wave*		0.0009		0.000002	
Wind		0.8		0.0004	
Oceanic thermal*		0.10		0.00	
Biomass		0.21		0.023	
Maximum Usable Amount (ZJ)					
Hydro-geothermal		0.41		0.001	
Dry hot rocks		310.13		0.00	
Total resources			Assured resources		
	(Mt)	(ZJ)	(Mt)	(ZJ)	
Uranium	12.31	598.2 (6.81)	4.72	227.1 (2.62)	0.03
Thorium	2.41	120.2	1.42	70.3	0.00
Lithium	#	#	8.3	175.3	0.00

Notes: 1. Number in "()" represents containing light water reactor.

2. The amount of lithium resources represents that available in Western countries.

3. An asterisk (*) specifies the mechanical and electrical power values.

4. A hash mark (#) denotes an undefined amount.

So if the energy consumes in such a rate than the total storage of energy in the world will be becoming a warning condition within 20-30 years (Tomabechi, 2010).

A huge amount of pollutant gases, such as CO, CO_2, NO_x, SO_2, and HC, are produced by burning fossil fuels. These gases are responsible for global warming, the greenhouse effect, air pollution, acid rain, climate change, and other environmental problems. Thus, electricity generation from fossil fuels has an adverse effect on the environment (Bose, 2010). The gradual reduction in natural fossil fuel reserves increases interest in the innovative use of PV solar cells (Hasnain et al., 1998). In recent decades, renewable forms of energy, such as PV, hydraulic, and wind energy, have exhibited the most potential among the different sources of energy. In 2007, approximately 19% of the total energy generated worldwide is obtained from renewable resources. In spite of the unavailability of natural silicon, the PV industry has constantly increased by approximately 30% annually. In 2008, Latin American countries yielded the highest amount of renewable energy (58% of total energy), most of which is from hydraulic energy. The present energy requirement in the world and its projected amounts until 2030 are shown in Table 2.2.

Table 2.2: Worldwide energy requirement in MTOE from 1980 to 2030 ("World Energy Outlook 2007," 2007)

	1980	**2000**	**2005**	**2015**	**2030**	**2005–2030[a]**
Coal	1786.0	2292.0	2892.0	3988.0 (3643.0)	4994.0 (3700.0)	2.20% (1.01%)
Oil	3106.0	3647.0	4000.0	4720.0 (4512.0)	5585.0 (4911.0)	1.30% (0.81%)
Gas	1237.0	2089.0	2354.0	3044.0 (2938.0)	3948.0 (3447.0)	2.10% (1.50%)
Nuclear	186.0	675.0	721.0	804.0 (850.0)	854.0 (1080.0)	0.71% (1.60%)
Hydro	147.0	226.0	251.0	327.0 (352.0)	416.0 (465.0)	2.01% (2.50%)
Biomass and waste	753.0	1041.0	1149.0	1334.0 (1359.0)	1615.0 (1738.0)	1.40% (1.70%)
Other renewable sources	12.0	53.0	61.0	145.0 (165.0)	308.0 (444.0)	6.70% (8.20%)

Note: Superscript “a” denotes the average increasing rate per annum.

The target of the European Union (EU) is to generate 20% of its total energy from renewable sources by 2020, and it is using approximately 15% at present. The United States also has a similar goal. Meanwhile, the goal of Asia-Pacific countries is to yield 35% of their total energy from renewable resources in the near future ("BP Statistical Review of World Energy ", 2008).

Umbach (2010) mentioned in his paper that the energy demand is expected to increase globally up to 55% by 2025/2030. Approximately 43% of total electricity generated is from renewable energy sources according to the forecasting of the International Energy Agency (IEA). Although solar energy is unstable because of weather fluctuations, it is the best alternative for fulfilling future energy demand (Hasnain et al., 1998). In 2009, the total power generated by solar cell plants was 22,928.9 MW, which was 46.9% higher than the total installed capacity in 2008, as reported in the BP statistical energy survey for 2010 (Othman et al., 2010). The recent progress and forecast until 2030 on the installation of solar PV energy systems in Japan, Europe, and the USA is presented in Table 2.3.

Table 2.3: Installation and development of PV plants for generating electricity in different countries ("WSPI. World Solar Power Introduction," 2010)

Year	USA (MW)	Europe (MW)	Japan (MW)	Worldwide (MW)
2000	140.00	150.00	250.00	1000.00
2010	3000.00	3000.00	5000.00	14,000.00
2020	15,000.00	15,00.00	30,000.00	70,000.00
2030	25,000.00	30,000.00	72,000.00	140,000.00

Tyagi et al. (2013) mentioned in his review that the increasing the number of solar PV plants generated approximately 23.5 GW power in 2010, and the power generated increased by approximately 35%–40% each year worldwide. PV technology is

forecasted to provide approximately 345 GW power in 2020, which will be approximately 4% of the total electricity generated. In 2030, this amount can increase by up to 1081 GW ("Solar photovoltaic electricity empowering the world," 2011).

2.3 Solar Energy

The sun is the source of all forms of energy. The transformation of hydrogen into helium and other heavy molecules through the process of nuclear fusion inside the sun can generate energy. Approximately 3.8×10^{26} J energy is produced every second through this process (Machacek et al., 2009). Approximately 1353±21 W/m^2 irradiance hits the atmospheric surface of the Earth (ASTM International, 1999), and approximately 1000 W/m^2 irradiance hits the surface of the Earth (ASTM International, 1992). Figure 2.1 shows the irradiation intensity inside and outside the atmosphere. Spectral irradiance, whose wavelength lies between 400 nm and 1300 nm, has a high photonic flux density (Goetzberger & Hoffmann, 2005). The marked area shows the irradiation density inside the atmosphere.

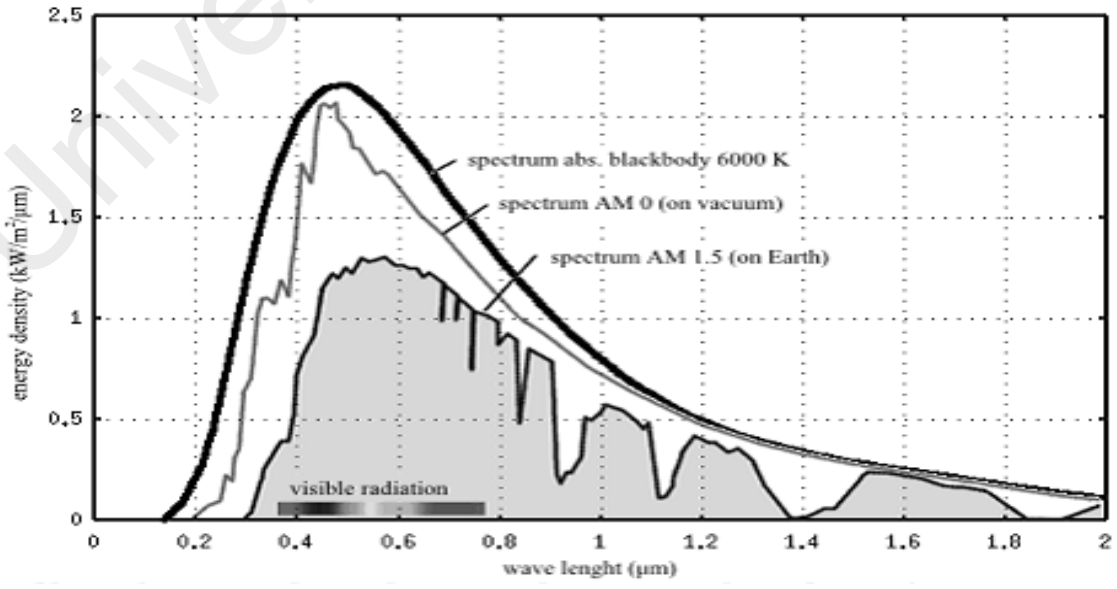

Figure 2.1: Irradiation intensity inside the atmosphere
(Limbra & Poulek, 2006)

Figure 2.1 shows that the visible radiation contains higher energy than the other irradiances (Limbra & Poulek, 2006; Murtinger et al., 2007). In general, light moves from one place to another through an electromagnetic wave. The wavelength of the electromagnetic spectrum can be 10^{-13} m to thousands of meters. However, the wavelength of the visible spectrum lies between 380 nm and 760 nm. The violet spectrum has the shortest wavelength, whereas the red spectrum has a wavelength of 760 nm (Limbra & Poulek, 2006). An electromagnetic spectrum has two characters: wave and corpuscles. A long-wavelength spectrum mainly has a wave character, whereas a short-wavelength spectrum exhibits a dominantly corpuscular character. A corpuscular spectrum is a flow of particles known as photons.

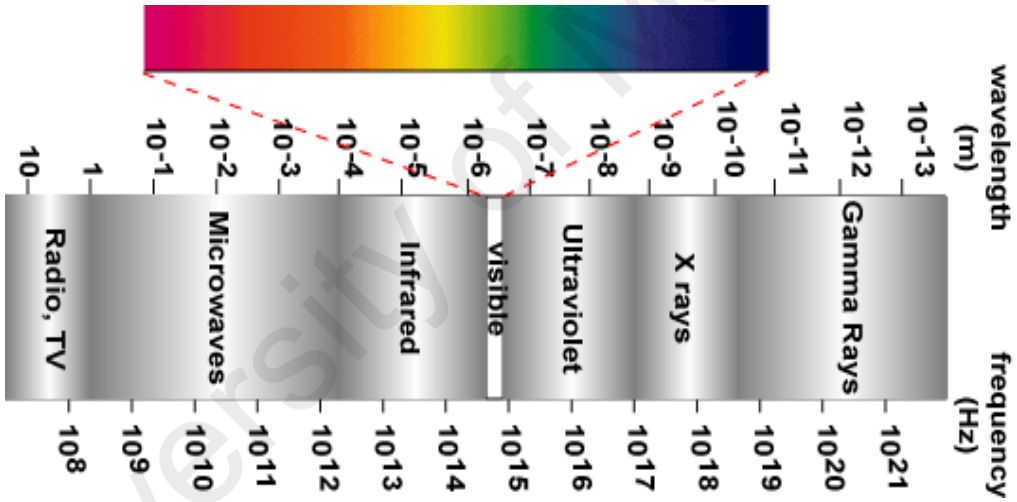

Figure 2.2: Wavelength and frequency of different spectra (PVEO, 2015)

The shorter the wavelength of the spectrum, the higher the photonic energy (Limbra & Poulek, 2006). The power density of a specific spectrum is represented by spectral irradiance ($W/(m^2 \cdot \mu m)$). Spectral irradiance is directly related to the wavelength of the spectrum. Figure 2.3 shows the spectral irradiances of sunlight and artificial light. If a light source has high spectral irradiance, then it has high energy or photon. As shown in

Figure 2.3, the spectral irradiance of sunlight is considerably higher than that of artificial light (PVEO, 2015).

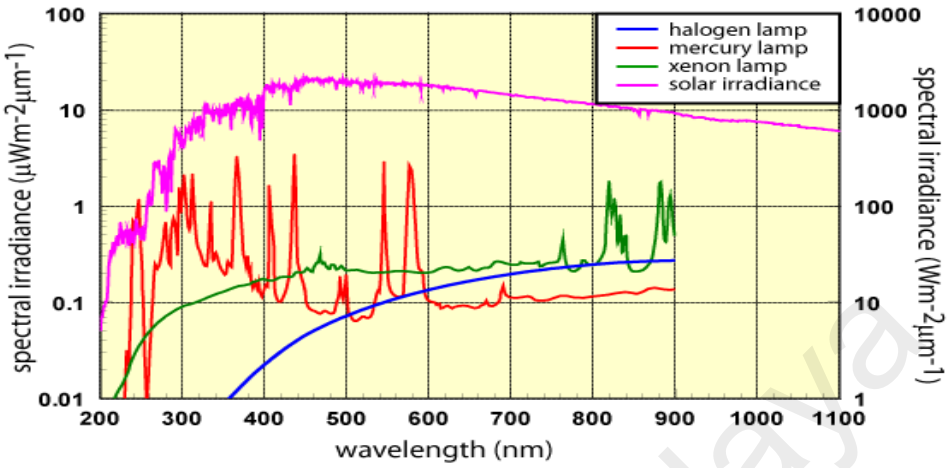

Figure 2.3: Spectral irradiances of sunlight and artificial light (PVEO, 2015)

2.4 Photovoltaic System

2.4.1 p-n Junction

The principle of p–n junctions provides an explicit idea of how solar cells work. A p–n junction is the combination of two types of semiconductors. The integration of a p-type semiconductor with a p-type semiconductor yields a p–n junction. Figure 2.4 shows that a semiconductor is doped with donor atoms in an n-type semiconductor. Donor atoms have more atoms than their base material atoms. A semiconductor is doped with acceptor atoms in a p-type semiconductor. Acceptor atoms have less atoms than their base material atoms; thus, holes are created. These holes are considered positive units, and they attract electrons and move throughout the base material. They contribute to the flow of electrons through the system. Through the recombination process, electrons and holes meet and annihilate each other.

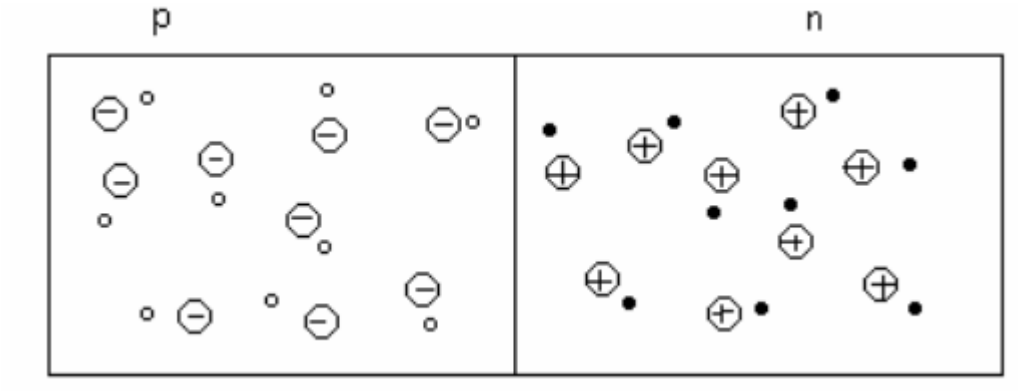

Figure 2.4: p-n junction
(Hettelsater, 2002)

2.4.2 Depletion Region

The combination of a p-type semiconductor with an n-type semiconductor produces an electron–hole concentration gradient. This concentration gradient produces a diffusion current by forcing the electrons to diffuse into the p-side and the holes to diffuse into the n-side. The location where this diffusion occurs is known as the depletion layer or the depletion region. When n-side electrons travel to the p-side and recombine with holes, positive charges on the n-side are created. In the same maner, when p-side holes recombine with n-side electrons, negative charges are created on the p-side. An internal electric field is in turn produced in the depletion layer because of the positive and negative charges (Hettelsater, 2002; Radziemska & Klugmann, 2002; Radziemska, 2002). Figure 2.5 shows that the electric field produced in the depletion layer inhibits further diffusion of electrons from the n-side to the p-side. Only a few electrons with sufficient energy can cross the electric field and diffuse. In equilibrium, the drift current (caused by the electric field) and the diffusion current are equal and opposite in directions; consequently, the resultant current is zero.

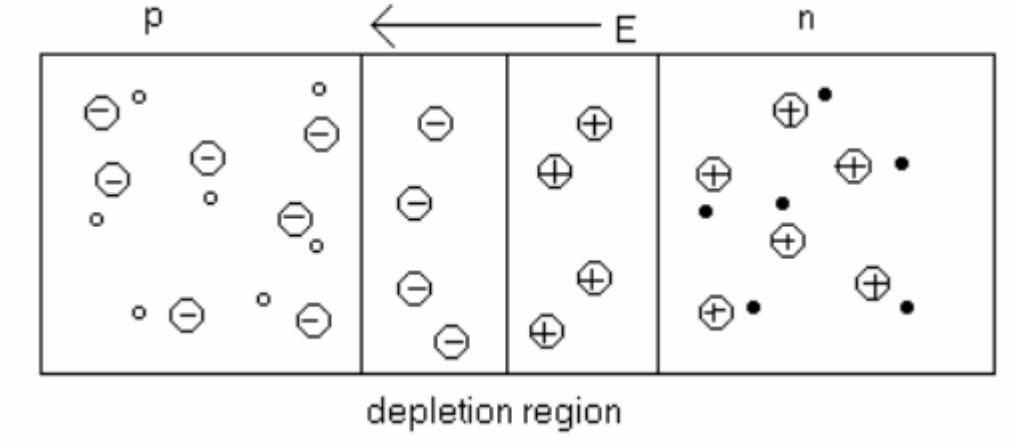

Figure 2.5: Generation of an internal electric field
(Hettelsater, 2002)

2.4.3 p-n Junction under an Applied Bias

The intensity of the internal electric field can be changed by applying an external voltage across the p–n junction. The internal electric field increases by applying a reverse bias or a negative voltage to the p-type surface of a p–n junction. Conversely, the internal electric field can be decreased by applying a forward bias or a positive voltage to the n-type layer of a p–n junction. When a forward bias is applied, the internal electric field is reduced and a certain number of electrons on the n-side gather sufficient energy to move through the depletion layer to the p-side. This moving electron number increases by a coefficient of eV/kT, where e is the electron charge, V is the voltage applied to the p–n junction, k is the Boltzmann constant, and T is the absolute temperature. The resultant electron current flows from the n-type layer to the p-type layer is defined by $I_{e0}\exp(eV/kT)$, where I_{e0} is the leakage current flowing from the p-type layer to the n-type layer. This leakage current is generated because of the presence of minority carriers in the p-type region.

2.4.4 Solar Cell Principles

A photon that contains energy higher than the band gap energy hits the semiconductor and generates an electron–hole pair on the semiconductor. This mechanism is clearly depicted in an energy band gap map of a semiconductor. The electrons in a semiconductor have three separate energy bands, as shown in Figure 2.6. The valence band of a semiconductor is completely filled with electrons, whereas no electrons are in the conduction band, which is distinct from the valence band by band gap energy. The electrons in the valence band cannot move freely to the conduction band and engage in electrical conduction. This phenomenon is explained by the Pauli exclusion principle. If an electron gains sufficient energy greater than the band gap energy, then it can move easily to the conduction band. A photon hitting a semiconductor has energy higher than the band gap energy, and thus, provides sufficient energy to the electron in the valence band to allow it to move to the conduction band. The holes created in the valence band and the electrons created in the conduction band participate in the current conduction working under an electric field (Kasap, 2002).

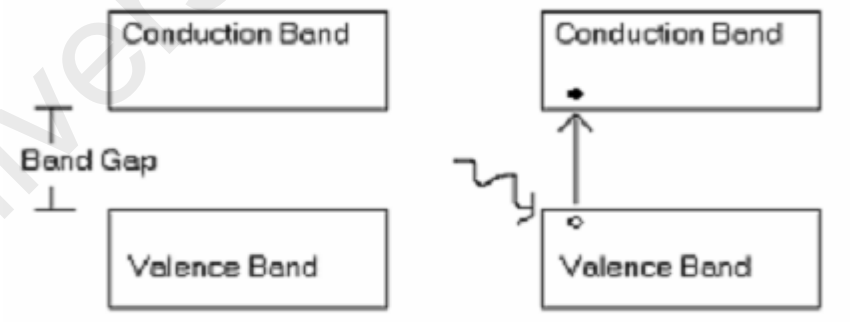

Figure 2.6: Band diagram and electron–hole pair generation (Kasap, 2002)

A heavily doped thinner n-type layer is placed on a thicker p-type layer during the manufacture of a PV module. The depletion layer most frequently exists on top of the the p-type layer, as shown in Figure 2.7. The incident light falls on the PV module through the n-type surface. A majority of the photons enter the p-type layer or the

depletion layer through the thinner n-type surface before the electron–hole coupling. After an electron–hole pair is generated in the depletion layer, the electric field forces the hole to move toward the p-type layer and the electron to move toward the n-type layer. Through this process, the previously neutral p-type layer gains a positive charge and the previously neutral n-type layer gains a negative charge. When the cell is connected to the load, the electrons are transported through the circuit. These transported electrons then recombine with the hole.

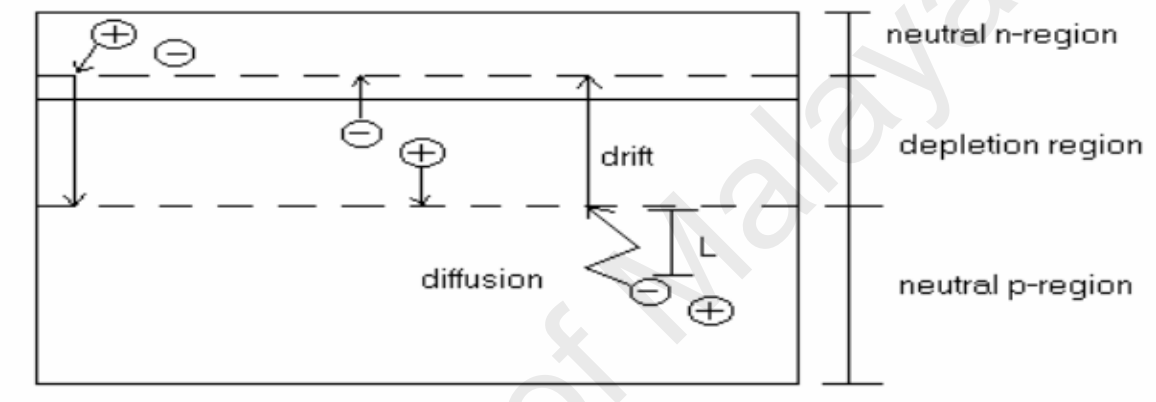

Figure 2.7: Electron-hole pair behavior in solar cell
(Kasap, 2002)

If incident irradiation occurs on the neutral p-type layer of the PV module, then an electron–hole pair is not created because of the absence of an electric field. Instead of creating an electron–hole pair, the hole and the electron move randomly on the material and neutralize each other when they meet. The average time between recombination and pair generation for an electron is τ_e. In the meantime, the electron moves an average distance, which is defined as $L_e = \sqrt{2 D_e \tau_e}$, where D_e is the coefficient of diffusion in the p-type layer. The electric field forces the electrons to diffuse into the depletion layer or move to the n-type layer when the hole–electron pair is produced within a distance of L_e. The greater the diffusion length, L_e, the better the performance of PV module. The hole–electron pair generation on the n-type layer follows a similar procedure. In silicon materials, the diffusion length of a hole is shorter than that of an electron; thus, the p-

type material forms a relatively thick layer, and the n-type material forms a thin upper surface layer. During the short circuit of a PV module, current flows in a direction opposite to the current flow of the diode. This current flow is a consequence of the electron–hole generation in the PV module and is known as photocurrent I_{ph}. The amount of photocurrent produced fully depends on incident irradiation intensity. If the circuit is connected through a resistance, then a voltage exists in the junction. This voltage functions as a forward bias, causing a diode current flow through the PV module (Hettelsater, 2002). A characteristic I–V curve of a PV cell is shown in Figure 2.8

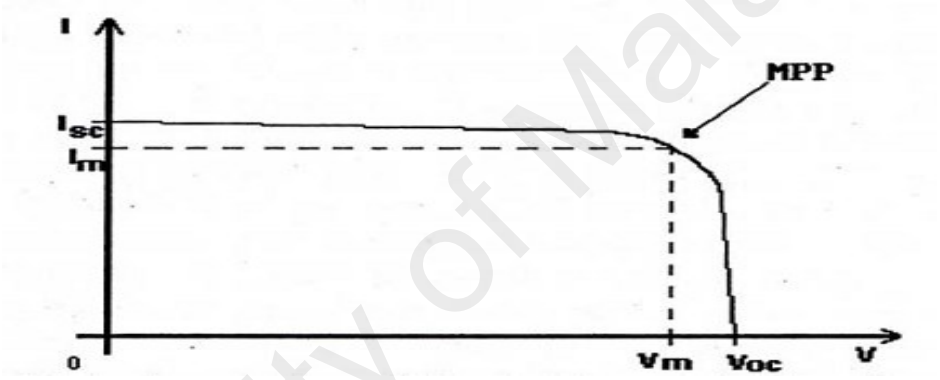

Figure 2.8: Typical I–V curve of a solar cell under illumination (MPP denotes the maximum power point of the cell.)
(Hettelsater, 2002)

2.5 PV Technology

Various methods have been used in the manufacturing process of PV technology. The three most popular types of solar cells are monocrystalline, polycrystalline, and amorphous solar cells (Floyd Associates, 2010). Detailed descriptions of these three types of solar modules are provided in the following subsections.

2.5.1 Monocrystalline Solar Cells

Monocrystalline solar PV cells are developed from a single silicon crystal, which is produced from molten silicon with high purity. These solar cells are truncated from a large single silicon crystal and formed into thin wafers 2–3 mm in length. Monocrystalline solar cells are regarded as the workhorse in the solar cell market because they are the most economical, efficient, and reliable type; however, they are also the most expensive in the present market (Renewables, 2010; Solar-Help, 2010). Tyagi et al. (2013) mentioned in his review that the efficiency of silicon solar cells in 1950 was only 15%, but it increased to 17% in 1970. Currently, silicon solar cells can generate power at an efficiency of approximately 28%.

Figure 2.9: Mono-crystalline solar cell
(Solar - Help, 2010)

In the commercial manufacturing of PV cells, crystalline silicon remains the first choice because of its abundance in nature. It also has a perfect band gap, which facilitates PV conversion , and a nontoxic property. The development of monocrystalline solar cells has been studied for years (Tobías et al., 2011). A monocrystalline solar cell has a highly definite crystal structure, and each of its atom possesses a prefixed position in a regular arrangement; consequently, a perfect band structure is formed.

Figure 2.10: Regular atomic structure of a monocrystalline solar cell (PVEO, 2013b)

Monocrystalline solar cells are generally made from a large wafer of a single silicon crystal with an extremely smooth surface (Ouma, 2013; Solar cells, 2013). A monocrystalline solar cell has the following components.

1. Glass cover: An outer layer made of glass that serves as the outer protection of the cell.
2. Transparent adhesive: This element attaches the glass to the solar cell.
3. Anti-reflective coating (ARC): A coating that prevents sunlight from bouncing off the cell surface to ensure that the cell can absorb the highest amount of energy.
4. Front contact: This component is used to transmit current.
5. n-Type semiconductor layer: A layer made of silicon doped with phosphorus atoms.
6. p-Type semiconductor layer: A thin surface of silicon doped with boron.
7. Back contact: This component is used to transmit current.

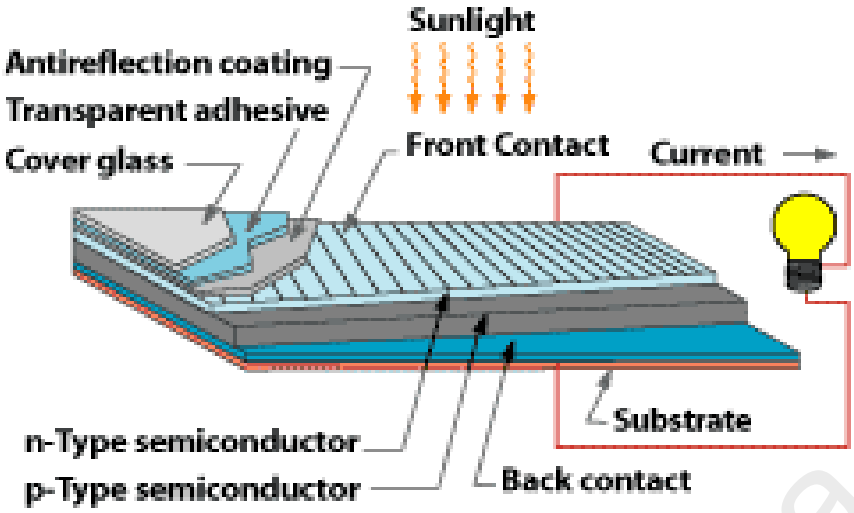

Figure 2.11: Structure of a monocrystalline solar cell
("How solar cells work," 2013)

2.5.2 Polycrystalline Solar Cells

Polycrystalline cells are slice from a silicon block. Unlike a monocrystalline silicon cell, a polycrystalline cell contains a large amount of silicon crystals integrated with rectangular conduit wires into ribbon-like panels. Its color, which is slightly lighter than that of a monocrystalline silicon cell, is marbled blue. Its cost and performance are lower than those of a monocrystalline cell. It requires mounting on a solid frame (Renewables, 2010; Solar-Help, 2010)

Figure 2.12: Polycrystalline solar cell
(Solar - Help, 2010)

A polycrystalline solar cell is easier to fabricate than a monocrystalline solar cell. The material quality of a polycrystalline solar cell is lower than that of a monocrystalline solar cell because the former has grain boundaries. These boundaries produce a high-density recombination region by introducing an extra defect energy level into the band gap, thereby reducing the life span of minority carriers in the cell material. Grain boundaries also hinder carrier flows and create a shunt through which current flows over the p–n terminal; consequently, solar cell performance is reduced.

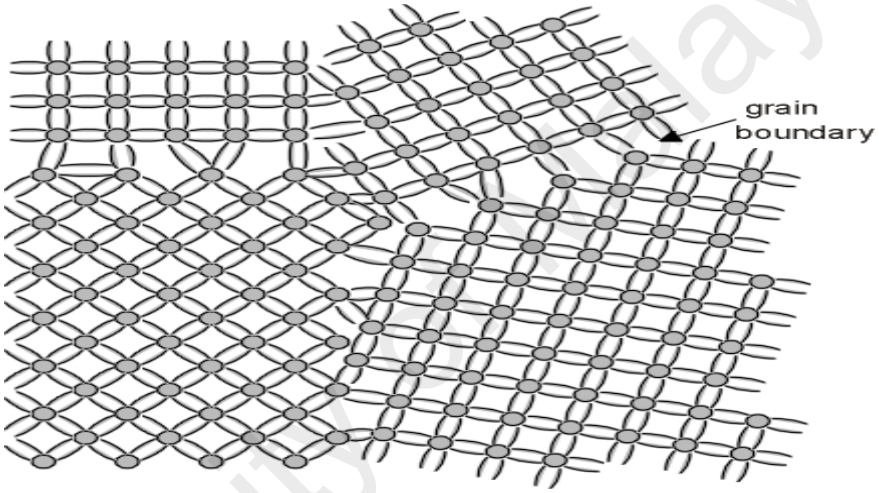

Figure 2.13: Multicrystalline silicon crystal structure with grain boundaries (PVEO, 2013a)

The best modules made using polycrystalline silicon generally have efficiencies of 2%–3%, which are lower than those of monocrystalline silicon and cost approximately 80% of the production cost of monocrystalline silicon cells (Miles et al., 2005).

2.5.3 Amorphous Silicon (a-Si) Solar Cells

An a-Si solar cell is made of an extremely thin layer of noncrystalline (amorphous) molecules of silicon. An a-Si film is a flexible layer; thus, it can be used in an extensive range of applications and on different layers. If an a-Si film is installed on a flexible layer, then the entire solar panel can be flexible. The efficiency of an amorphous solar cell is low, and it has the lowest cost among the three popular types of solar cells. It

exhibits high efficiency during installation, but its efficiency decreases with time and reaches a stable condition within a few months. Thus, the reported output of a-Si is the highest output offered under this stable condition. a-Si PV cells are made without any crystal module, thereby resulting in their lower cost and lower efficiency but good performance (Renewables, 2010; Solar - Help, 2010).

Figure 2.14: Amorphous PV panel on a garage roof
(Renewables, 2010)

The substrate configuration of an a-Si solar cell fabricated through the ASTER process is a substrate/Ag/ZnO:Al/n/i/p/ITO/Au grid line. From this configuration, the following three types of solar cells can be produced:

1. substrate/Ag/ZnO:Al/n-nc-Si/i-Si/buffer layer/p-nc-Si/ITO/Au grid line (single doped n-layer of nanocrystalline silicon [nc-Si] material)
2. substrate/Ag/ZnO:Al/n-nc-Si/n-a-Si/i-Si/buffer layer/p-nc-Si/ITO/Au grid line (double n-layer)
3. substrate/Ag/ZnO:Al/n-nc-Si/n-a-Si/i-Si/p-a-Si/ITO/Au grid line (double n-layer + amorphous p-layer)

Rath et al. (2010) described the fabrication process for thin-film silicon (a-Si or nc-Si) PV cells. They designed a structure through the direct deposition of a thin film of silicon (a-Si/nc-Si) on a plastic substrate. Their designed structure delivered primary

efficiencies of approximately 6.2% and 5.9% for PEN and PET substrates, which are made of n-i-p a-Si. Their designed structure are given below.

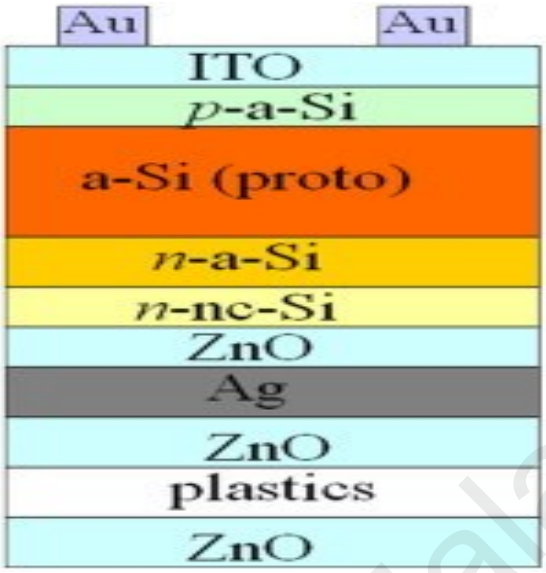

Figure 2.15: Cross-sectional schematic view of an n-i-p a-Si solar cell on a PEN/PET plastic substrate (direct deposition process)
(Rath et al., 2010)

Rath et al. (2010) also designed an a-Si cell by transferring the cell on a polyester substrate. Through this method, a tandem a-Si/nc-Si PV cell yielded an efficiency of approximately 8.12%, and an a-Si single junction solar cell generated an efficiency of 7.7%. The difference between a single crystal and an a-Si material is that the latter lacks a long-range crystal order. The neighborhood of an atom inside a lattice is similar to that of a crystalline silicon atom, with only slight variations in the bond angles.

2.6 Effect of Various Operating Parameter on PV Module Performance

2.6.1 Effects of Temperature and Irradiation on PV module

PV solar cells are manufactured using p–n junction semiconductor materials, which directly convert sunlight into electric current (Muneer et al., 2005). Although the potential of solar cells in the renewable energy sector is considerable, they are not cost-

efficient. Thus, improving the efficiency of PV solar cells is essential to minimize their cost (Sanusi et al., 2011). Many investigators have used numerical, experimental, and analytical methods to study the effects of various operating parameters on the degradation of PV module performance and to search for possible techniques that can enhance the performance of PV modules. PV modules practically transform approximately 15%–20% of the solar rays hitting its surface; the remainder of the incident rays increases the cell temperature of the module (Jie et al., 2007; Teo et al., 2012). PV module efficiency decreases with an increase in its temperature (Shan et al., 2014). Sanusi et al. (2011) performed an experiment to determine the effect of ambient temperature on the performance of an a-Si PV cell in a tropical zone in Nigeria in 2006, 2007, and 2008. They discovered that the output power of the a-Si cell is directly proportional to ambient temperature, and that this type of PV cell can operate better in high-ambient-temperature periods than in low-atmospheric-temperature periods (Sanusi et al., 2011). Ray (2010) conducted an experiment on PV cell efficiency at a high temperature. Polymer, copper indium diselenide (CIS), and a-Si type solar modules were used and irradiated under an AM 1.5 solar simulator with a capacity of 973 W/m^2. The efficiency of the CIS solar module was 12% at 12 °C cell temperature, and efficiency dropped nonlinearly to 10% at 105 °C cell temperature. Peak efficiency was reached at 80 °C and 40 °C. Such results are unexpected. The efficiency of the a-Si module reached 4% at a cell temperature of 45 °C, decreased linearly with increasing cell temperature, and became 3% at 80 °C. The efficiency of the polymer cell dropped from 1.1% to 1% when the temperature was increased from 45 °C to 60 °C. The polymer cell was destroyed when cell temperature reached 100 °C. Therefore, CIS and a-Si cells were considered suitable for solar hybrid power generation (Ray, 2010). Hanif et al. (2012) experimentally observed the output power of a PV module at an operating temperature range of 15 °C–45 °C and different tilt angles. The module produced

maximum power at 15 °C and 35° tilt angle (Hanif et al., 2012). Output power and electrical efficiency decreased by 0.5% and 0.05%, respectively, with each 1 °C increase in ambient temperature (Jong et al., 2011). Malik et al. (2010) experimentally observed that the increase in the temperature of a polycrystalline solar module decreased both output power and efficiency, thereby reducing module output power by as much as 97%. The output power of an a-Si PV module is strongly related to spectrum range. It demonstrates maximum power in a blue-rich spectrum. By contrast, the performance of monocrystalline PV module depends on cell temperature but not on the spectrum range of irradiation (Minemoto et al., 2007). Park et al. (2010) observed that output power decreased by 0.48% at STC under indoor operating conditions and 0.52% under outdoor operating conditions at 500 W/m^2 solar irradiation level per 1 °C increment in cell temperature of a BIPV module. In the experiment of Radziemska (2003), approximately 0.65% output power, 0.2% filling factor, and 0.081% electrical efficiency of the solar device were decreased per 1 K increment in module surface temperature. The performance of PV conversion mainly depends on a few factors, such as semiconductor type, solar spectrum range, cell sensitivity to the spectrum, and cell surface reflectivity. In the study of Olchowik et al. (2006), the output efficiency of a PV module also decreased with an increment in cell temperature. The decrease in efficiency caused by increasing temperature is greater for a monocrystalline PV cell than for an a-Si solar cell. Kumar and Rosen (2011) reported that when temperature rises from 300 K to 330 K, the efficiency of a monocrystalline PV cell was reduced by approximately 15%, whereas the efficiency of an a-Si PV only decreased by 5%. Ugwuoke and Okeke (2012) practically observed that the conversion efficiencies of monocrystalline, polycrystalline, and amorphous PV modules were 12.97%, 9.67%, and 4.94%, respectively, at 600 W/m^2 irradiation level; however, at 1000 W/m^2 irradiation level, efficiency dropped to 9.61%, 7.65%, and 3.62%, respectively. Conversion efficiency

dropped by approximately 30.6%, 42.32%, and 31.88% for amorphous, polycrystalline, and monocrystalline PV cells with a 400 W/m^2 increment in solar irradiation level (Ugwuoke & Okeke, 2012). Jong et al. (2011) numerically determined that open-circuit voltage decreased and short-circuit current increased with an increase in module temperature from −25 °C to 50 °C. The increment in module temperature increases dark current flow, thereby causing an increase in short-circuit current and free-carrier losses; thus, the output performance of the PV module in the study of Malik et al. (2010) decreased. The forward voltage decreased by 2 mV and 1 mV for PV cell and silicon diode, respectively, with each degree increment in operating temperature, whereas the forward current was constant at 100 mA. The series resistance values of a solar cell and a diode were both increased by approximately 0.65% for every 1 K temperature increment at an operating temperature range of 295 K to 373 K (Radziemska, 2006). Shenck (2010) reported that both PV output power and efficiency decreased with increasing temperature because of the retraction of the band gap of the atoms with an increase in temperature. Thus, open-circuit voltage drops for the same reason (Shenck, 2010). When temperature increases, the flow of free electrons from the valence band to the conduction band intensifies and reduces the band gap; consequently, short-circuit current increases, open-circuit voltage drops, and efficiency decreases (Dinçer & Meral, 2010). Kalogirou (2009) plotted a graph showing the relationship between the temperature of a PV module and the short-circuit output current and open-circuit output voltage of the module.

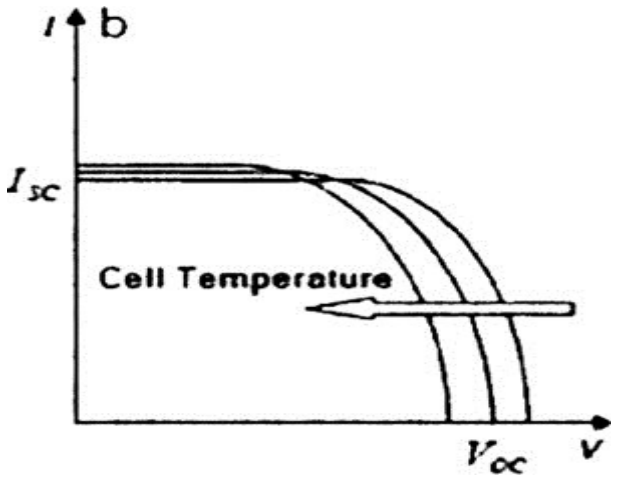

Figure 2.16: Temperature effect on the performance of PV cells (Kalogirou, 2009)

Singh and Rabindra (2012) analytically investigated the temperature-dependent performance of a PV cell at an operating temperature range of 273 K to 523 K. They reported that the increment in cell temperature enhanced the reverse charge flow, and consequently, reduced open-circuit voltage and fill factor; as result, output efficiency was also decreased (Singh & Ravindra, 2012). With increasing cell temperature, the band gap is reduced; thus, the short-circuit current increases and the open-circuit voltage, output power, and efficiency decrease (Singh & Ravindra, 2012).

2.6.2 Effect of Cooling on PV Module Performance

Tonui and Tripanagnostopoulos (2007) experimentally investigated the electrical and thermal efficiency of a PV/T hybrid thermal collector under natural and forced airflows. They observed that the electrical efficiency of the PV module reached 12.5% at 26 °C cell temperature and dropped to 9% at 68 °C cell temperature; furthermore, thermal efficiency was 30% for an airflow of 60 m^3/h^{-1} through a 15 cm air channel with fins, 28% for a thin metal sheet, and 25% for a typical cooling system (Tonui & Tripanagnostopoulos, 2007). Qunzhi and Leilei (2012) experimentally showed that the electrical efficiency of an a-Si module was increased by approximately 3% by using a

water cooling system; water cooling was more effective than air cooling in reducing the cell temperature of the a-Si module. Dubey et al. (2009) reported that PV module efficiency was 9.75% without cooling. After applying the air cooling method, it increased to 10.41% (Dubey et al., 2009). Odeh and Behnia (2009) increased PV module efficiency by 15% under a high irradiation level through a water trickling arrangement on the top surface of the PV module (Odeh & Behnia, 2009). Hosseini et al. (2011) used a thin film of water flowing over the upper surface of a PV module to reduce reflection loss and top surface temperature, thereby significantly increasing the output power and electrical efficiency of the PV module. Teo et al. (2012) observed that the efficiency of a polycrystalline PV system without cooling was 8%–9%, but after a steady airstream was applied through a parallel duct attached to the back layer of the PV device, efficiency increased to 12%–14%. Bahaidarah et al. (2013) reduced 20% of the cell temperature of a monocrystalline PV module via an effective water cooling method, in which a heat exchanger device was attached to the back surface of the module, and increased cell efficiency by up to 9%. The experimental and mathematical results are nearly the same (Bahaidarah et al., 2013). Chandrasekar et al. (2013) reduced the cell temperature of a PV module by 30% and consequently increased its output power by 6.5 W and electrical efficiency by 1.4% using various coolants, such as Al_2O_3/water, CuO/water-based nanofluid, and water through a cotton-wick cooling structure. Both the thermal and electrical performances of the PV module increased through this process (Chandrasekar et al., 2013). Valeh-e-Sheyda et al. (2013) used both water flow and airflow through a microchannel to reduce the cell temperature of a PV module and increased its output power by 38%. Ceylan et al. (2014) applied a stream of water through a spiral tube heat exchanger panel to reduce the surface temperature of a monocrystalline PV module and consequently increased its electrical efficiency to 13%; the electrical efficiency of the PV module was 10%without cooling. Alami (2014)

decreased the temperature of a PV cell with an artificial mud layer with water molecules attached to the bottom part of the PV device and by dissipating the heat on the surface through evaporation; consequently, output power and resultant voltage increased by 19.1% and 19.4%, respectively. The electrical efficiency of a PV module improved by approximately 8.2%, 9.01%, and 9.75% with respect to electrical efficiency without cooling by using water, 1 wt.% silica–water nanofluid, and 3 wt.% silica–water nanofluid, respectively, as coolants (Sardarabadi et al., 2014)

2.6.3 Effects of Dust and Humidity on PV Module Performance

Dust and humidity potentially decrease PV cell output power (Panjwani & Narejo, 2014; Mekhilef et al., 2012.). An increase in the amount of dust accumulating on the top surface of a PV module decreases the electrical efficiency of the module (Beattie et al., 2012). A previous investigation showed that 100 days worth of accumulated dust decreased efficiency by 10%. The dust that accumulated on the upper surface of a module could reduce 50% of system efficiency according to Sulaiman et al. (2011). The reduction in the efficiency of a PV module increased from 0% to 26% with a corresponding increase in dust deposition from 0 g/m^2 to 22 g/m^2 (Hai et al., 2011). Said and Walwil (2014) found that the spectral transmittance and overall transmittance of a PV module decreased by 85% and 20%, respectively, because of the 45-day dust deposition (5 g/m^2) on the PV module; consequently, PV module efficiency dropped. In another investigation, dust accumulation reduced glass transmittance by approximately 19.17%, 13.81%, and 5.67% at 0°, 45°, and 90° tilt angles of a solar module, respectively; the reduction in glass transmittance decreased PV module efficiency (Nahar & Gupta, 1990). Efficiency is also decreased by an increase in RH (Touati et al., 2012). A PV module showed high conversion efficiency at a low RH (Ettah et al., 2012.). Katkar et al. (2011) reported a solar efficiency of 9.7% at 60% RH and 12.04%

at 48% RH (Katkar et al., 2011). Omubo-Pepple et al. (2009) showed that the efficiency of a solar module increased with decreasing RH under a constant irradiation level. Humidity is the existence of water vapor particles in atmospheric air. The presence of these particles leads to the reflection, refraction, and diffraction of the direct irradiance hitting a PV module surface; consequently, the efficiency of the PV module decreases (Gwandu & Creasey, 1995).

The objective of the current research is to investigate the effects of solar cell temperature, varying irradiation levels, water and air cooling, dust, and humidity on the output performance of PV modules under both indoor and outdoor operating conditions. A finned semi-circular copper sheet attached to the copper tube heat exchanger, through which cooling water flows, is used to observe the cooling performance of a PV module.

CHAPTER 3 : RESEARCH METHODOLOGY

3.1 Introduction

This chapter presents a short discussion of the methodology followed in conducting the experiment, including experimental setup, data collection and processing techniques, and detailed mathematical modeling. Certain theoretical concepts of the heat transfer phenomena with regard to the heat exchanger used in a solar cell module are also discussed. Different equations and calculation methods related to PV technology are described. A brief description of the experimental setup and instruments are also mentioned in this chapter.

The experiments were conducted at the Solar Thermal Lab, Level 15 and Solar Garden, Level 3, University of Malaya Power Energy Dedicated Advanced Center (UMPEDAC), Wisma R & D, University of Malaya.

3.2 Experimental Setup

The experiments are conducted indoors at an ambient temperature of 27 °C and outdoors at a maximum ambient temperature of 35 °C. The setup mainly consists of a monocrystalline PV module, a solar simulator, a centrifugal pump, a cooling radiator, a heat exchanger, and an air blower.

Figure 3.1 shows a schematic of the current experimental setup.

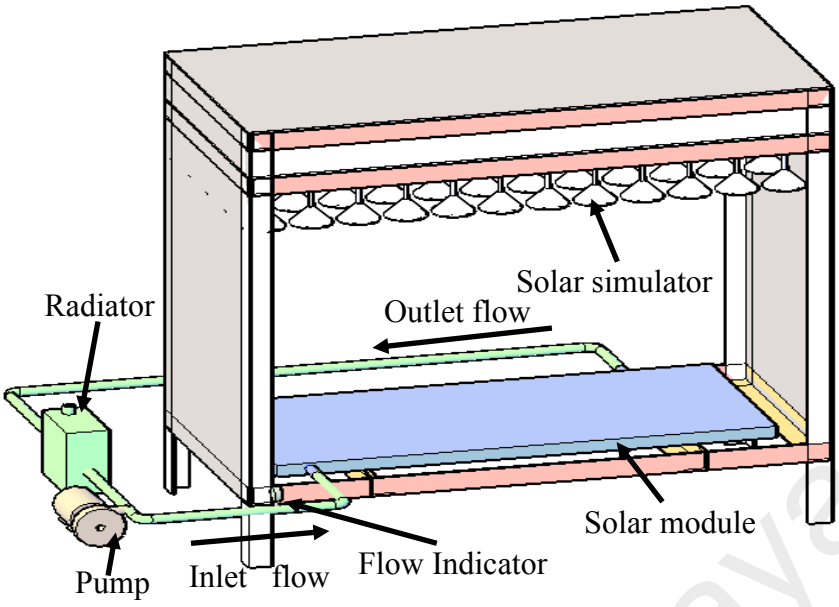

Figure 3.1: Schematic diagram of the experimental setup

3.2.1 Solar Simulator

A solar simulator, manufactured using 90 OSRAM halogen bulbs, is used to produce the variable irradiation levels applied to the PV module.

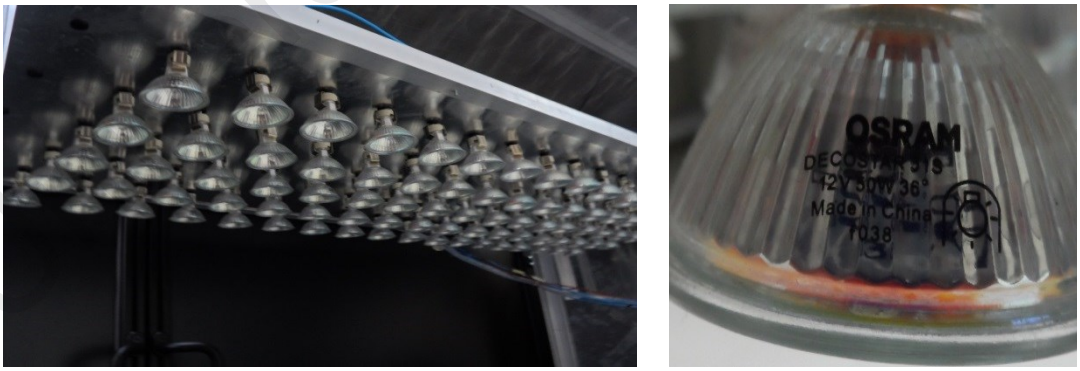

Figure 3.2: Solar simulator and halogen bulbs

The simulator is shown in Figure 3.2. A total of 90 bulbs are used in the experiment. Each bulb has a capacity of 50 W, a supply voltage of 12 V, and a current of 4.17 A. Thus, the simulator is capable of providing 4500 W irradiation. Given that 15 bulbs are

connected in series, a total of 6 series connections are prepared for the simulator. A total of 3 variable-controlled AC power supply transformers are used to supply power to the simulator and generate variable irradiation. The capacity of each transformer is 3 kVA. Each transformer supplies power to two series circuits in a parallel connection. This simulator is designed to fully operate under indoor conditions.

3.2.1.1 PV Module

A new monocrystalline PV module (SY 90M model) made by Shaiyang in Hebei, China (Mainland) is used in the experiments. The module is shown in Figure 3.3.

Figure 3.3: Monocrystalline PV module

The PV module has a total of 36 cells, each with dimensions of 125 mm × 125 mm. The total dimensions of the module are 1200 mm × 545 mm × 35 mm, and its maximum output power is 90 W. The detailed specifications of the solar module at STC are given in the Table 3.1. In general, a monocrystalline PV has the following layers, which have different material compositions: (1) a glass upper shield, (2) an ARC, (3) a monocrystalline silicon layer, (4) a layer made of ethylene vinyl acetate (EVA), (6) a metal back contact sheet, and (6) a Tedlar PVF layer. These layers are mounted on a metallic frame (Jones, 2001).

Table 3.1: Specifications of an SY 90M monocrystalline module

Place of Origin	**Hebei, China (Mainland)**
Brand Name	Shaiyang
Model Number	SY-90M
Material	Monocrystalline silicon
Size	1200 mm × 545 mm × 35 mm
Number of Cells	4×9
Maximum Power	90 W
Open-circuit voltage (V)	22.04
Short-circuit current (A)	5.31
V_{mp} (V)	18.37
I_{mp} (A)	4.91
Weight of module (kg)	7.01
Cell dimension (mm)	125×125

Table 3.2: Properties of a PV layer (Armstrong & Hurley, 2010; Notton et al., 2005; Jones & Underwood, 2001; Jooss, 2002; Lai et al., 1997; Lu & Yao, 2007; Phylipsen & Alsema, 1995; Hatch, 1984;)

Layers	**Thickness, t (m)**	**Thermal conductivity, k (W/m·K)**	**Density, ρ (kg/m^3)**	**Specific heat capacity (J/(kg·K))**	**Heat capacity, c (J/K)**
Glass	0.0031	1.80	3000.0	500.0	2943
ARC	100×10^{-9}	32.0	2400.0	691.0	0.11
Monocrystalline cell	225×10^{-6}	148.0	2330.0	677.0	232
EVA	500×10^{-6}	0.35	960.0	2090.0	656
Back contact	10×10^{-6}	237.0	2700.0	900.0	16
Tedlar PVF layer	0.00011	0.20	1200.0	1250.0	98

The thickness (t), thermal conductivity (k), density (ρ), and heat capacity (c) of each PV layer is shown in Table 3.2. The properties of the PV panel materials are assumed to be independent of temperature. The prevailing wind conditions and varying ambient temperatures also have significant effects on the thermal response time of the PV panel.

3.2.2 Heat Exchanger

In the experiment, a rectangular heat exchanger composed of copper tubes, each with a diameter of 22 mm, is used to cool the PV module, as shown in Figure 3.4

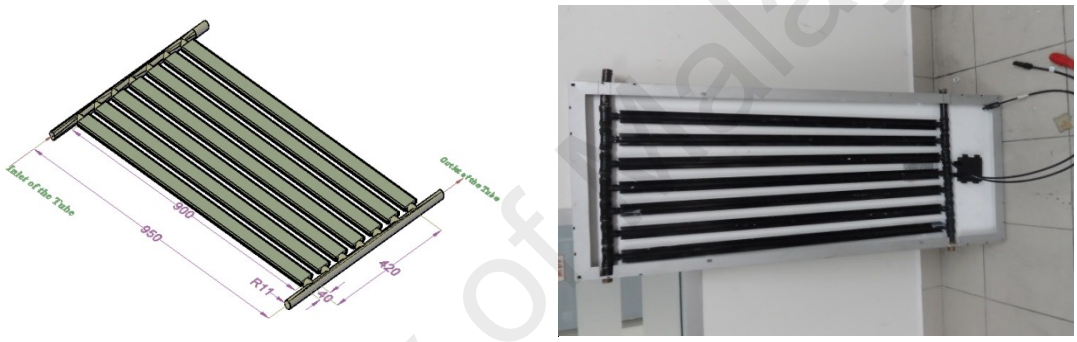

Figure 3.4: PV module heat exchanger device

The length of the device is 950 mm, and its width is 420 mm. Seven circular parallel copper tubes are used in the device. A semi-circular finned plane sheet is used on the upper half round of each parallel tube so that the bottom of the PV device is attached to the system for smooth heat transfer flow. The finned plane sheet is used to increase the heat transfer rate from the bottom surface.

3.2.3 Centrifugal Pump

A Pentax CP45 centrifugal pump (Figure 3.5) is used in the current investigation. This pump operates at various voltages and creates different flow rates of water flowing

through the heat exchanger device. The pump has a capacity range of 5–35 L/min, a delivery head range of 9–35 m, and an operating horsepower of 0.5 kW.

Figure 3.5: Pentax CP45 centrifugal pump.

3.2.4 Air Blower

An air blower (Figure 3.6) with a capacity of 34 L/min is used in the experiment for the air cooling of the PV module. It operates at 115/230 V AC and 40 W power.

Figure 3.6: BOYU S-60 air pump.

The specifications of the BOYU S-60 air pump are provided in Table 3.3. It can generate a maximum airflow of 34 L/min. Air is circulated in an open channel flow.

Table 3.3: Specifications of the BOYU S-60 air pump.

Parameters	Value
Volt	AC230/115 V
Frequency	50/60 Hz
Power	40 W
Pressure	0.030 MPa
Output	34 L/min
Weight	4.40 kg
Size	290 mm × 210 mm × 165 mm

3.2.5 Humidifier

To generate humidity around the PV module, an anion atomized ultrasonic humidifier (Figure 3.7) is used in the experiment.

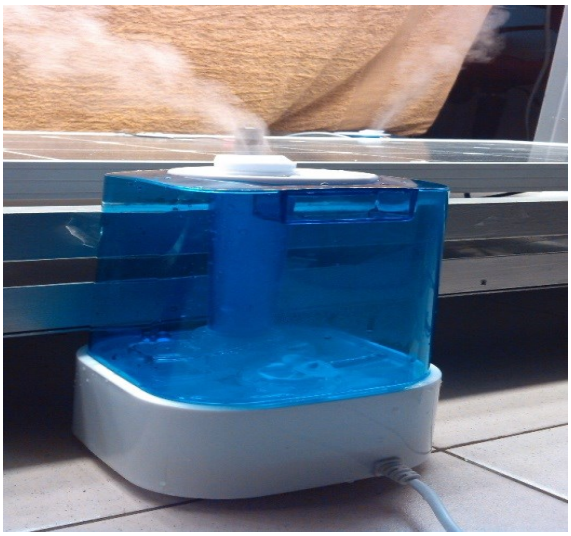

Figure 3.7: Anion humidifier

The capacity of the humidifier is 2 L, and its mist discharge rate is 350 L/h. The power rating of this humidifier is 28 W, and its voltage rating is 220 V/50 Hz. It operates in a super silent mode with a 360° rotating capacity. The humidifier runs continuously beside the solar module to generate humidity around the top surface area of the module.

3.2.6 Radiator

An HKS cooling radiator with a 1.3 kg/cm^2 capacity is used to cool the heated water, as shown in Figure 3.8.

Figure 3.8: HKS radiator

The detailed design parameters of the experimental setup are provided in Table 3.4.

Table 3.4: Detailed design parameters of the experimental setup

Parameters	**Value**
Incident irradiation intensity, G (W/m^2)	400–1000
Area of solar cell, A_{sc} (m^2)	0.65
Ambient temperature, T_a (°C)	27.0
Area of the inside rectangular half round, A_h (m^2)	0.218
Total area of the plate attached to the bottom surface of the module, A_{sheet} (m^2)	0.25
Unfinned area of the two sides of the rectangular half round, A_{unfin} (m^2)	0.0144
Finned area of the two sides of the rectangular half round, A_{fin} (m^2)	0.0864
Cross-sectional area of a fin, A_c (m^2)	0.0018
Perimeter of a fin, p (m)	1.804
Fin characteristic parameter (m)	3.88902
Corrected length of the rectangular fin, L_c (m)	0.0061
Mass flow rate of the fluid, m_f (kg/s)	0.01–0.04

3.3 Experimental Instrumentation

Several instruments, such as a data taker, an I–V tracer, a flow meter, thermocouples, a pyranometer, and a humidity sensor, are used to measure the different parameters pertinent to the investigation.

3.3.1 Data Taker

A digital data taker (model DT80) is used to measure the different temperature and irradiation readings. Its web-based dEX graphical interface can trace data more rapidly and more easily. The recorded data can be retrieved through a web browser or copied to

any portable USB drive. The data taker uses a programming language that can interface with any complex system. DT80 is an operator-friendly data taker, which facilitates communication through an serial sensor port and other communication ports. It also has low power consumption during operation.

Figure 3.9: Data taker DT80

The DT80 data taker provides five analog input channels (numbered 1 to 5). Depending on the wiring configuration used, these channels allow the measurement of 5 and 15 separate voltages. Each analog input channel is a 4-wire input, which allows the measurement of voltage, current, resistance, and frequency. These are the fundamental signal outputs of most sensors. Using all 4 terminals on each channel is unnecessary; 2 terminals are frequently adequate.

3.3.2 I-V Tracer

An I–V tracer as shown in the Figure 3.10, is used to measure the module output in terms of current and voltage. The tracer is used to measure and control the open-circuit voltage (V_{oc}), short-circuit current (I_{sc}), maximum power (P_{max}), maximum voltage (V_m), and maximum current (I_m) generated by the module.

Figure 3.10: I-V tracer developed by UMPEDAC

The MPP tracker (MPPT) or I–V tracer can trace power up to 2000 W. It is generally used to test the properties of a PV module or a single solar cell both in indoor simulation and outdoor irradiation. The performance of the solar module is characterized using the I–V curve or the maximum power point from the MPPT/I–V tracer. The operating specifications of the I–V tracer are provided in Table 3.5.

Table 3.5: Specifications of the I–V tracer

Notation	Parameter	Minimum value	Maximum value
V_{oc}	Open-circuit voltage	1 V	600 V
I_{sc}	Short-circuit current	0.5 A	7 A
P_{max}	Maximum power	0 W	3000 W

3.3.3 Flow Meter

A variable area flow meter (Figure 3.11) is used to measure the discharge rate and velocity of water flow and airflow.

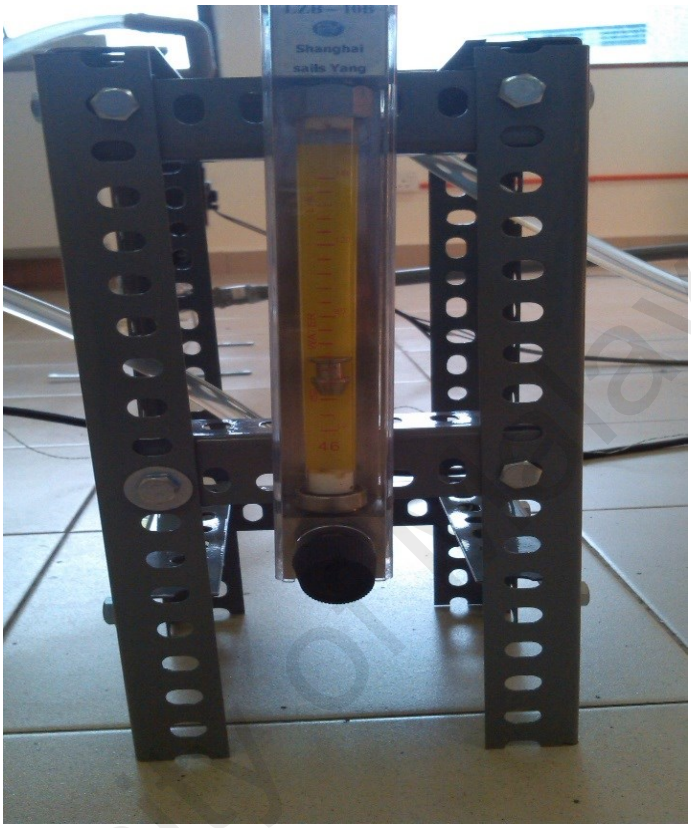

Figure 3.11: LZB -10B flow meter

The model of the water flow meter used in the experiment is LZB-10B. It can measure flow rates within the range of 16–160 L/h. The various water flow rates measured using the flow meter are 0.01, 0.02, 0.03, and 0.04 kg/s. It also measures fluid flow rate based on the pressure difference between the upper and lower parts of the float.

3.3.4 Thermocouples

Two K-type thermocouples (Figure 3.12), each with a PTFE uncovered welded tip, are used to measure the temperatures of the top and bottom surfaces of the module. Two more thermocouples are used to measure the inlet and outlet temperatures of the cooling tube.

Figure 3.12: K-type PTFE twin twisted pair thermocouple cable

The thermocouples exhibit good mechanical strength; flexibility; and resistance to oils, acids, and other harsh fluids. These sensors are designed for testing and development applications, and data can be collected using an ideal data logger. The temperature-measuring range of this sensor is −75 °C to 250 °C.

3.3.5 Pyranometer

A LI-COR PY82186 pyranometer (Figure 3.13) is used in the experiment to measure the irradiance of the solar simulator. This type of pyranometer is used in different countries for PV investigations as well as climatological and agronomic research to measure incident irradiation intensity . The LI-COR pyranometer can be calibrated easily with any digital pyranometer on a sunny day.

Figure 3.13: LI-COR PY82186 model pyranometer

The irradiance measuring range of this pyranometer is from 0 W/m^2 to 1500 W/m^2, its spectral range is from 300 nm to 1100 nm, and its operating temperature range is from −40 °C to 95 °C. The pyranometer is thoroughly calibrated using a digital pyranometer before its use.

3.3.6 Spectroradiometer

A spectroradiometer detects an optical character by calculating specific optical responses. The spectroradiometer used in this investigation is manufactured by Bentham, and it can measure spectral irradiance from 150 nm to 30 μm. It can perfectly detect all types of UV radiometric, colorimetric, and photometric characters by calculating spectroradiometric measurements.

Figure 3.14: Spectroradiometer

However, Bentham also supplies a range of filter-based radiometers/photometers that closely match spectral responses for simple integral-type measurements.

Figure 3.15: D7-H and IS75-ENV cosine response diffusers

The spectroradiometer uses a D7-H PTFE horizontal optical input device for the accurate measurement of spectral responses. It can measure spectral irradiance within the 200–1100 nm range. A fiber-coupled IS75-ENV quartz dome is used to measure the extended wavelengths of irradiances within the range of 200–2500 nm.

3.3.7 Humidity Sensor

A humidity sensor (model HU1030NA) is used to measure humidity in the PV module enclosure. It can measure humidity within the range of 20%–90% RH. Images of this sensor are presented in Figure 3.16. The operating specifications of this sensor are provided in Table 3.6.

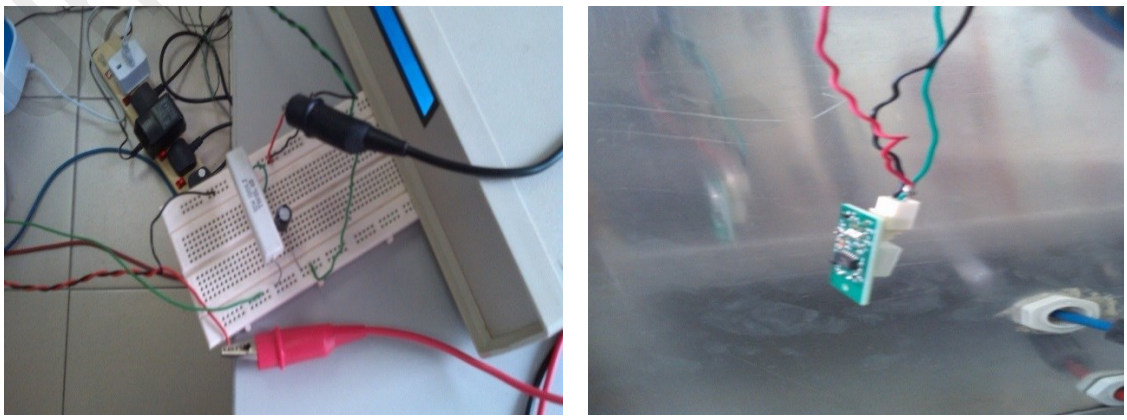

Figure 3.16: HU1030NA humidity sensor.

Table 3.6: Specifications of the humidity sensor

Item	**Value/description**
Humidity sensor type	Polymer Humidity Sensor HS-30P
Maximum current	≤ 2 mA at 5.0 V
Output voltage range (DC)	1.0–3.0 V
Output impedance	~2.5 kΩ
Accuracy (Humidity calibration)	≤± 5% RH at 25 °C, 25%–90% RH at 5.0 V ≤±10% RH at 5 °C–90 °C, 20%–100% RH at 5.0 V ※Output voltage (V) = 0.02 × H + 1 (H: Relative humidity % RH)
Operating temperature range	0 °C–90°C
Operating humidity range	20%–90% RH (without condensation)
Response time (90%)	≤3 milS

3.4 Experiment Test Conditions and Data Acquisition

This study aims to determine the influences of different environmental operating conditions on the performance of a PV module. The indoor test conditions are as follows: 27 °C ambient temperature, 400–1000 W/m^2 irradiation level, 40–160 L/h mass flow rate, and 40%–60% RH. The environmental parameters include solar irradiance and RH. The operating parameter cooling water flow rate is varied in the experiment. The parameters are varied independently of one another. Only one variable is varied while the others are kept constant. The irradiation levels are 400, 600, 800, and 1000 W/m^2. Each level is kept constant when investigating the effects of temperature and irradiation intensity on the performance of the PV module. A photograph of the experimental setup is shown in Figure 3.17

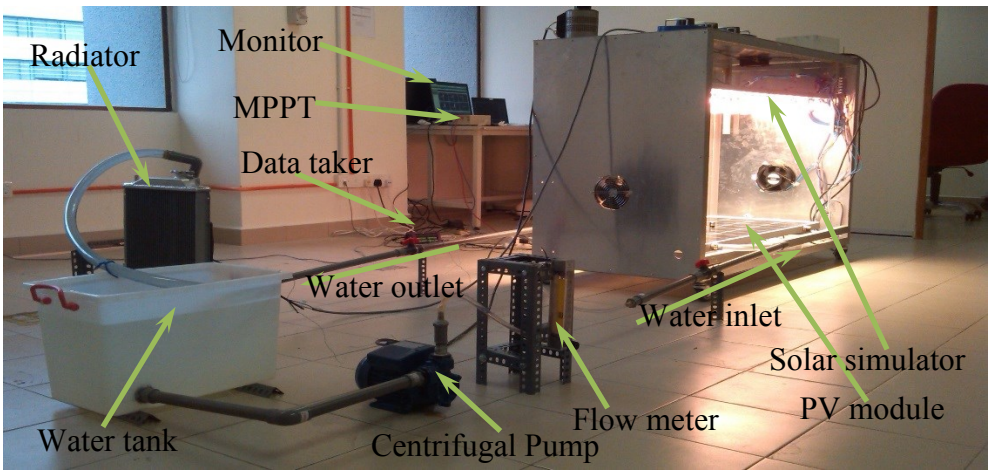

Figure 3.17: Experimental setup

To determine the optimal cooling water flow rate, water flows through the heat exchanger device at various flow rates, including 40, 80, 120, and 160 L/h, at a constant irradiation level of 1000 W/m^2 irradiation. The PV module output performance is observed during irradiation. To investigate the effect of cooling on the performance of the PV module, irradiation intensity is varied at different levels, including 1000, 800, 600, and 400 W/m^2, and a constant 80 L/h cooling water flow rate is applied. The effects of irradiation intensity on the PV module temperature and conversion performance are observed by applying this cooling condition. Various RH levels, including 60%, 50%, and 40%, are maintained in the surrounding area of the PV module under indoor conditions and at 800 W/m^2 irradiation level to investigate the effect of humidity on the performance of the PV module.

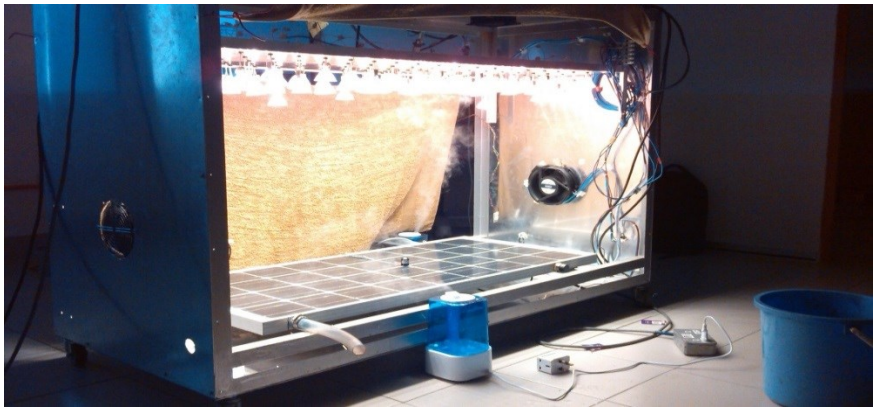

Figure 3.18: Experimental setup for the investigation on the effect of humidity on the output performance of the PV module at 800 W/m^2 irradiation level.

Approximately 0.012 g/cm^2 dust is spread on the top surface of the solar module to investigate the effect of dust on the performance of the PV module at 800 W/m^2 irradiation level, as shown in Figure 3.19.

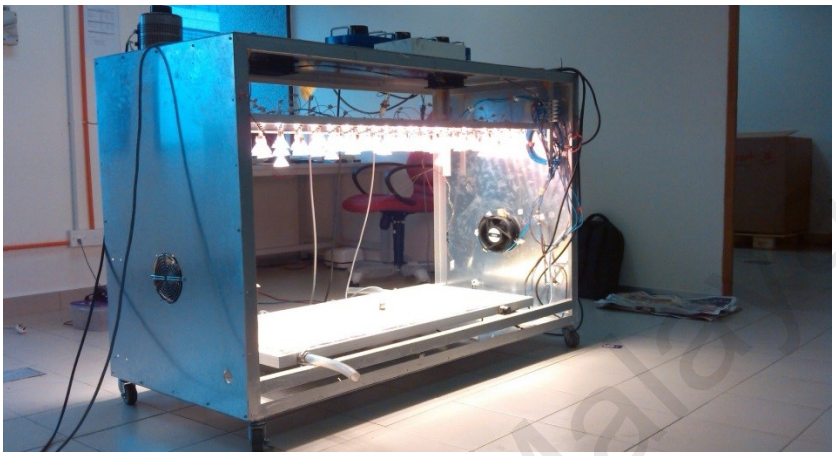

Figure 3.19: Experimental setup for the investigation on the effect of dust on the output power of the PV module at 800 W/m^2 irradiation level

The data taker collects the temperature data from the thermocouples at a pre-defined time interval from the front and back of the PV module and from the entry and exit positions of the cooling water flow. The data taker also collects data from the humidity sensor and pyranometer. The I–V tracer measures the open-circuit voltage (V_{oc}), short-circuit current (I_{sc}), maximum power (P_{max}), maximum voltage (V_m), and maximum current (I_m) of the PV module. Data are gathered every minute. All the gaskets are checked for water tightness, and the thermocouples are attached carefully to collect data correctly.

To compare the indoor outputs under practical operating conditions, outdoor data are also collected in outdoor conditions. Another experimental setup is constructed at Solar Park, Level 3, Wisma R&D, University of Malaya to collect outdoor data. The data are collected on sunny days from January 2015 to March 2015, with cooling and without cooling conditions. From January to March, the solar park of UMPEDAC is completely covered by building shading after 12:40 p.m. Thus, the data are collected from 09:00

a.m. to 12:40 p.m., during which solar irradiation level varied from approximately 300 W/m^2 to 1000 W/m^2. Figure 3.20 shows a photograph of the outdoor experimental setup.

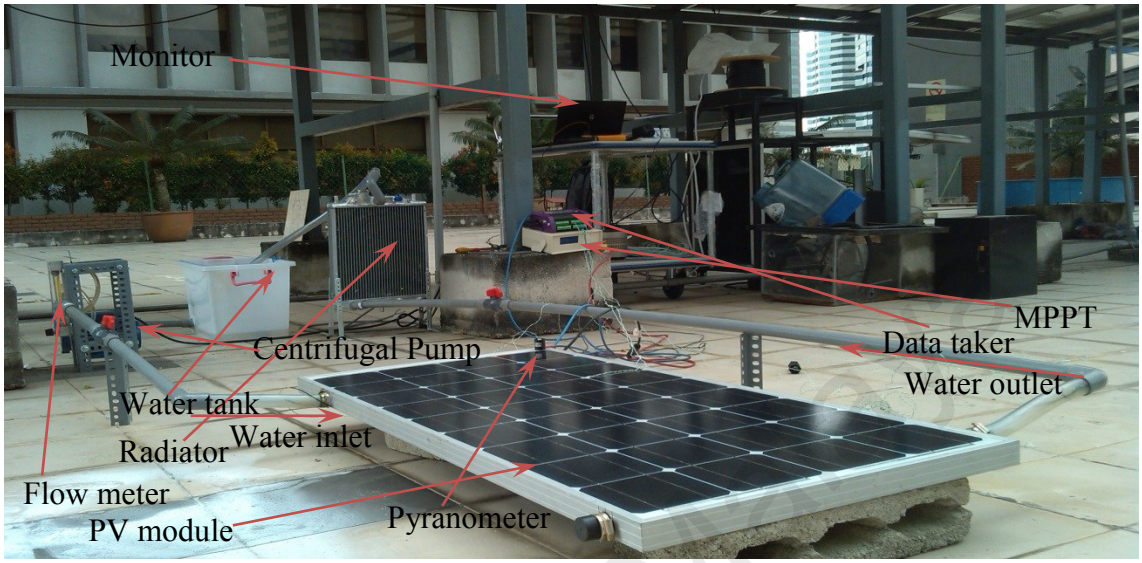

Figure 3.20: Outdoor experimental setup

Ambient temperature varies from approximately 29 °C to 35 °C. The data used in the analysis are collected under similar meteorological conditions on different days. The efficiency of the solar module is observed when solar irradiation intensity and cell temperature increase. The mass flow rates of the cooling water flowing through the heat exchanger of the PV module applied in the outdoor experiment are 30, 60, 90, and 180 L/h. The effects of irradiation levels on solar cell temperature and output performance are observed under cooled condition. To investigate the effect of humidity on the performance of the PV module under outdoor operating conditions, data are collected on five sunny days with different RH conditions but similar irradiation levels at peak operating period. To investigate the effect of dust on PV module performance under outdoor conditions, 0.012 g/cm^2 dust is spread on the top surface of the PV module, and the data collected are compared with those collected when the PV module has no dust under similar meteorological conditions. The data taker collects the temperature data from the thermocouples on the lower and upper surfaces of the PV module and at the

entry and exit points of the cooling water flowing through the heat exchanger. The data taker also collects data from the pyranometer located on the top surface of the PV module. Data are collected at regular 10-minute intervals throughout the experiment. The I–V tracer measures the open-circuit voltage (V_{oc}), short-circuit current (I_{sc}), maximum power (P_{max}), maximum voltage (V_m), and maximum current (I_m) of the PV module. The objective of the outdoor experiment is to compare the parametric effects, such as temperature effect, cooling effect, and irradiation effect, under indoor and outdoor operating conditions. The collected data are used to analyze the performance of the monocrystalline PV module subjected to cooling and increases in irradiation intensity, temperature, dust, and RH under practical operating conditions.

3.5 Mathematical Formulation

3.5.1 Heat Transfer from the Top Surface of the Module

The energy balance formulae proposed by Tiwari et al. (2006), Dubey and Tiwari (2008), and Dubey and Tay (2013) indicate that the overall energy consumed by the upper layer of the PV module can be calculated by

$$E_{ab} = \tau_g \alpha_{sc} p_{sc} G A_{sc} \tag{3.1}$$

The energy wasted from the top surface of the PV module as a result of the convection process is

$$E_{ctop} = U_{sca} \left(T_{sc} - T_a\right) A_{sc} \tag{3.2}$$

The total energy conducted from the top surface to the back of the PV module can be written as

$$E_b = U_t (T_{sc} - T_b) A_{sc} \tag{3.3}$$

The electrical energy generated from the incident solar radiation can be written as

$$E_e = \eta_{sc} p_{sc} G A_{sc} \tag{3.4}$$

Thus, the energy balance equation for the top surface of the module can be written as

$$E_{ab} = E_{ctop} + E_b + E_e \tag{3.5}$$

The formula for the solar cell temperature can be derived from Equations 3.3–3.5 as follows:

$$T_{sc} = \frac{p_{sc} G (\tau_g \alpha_{sc} - \eta_{sc}) + (U_{sca} T_a + U_t T_b)}{(U_{sca} + U_t)} \tag{3.6}$$

3.5.2 Heat Transfer by Fins

Newton's cooling law defines the amount of heat convected from a solid surface to its surrounding area, and the transferred heat is formulated as follows (Cengel, 2006):

$$Q_{conv} = h_{air} A_s (T_s - T_\alpha) \tag{3.7}$$

Fourier's law of heat conduction suggests that the heat transferred through a finned surface can be expressed as follows (Cengel, 2006);

$$Q_{adiabatic\_tip} = \sqrt{h_{air} pkA_c} (T_b - T_\infty) \tanh ml \tag{3.8}$$

where, $m = \sqrt{\frac{h_{air} p}{kA_c}}$ (3.9)

Fin length should be corrected if the heat transferred by convection is considered. The following equation can be used to determine the modified length of a fin: $L_c = L + \frac{A_c}{p}$.

The corrected length of a rectangular fin is $L_c = L + \frac{t}{2}$ and that of a cylindrical fin is $L_c = L + \frac{D}{4}$.

The fin can transfer the maximum amount of heat if the fin material has infinite conductivity, and this amount of heat can be calculated using the following equation:

$$Q_{fin,\max} = h_{air} A_{fin} (T_b - T_a) \tag{3.10}$$

The efficiency of a fin can be described by

$$\eta_{fin} = \frac{Q_{fin}}{Q_{fin,max}} = \frac{\text{actual heat transfer rate from the fin}}{\text{maximum heat transfer from the fin in ideal case}} \tag{3.11}$$

However,

$$Q_{fin} = \eta_{fin} Q_{fin,\max} = \eta_{fin} h_{air} A_{fin} (T_b - T_a) \tag{3.12}$$

The efficiency of an extremely long fin is as follows:

$$\eta_{longfin} = \frac{Q_{fin}}{Q_{fin,\max}} = \frac{\sqrt{h_{air} pkA_c}(T_b - T_a)}{h_{air} A_{fin} (T_b - T_a)} = \frac{1}{L}\sqrt{\frac{kA_c}{h_{air} p}} = \frac{1}{ml} \tag{3.13}$$

The efficiency of a fin with an adiabatic tip can be calculated by

$$\eta_{adiabatic,tip} = \frac{Q_{fin}}{Q_{fin,\max}} = \frac{\sqrt{h_{air} pkA_c}(T_b - T_a)\tanh ml}{h_{air} A_{fin} (T_b - T_a)} = \frac{1}{L}\sqrt{\frac{kA_c}{h_{air} p}} = \frac{\tanh ml}{ml} \tag{3.14}$$

The cumulative heat transferred from the unfinned and finned areas determines the total heat transfer rate from the finned area, as shown in the following equation:

$$Q_{total,fin} = Q_{unfin} + Q_{fin} = h_{air} A_{unfin} (T_b - T_a) + \eta_{fin} h_{air} A_{fin} (T_b - T_a) \tag{3.15}$$

Table 3.7: Thermal characteristics of the system (Dubey & Tay 2013)

Parameters	**Value**
Transmissivity of the glass cover, τ_g	0.961
Solar module absorptivity, α_{sc}	0.90
Solar module packing factor, p_{sc}	0.80
Overall heat transfer coefficient through the glass cover from the top surface of the module to the ambient environment, U_{sca} ($W/(m^2 \cdot K)$)	7.141
Overall heat transfer coefficient from the top surface of the module to the Tedlar back surface, U_t ($W/(m^2 \cdot K)$)	150.00
Thermal conductivity of the copper fin, k ($W/(m^2 \cdot K)$)	385.00
Specific heat of water, C_f ($J/(kg \cdot K)$)	4200.00

CHAPTER 4 : RESULTS AND DISCUSSION

4.1 Indoor Performance of the PV Module

4.1.1 Effect of Temperature on PV Module Performance

The effect of temperature on PV module performance is investigated by observing the output power and efficiency of the module at 1000, 800, 600, and 400 W/m^2 irradiation levels, as shown in Figure 4.1 and Figure 4.2. At an irradiation level of 1000 W/m^2 without cooling, the initial module temperature is 30.11 °C, the efficiency is 7.63%, and the output power is 49.89 W. After a stable condition is attained, the module temperature increases to 73.23 °C, the efficiency decreases to 4.50%, and the output power decreases to 29.42 W. From the initial values, 3.13% electrical efficiency and 20.47 W output power are reduced because of the 43.12 °C increment in solar module temperature, thereby resulting in an output performance that is 41.03% lower than the preliminary output performance. At 1000 W/m^2 irradiation level without cooling, electrical efficiency decreased by 0.07%, and output power declined by 0.47 W per 1 °C increase in module surface temperature.

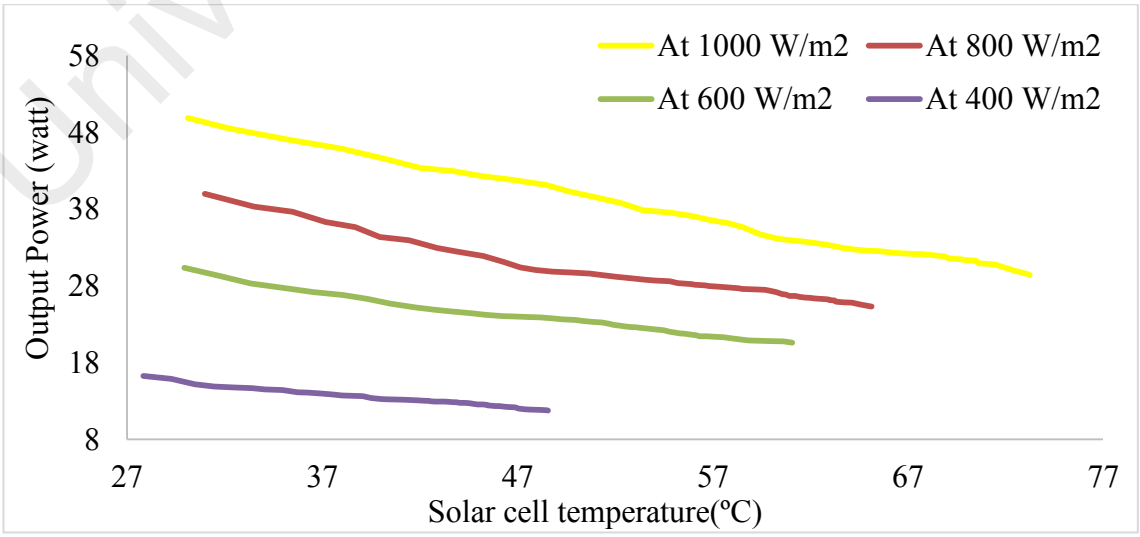

Figure 4.1: Output power vs. module temperature at different irradiation levels (without cooling).

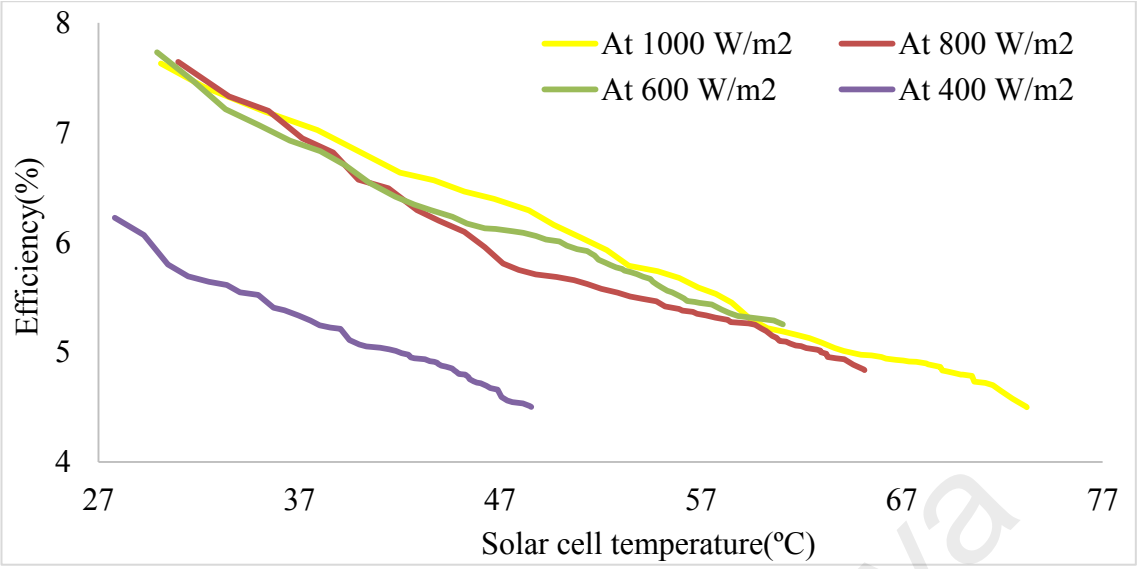

Figure 4.2: Efficiency vs. module temperature at different irradiation levels (without cooling)

Bahaidarah et al. (2013) observed that electrical efficiency decreased by 0.03% per one degree increment in PV module temperature without cooling condition. This result is in good agreement with the present experimental result. Chandrasekar et al. (2013) found a 0.05% electrical efficiency reduction for every degree increment in PV module surface temperature (Chandrasekar et al., 2013). This result also agrees well with the result of the current investigation. Deviations exist between the previous experiments and the present experiment under different environmental operating conditions. In the current investigation, the ambient temperature and other operating conditions are kept constant as the experiment is performed indoors. Bahaidarah et al. (2013) and Chandrasekar et al. (2013) conducted their investigations under open-air conditions at different irradiation levels, ambient temperatures, and wind velocities, among other parameters that affect the output performance of the PV module. The spectral irradiance (W(m·μm)) of sunlight is also considerably higher than that of halogen light. In the current investigation, a spectroradiometer is used to measure the spectral irradiance ($W/(m^{-2}\cdot\mu m)$) of artificial light and sunlight.

The efficiency of the PV module at 400 W/m^2 irradiation level is significantly lower than those at 600, 800, and 1000 W/m^2 irradiation levels. When a photon with an energy higher than the band gap energy hits a semiconductor, it provides the electrons located in the valence band with sufficient energy to travel to the conduction band. Both the holes created in the valence band and the electrons created in the conduction band participate in current flow in a potential ground (Kasap, 2002). At 400 W/m^2 irradiation level, halogen bulbs cannot provide a sufficient amount of photonic energy to the electrons in the valence band to allow them to move from the valence band to the conduction band.

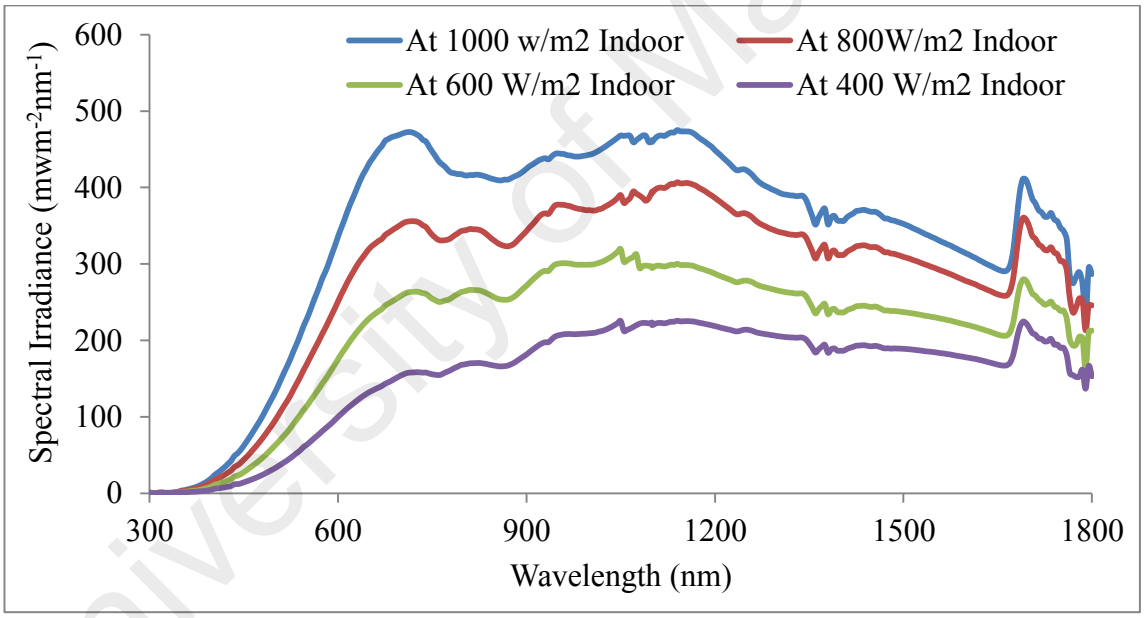

Figure 4.3: Spectral irradiance of halogen lights

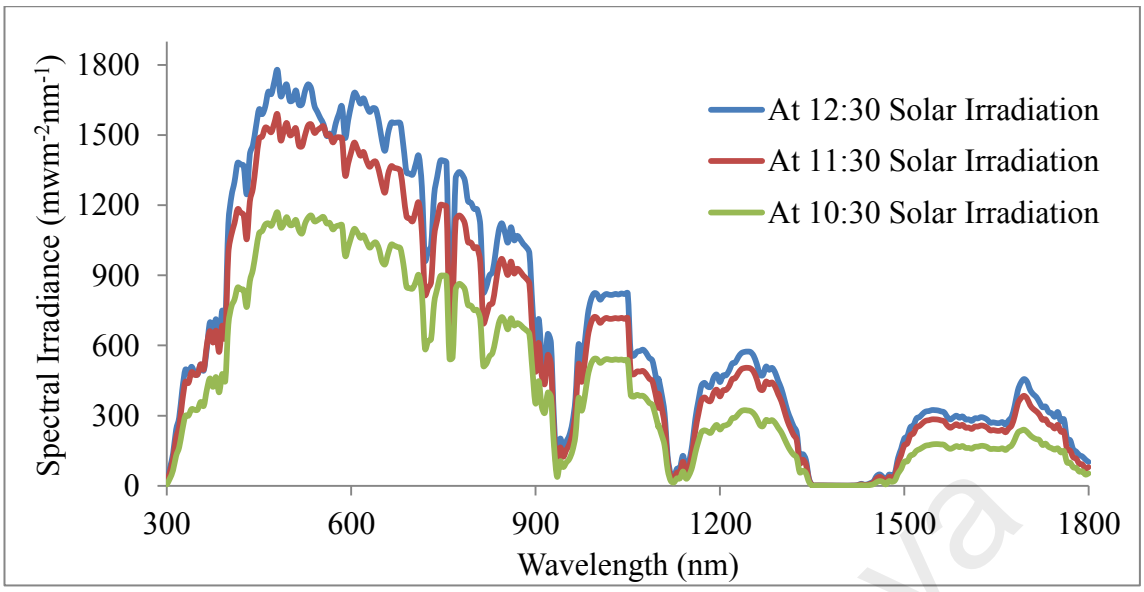

Figure 4.4: Spectral irradiance of sunlight

Figure 4.3 and Figure 4.4 show the spectral irradiances of halogen light and sunlight. Halogen light produces more heat than sunlight as the former has less photonic energy (education.org, 2015).

Consequently, the experimental results of Bahaidarah et al. (2013) and Chandrasekar et al. (2013) deviate from the current experimental results to a certain extent. Table 4.1 shows a comparison of the electrical efficiency results in the studies of Bahaidarah et al. (2013) and Chandrasekar et al. (2013), and the current investigation.

Table 4.1: Comparison of the efficiency reduction rates per 1 °C increase in cell temperature of the PV module in different investigations

Authors, year, time, location, and coordinates	Irradiation (W/m^2)		Operating temperature (°C)		Efficiency (%)		Maximum ambient temperature (°C)	Reduction of efficiency (%) per 1 °C increment in cell temperature	Comparison with present investigation
	Starting period	Peak period	Starting period	Peak period	Starting period	Peak period			
Current experimental results; Solar Thermal Lab, UMPEDAC, University of Malaya; Latitude 26°18'N, Longitude 50°08'E	1000	1000	30.11	73.23	7.63	4.5	27	0.07	Agree with previous investigations
Bahaidarah et al. (2013); February 2012; KFUPM, Dhahran, Saudi Arabia; Latitude 26°18'N, Longitude 50°08'E	240	979	25	44	15.7	15.2	21	0.03	Agree well with current investigation
Chandrasekar et al. (2013); April 2013; Anna University, BIT Campus, Tiruchirappalli, India; Latitude 10°39'N, Longitude 78°44'E	600	1300	37	65	10.3	9	37	0.05	Agree well with current investigation

At an irradiation level of 800 W/m^2 without cooling, the initial module temperature is 30.97 °C, electrical efficiency is 7.64%, and output power is 39.99 W. After a stable condition is attained, module temperature increases to 65.14 °C, efficiency decreases to 4.84%, and output power decreases to 25.31 W. Approximately 2.81% electrical efficiency and 14.68 W output power are reduced from the initial values because of the

34.16 °C increment in solar module temperature; consequently, the output performance is 36.71% lower than the preliminary output performance. At an irradiation level of 800 W/m^2 without cooling, approximately 0.08% electrical efficiency and 0.43 W output power decreases occur for every 1 °C enhancement of the module surface temperature.

At an irradiation level of 600 W/m^2 without cooling, the initial module temperature is 29.92 °C, efficiency is 7.73%, and the output power is 30.34 W. After a stable condition is attained, module temperature increases to 61.07 °C, efficiency decreases to 5.25%, and output power decreases to 20.61 W. Approximately 2.48% electrical efficiency and 9.73 W output power are reduced from the initial values as a consequence of the 31.15 °C increment in solar module temperature; thus, the output performance is 32.06% lower than the preliminary output performance. At an irradiation level of 600 W/m^2 without cooling, electrical efficiency decreases by 0.08%, and output power decreases by 0.31 W per 1 °C increase in module surface temperature.

At an irradiation level of 400 W/m^2 without cooling, the initial module temperature is 27.82 °C, electrical efficiency is 6.22%, and output power is 16.28 W. After a stable condition is attained, module temperature increases to 48.55 °C, efficiency decreases to 4.5%, and output power decreases to 11.78 W. Approximately 1.72% electrical efficiency and 4.50 W output power are reduced from the initial values because of the 20.73 °C increment in solar module temperature; consequently, output performance is 27.65% lower than the preliminary output performance. At an irradiation level of 400 W/m^2 without cooling, approximately 0.08% electrical efficiency and 0.22 W output power are reduced per 1 °C enhancement of module surface temperature.

Figure 4.5 and Figure 4.6 present the temperatures of the solar cell, Tedlar back surface, and glass front surface of the PV module, with and without cooling.

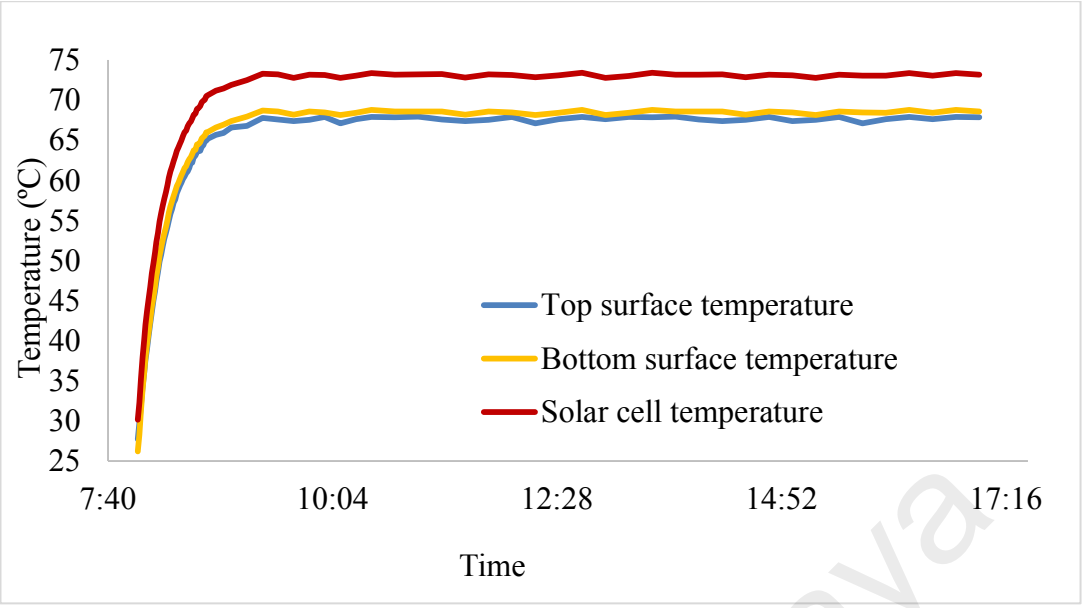

Figure 4.5: Top surface, bottom surface, and solar cell temperatures at an irradiation level of 1000 W/m^2 without cooling

In the current investigation, the maximum cell temperature (73.23 °C) is observed in steady state at an irradiation level of 1000 W/m^2 without cooling and under indoor operating conditions. Chandrasekar et al. (2013) found that cell temperature was 65 °C at an irradiation level of 1300 W/m^2 without cooling during peak operating periods at Anna University, BIT Campus, Tiruchirappalli, India. Their experiment was conducted in April 2012, when the highest ambient temperature was 37 °C (Chandrasekar et al., 2013). Bahaidarah et al. (2013) observed that solar cell temperature was 44 °C at an irradiation level of 979 W/m^2 without cooling at King Fahd University for Petroleum and Minerals (KFUPM), Dhahran, Saudi Arabia. Their experiment was conducted in February 2012, with 21 °C being the highest ambient temperature (Bahaidarah et al., 2013). Thus, solar cell temperatures in the current investigation are slightly different from those recorded by Chandrasekar et al. (2013) and Bahaidarah et al. (2013). The current investigation is conducted indoors, and the properties of halogen radiation are different from those of sunlight to some extent. The spectral irradiance (W/(m^2·μm)) of solar rays is considerably higher than that of artificial light. Synthetic halogen light produces higher heat than solar rays because of its lower photonic energy

(education.org, 2015). Thus, deviations are expected among the experimental outcomes of the investigations of Chandrasekar et al. (2013), Bahaidarah et al. (2013), and the current investigation.

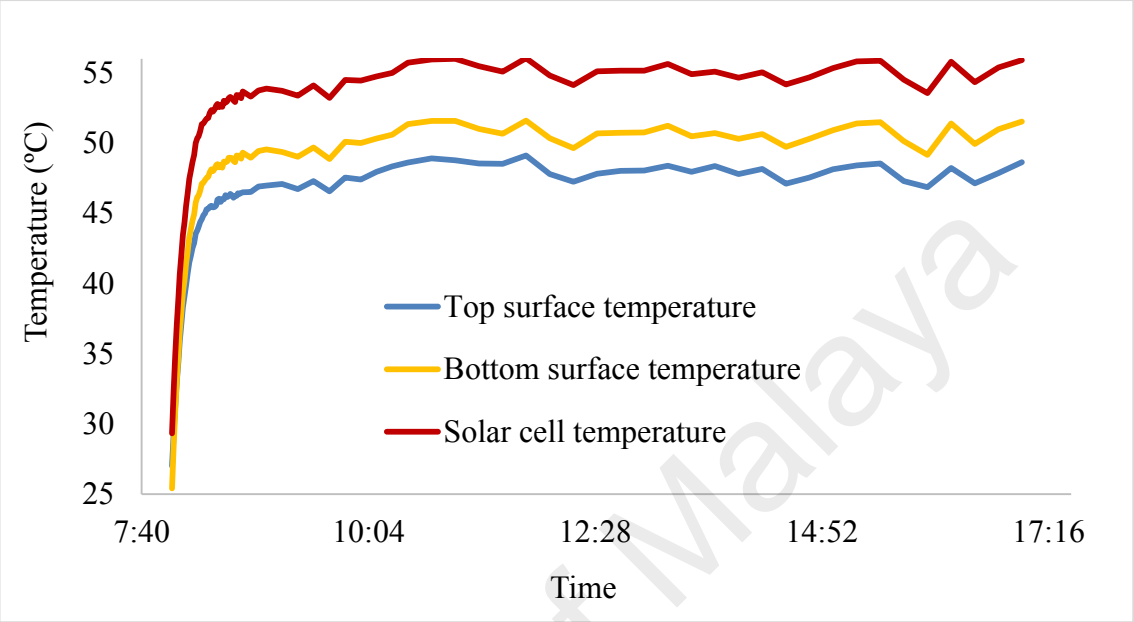

Figure 4.6: Top surface, bottom surface, and solar cell temperatures at an irradiation level of 1000 W/m^2 with cooling

In the current investigation, maximum cell temperature (56.02 °C) is observed in steady state at an irradiation level of 1000 W/m^2 with water cooling. Chandrasekar et al. (2013) found that solar cell temperature was approximately 50 °C at an irradiation level of 1300 W/m^2 with cooling under peak operating conditions at Anna University, BIT Campus, Tiruchirappalli, India. Their experiment was conducted in April 2012, when the highest ambient temperature was 37 °C (Chandrasekar et al., 2013). Bahaidarah et al. (2013) observed that solar cell temperature was 35 °C at an irradiation level of 979 W/m^2 with cooling at KFUPM, Dhahran, Saudi Arabia. Their experiment was conducted in February 2012, with 21 °C being the highest ambient temperature (Bahaidarah et al., 2013). The current investigation is conducted indoors. The spectral band quality of sunlight and halogen light are different. Halogen light has lower photonic energy and higher wavelength, thereby producing extra heat on the solar cell

surface (education.org, 2015). Thus, its spectral irradiance value (W/(m2·μm)) is significantly lower than that of solar rays. Inevitably, deviations exist among the experimental results of Chandrasekar et al. (2013), Bahaidarah et al. (2013), and the current study.

Approximately 15%–20% of the sunlight hitting a PV module is harnessed for electricity generation on the solar cell surface, whereas the remaining incident solar radiation generates heat on the system (Teo et al., 2012). A portion of the produced heat energy from the incident solar radiation on the PV module surface is transferred to the surroundings through convection, whereas the remaining portion is transmitted to the Tedlar back layer. The Tedlar back surface of the solar module directly absorbs a portion of the incident solar radiation because the packing factor passess additional heat on the back surface (Dubey & Tay, 2013). Approximately 96% of the incident solar radiation passes through the upper glass sheet to the PV cell layer. The coefficient of the heat transferred from the surface glass sheet to the surrounding air, U_{sca}, is 7.14 W/(m^2·K). However, the coefficient of the heat transferred from the Tedlar back layer to the ambient air, h_{air}, is 5.81 W/(m^2·K). Thus, the glass sheet on the top surface of the module loses more heat than the Tedlar back sheet. Consequently, the top glass surface of a PV module has a lower temperature than the Tedlar bottom layer (Dubey & Tay, 2013; Dubey & Tiwari, 2008). The temperature of the solar cell surface depends directly on the amount of incident solar radiation, Tedlar back surface temperature, and ambient temperature, as shown in Equation (3.6). Table 3.2 shows that the heat capacity of the Tedlar back surface is significantly lower than that of the solar cell layer of the monocrystalline PV module. Therefore, the PV cell heats up rapidly as it absorbs additional heat. Consequently, the Tedlar back surface temperature is lower than the PV cell temperature.

4.1.2 Effect of Irradiation Level on PV Module Performance

Cell temperature and output power fully depend on the intensity of solar irradiation, as shown in Table 4.2.

Table 4.2: Solar cell temperature, output power, and efficiency values in steady state at different irradiation levels, with cooling and without cooling

Irradiation level (W/m2)	Without cooling		With cooling	
	Solar cell temperature (°C)	Output power (W)	Solar cell temperature (°C)	Output power (W)
400	48.55	11.78	41.90	11.38
600	61.07	20.61	46.62	23.10
800	65.14	25.31	52.40	29.58
1000	73.23	29.42	56.02	37.46

Figure 4.7 shows that solar cell temperature increases with increasing irradiation level

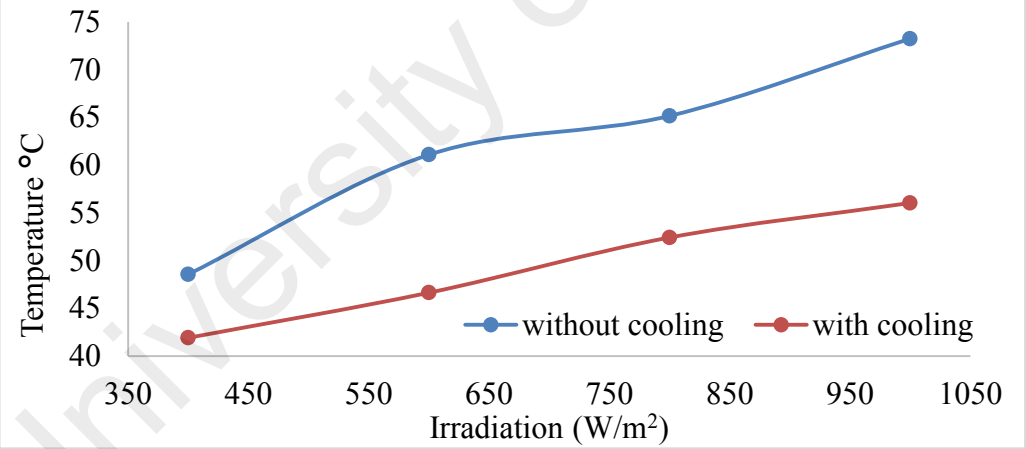

Figure 4.7: Irradiation level vs temperature

Table 4.2 and Figure 4.7 show that solar cell temperature increase by approximately 2.35 °C and 4.11 °C with each 100 W/m^2 increase in the irradiation level, with and without cooling, respectively.

Teo et al. (2012) conducted an experiment on the rooftop of the EA Building at the National University of Singapore in September 2009. At an irradiation level range of

280–1200 W/m^2 without cooling, solar cell operating temperatures ranged from 47 °C to 65 °C. At an irradiation level range of 550–1050 W/m^2 with cooling, solar cell operating temperatures ranged from 41 °C to 48 °C. Approximately 1.8 °C and 1.4 °C were added to solar cell temperature each time the irradiation level was increased by 100 W/m^2 without cooling and with air cooling, respectively (Teo et al., 2012).

Bahaidarah et al. (2013) conducted an experiment at KFUPM, Dhahran, Saudi Arabia in February 2012, when the highest ambient temperature was 21 °C. The incident solar radiation limit ranged from 240 W/m^2 to 979 W/m^2. Without cooling, the range of module operating temperature in their experiment was 25 °C–44 °C. With cooling, module operating temperature range was 21 °C–35 °C. Approximately, 2.6 °C and 1.9 °C were added to solar cell temperature with each 100 W/m^2 increase in the irradiation level, without cooling and with water cooling, respectively (Bahaidarah et al., 2013).

Chandrasekar et al. (2013) conducted their investigation at Anna University, BIT Campus, Tiruchirappalli, India in April 2012, when the highest ambient temperature was 37 °C. The incident solar radiation ranged from 600 W/m^2 to 1300 W/m^2. Without cooling, cell temperature ranged from 37 °C to 65 °C. With cooling, the module operating temperature range was 40 °C–50 °C. Solar cell temperature increased by approximately 4 °C and 1.4 °C for every 100 W/m^2 increase in irradiation level, without cooling and with water cooling, respectively (Chandrasekar et al., 2013). The increases in cell temperature per 100 W/m^2 increment in the irradiation level in the present experiment and previous experiments are summarized in Table 4.3.

Table 4.3: Comparison of cell temperature increments resulting from every 100 W/m^2 increase in irradiation level in different investigations

Authors, year, time, location, and coordinate		Irradiation level (W/m^2)		Operating temperature (°C)		Maximum ambient temperature (°C)	Cell temperature increment per 100 W/m^2 irradiation level increase	Comparison with present investigation
		Starting period	Peak period	Starting period	Peak period			
Current experimental results; Solar Thermal Lab, UMPEDAC, University of Malaya; Latitude 26°18'N, Longitude 50°08'E	Without cooling	400	1000	48.55	73.23	27	4.11	Agrees with two of the three previous investigations
	With cooling	400	1000	41.90	56.02	27	2.35	
Teo et al. (2012); September 2009; EA Building, National University of Singapore; Latitude 1° 17′ N, Longitude 103° 46′ E	Without cooling	280	1200	47	65		1.8	Deviates because of different operating conditions
	With cooling	550	1050	41	48		1.4	
Bahaidarah et al. (2013); February 2012; KFUPM, Dhahran, Saudi Arabia; Latitude 26°18'N, Longitude	Without cooling	240	979	25	44	21	2.6	Agrees well with current investigation
	With cooling	240	979	21	35	21	1.9	
Chandrasekar et al. (2013); April 2013; Anna University, BIT Campus, Tiruchirappalli, India; Latitude 10°39′N, Longitude 78°44′E	Without cooling	600	1300	37	65	37	4	Agrees well with current investigation
	With cooling	600	1300	40	50	37	1.4	

The results of the present experiment deviate from those of the experiment of Teo et al. (2012) because of the variations in ambient temperature, operating irradiation level, heat

removal capacity of the coolant, wind velocity, and operating module temperature. By contrast, the present experimental results are consistent with those of Bahaidarah et al. (2013) and Chandrasekar et al. (2013). Given that the current experiment is conducted indoors, its operating conditions are kept constant, except for irradiation level. Thus, the output performance of the PV module indoors is not influenced by ambient temperature, irradiation fluctuation, and air velocity unlike that of the PV module operating under outdoor conditions. The spectral irradiance (W/(m^2·μm)) of solar radiation is also significantly higher than that of artificial halogen lamp radiation. Halogen irradiation produces higher heat than solar irradiation because the former provides lower photonic energy (education.org, 2015). Consequently, the results of the current experiment show deviations from those of Teo et al. (2012). The output power of the PV module increases with an increment in the intensity of incident solar radiation or irradiation level, as shown in Figure 4.8.

Table 4.2 and Figure 4.8 show that output power increases by 4.35 W and 2.94 W, respectively, with and without cooling, for every 100 W/m^2 increase in irradiation level.

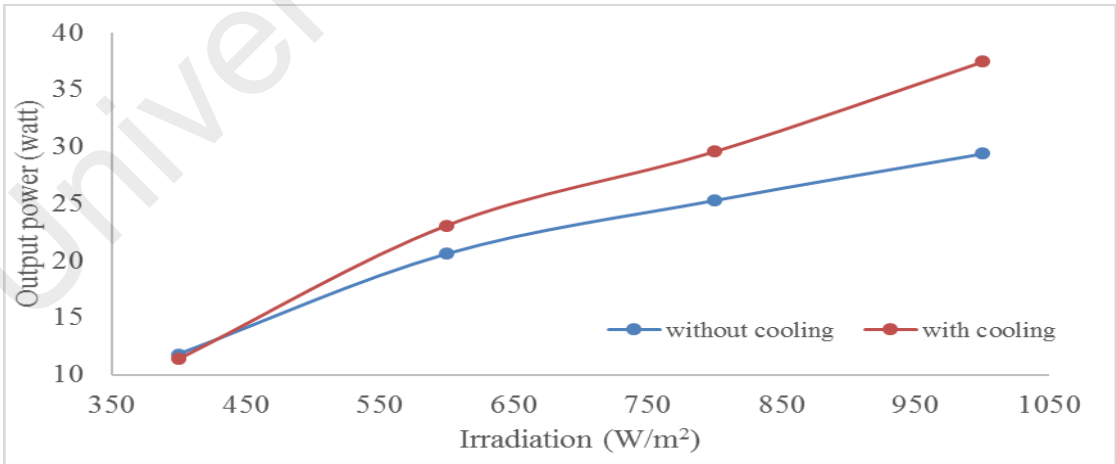

Figure 4.8: Irradiation level vs output power

4.1.3 Effect of Cooling on PV Module Performance

For the investigation on the effect of cooling on PV module performance, the irradiation level is set to 1000 W/m^2, and various flow rates (40, 80, 120, and 160 L/h) of the cooling water passing through the heat exchanger tube are applied to remove heat from the PV module.

Table 4.4: Values of output power and efficiency in steady state at different flow rates and 1000 W/m^2 irradiation level

Flow rate(L/h)	Solar cell temperature in steady state	Output power (W)	Efficiency (%)
40.0	57.54	36.582	5.594
80.0	56.02	37.461	5.731
120.0	54.70	37.543	5.743
160.0	53.97	37.682	5.761

Table 4.4 shows the efficiency, output power, and solar cell temperature values of the PV module in stable state at different cooling water flow rates. A flow rate of 120 L/h or 160 L/h minimally increases output power, whereas a flow rate of 80 L/h increases output power twofold. The pump expends significantly higher power to achieve a flow rate of 120 L/h or 160 L/h than to achieve a flow rate of 80 L/h. As shown in Table 4.4, 0.02 kg/s or 80 L/h cooling-water flow rate is clearly the optimal flow rate compared with the other flow rates in terms of power consumption. Thus, this flow rate of cooling water is used throughout the experiment at different irradiation levels to observe the cooling performance of the PV module.

PV module temperature is decreased by having cooling water pass through the heat exchanger device at a rate of 80 L/h and studied at 400, 600, 800, and 1000 W/m^2 irradiation levels. Figure 4.9 and Figure 4.10 show that, at an irradiation level of 1000 W/m^2, the initial module temperature is 29.33 °C and the electrical efficiency and

output power are 7.65% and 50.02 W, respectively, under cooling operating conditions, with 80 L/h as the cooling water flow rate.

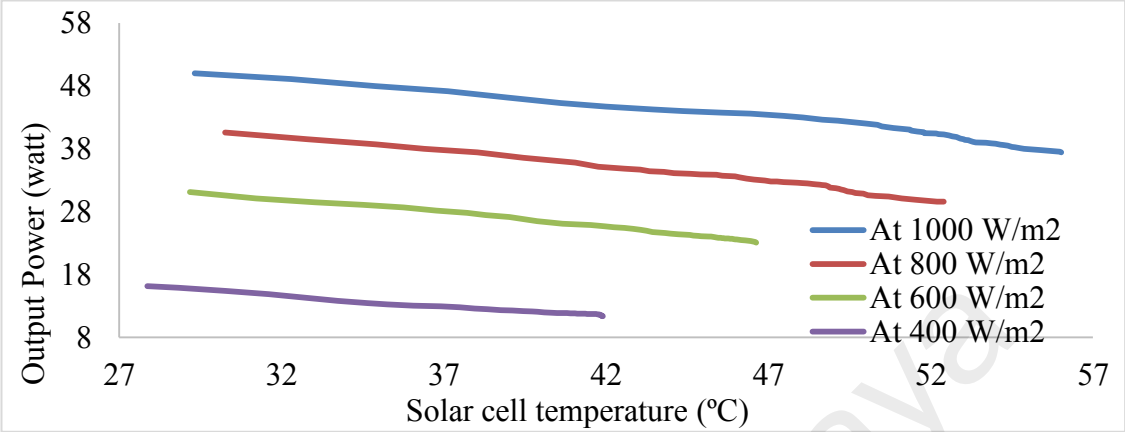

Figure 4.9: Output power vs. module temperature at different irradiation levels with cooling at 80 L/h flow rate

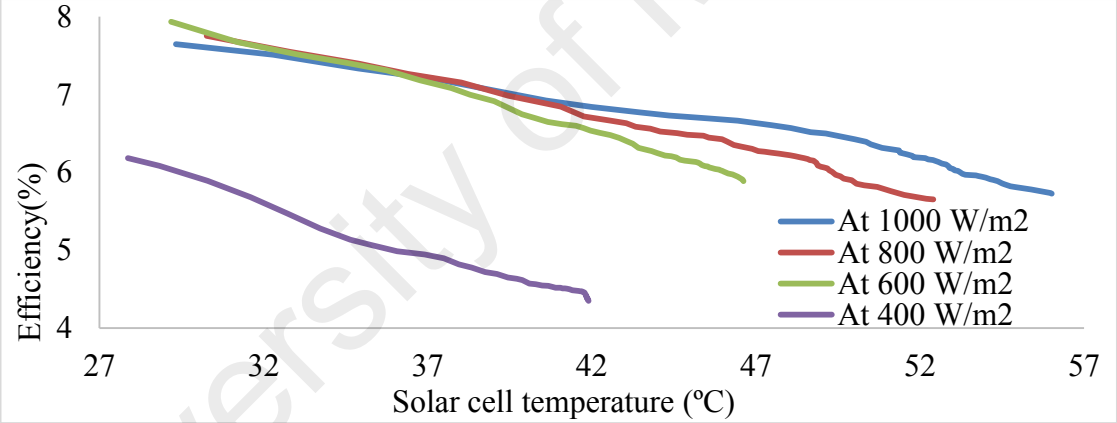

Figure 4.10: Efficiency vs. module temperature at different irradiation levels with cooling at 80 L/h flow rate

After a stable condition is attained, module temperature increases to 56.02 °C, efficiency decreases to 5.73%, and output power decreases to 37.46 W. Approximately 1.92% electrical efficiency and 12.56 W output power are reduced from the initial values as a result of the 26.60 °C increment in solar module temperature; consequently, the output performance under these conditions is 25.11% lower than the preliminary output performance. Under cooling operating conditions with 80 L/h cooling water flow rate at an irradiation level of 1000 W/m^2, electrical efficiency decreases by 0.07%, and

the output power is reduced by 0.47 W per 1 °C enhancement of module surface temperature.

Under the same cooling operating conditions and at an irradiation level of 800 W/m^2, the initial module temperature is 30.26 °C, electrical efficiency is 7.76%, and output power is 40.58 W. After a stable condition is attained, module temperature increases to 52.40 °C, efficiency decreases to 5.65%, and output power decreases to 29.58 W. Approximately 2.10% electrical efficiency and 11 W output power are reduced from the initial values because of the 22.14 °C increment in solar module temperature; consequently, output performance under these conditions is 27.10% lower than the preliminary output performance. Under cooling operating conditions with 80 L/h cooling water flow rate at an irradiation level of 800 W/m^2, approximately 0.09% electrical efficiency and 0.50 W output power decreases occur per 1 °C increase in module surface temperature.

Under the same cooling operating conditions and at an irradiation level of 600 W/m^2, the initial module temperature is 29.18 °C, electrical efficiency is 7.94%, and output power is 31.14 W. After a stable condition is attained, module temperature increases to 46.62 °C, efficiency decreases to 5.89%, and output power decreases to 23.10 W. Approximately 2.05% electrical efficiency and 8.04 W output power are reduced from the initial values because of the 17.44 °C increment in solar module temperature; consequently, output performance under these conditions is 25.82% lower than the preliminary output performance. Under cooling operating conditions with 80 L/h cooling water flow rate at an irradiation level of 600 W/m^2, electrical efficiency and output power declined by approximately 0.12% and 0.46 W, respectively, per 1 °C increment in module surface temperature.

Under cooling operating conditions with 80 L/h cooling water flow rate at an irradiation level of 400 W/m^2, the initial module temperature is 27.87 °C, electrical efficiency is 6.18%, and output power is 16.17 W. After a stable condition is attained, module temperature increases to 41.90 °C, efficiency decreases to 4.35%, and output power decreases to 11.38 W. Approximately 1.83% electrical efficiency and 4.79 W output power are reduced from the initial values because of the 14.04 °C increment in solar module temperature; consequently, output performance under these operating conditions is 29.65% lower than the preliminary output performance. Under cooling operating conditions with 80 L/h cooling water flow rate at an irradiation level of 400 W/m^2, approximately 0.13% electrical efficiency and 0.34 W output power decreases occur per 1 °C enhancement of module surface temperature.

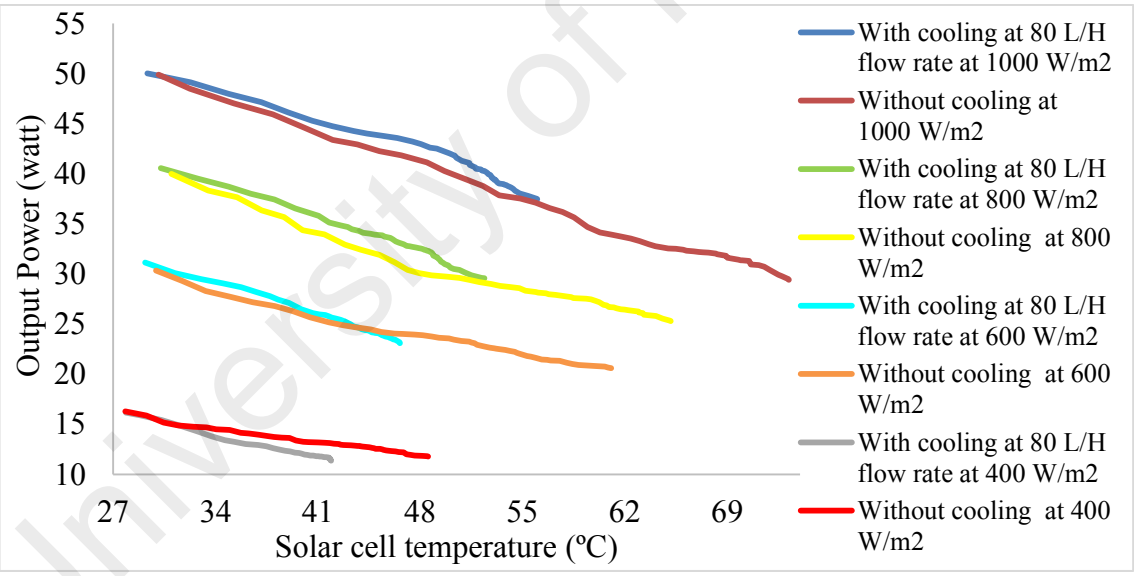

Figure 4.11: Output power is increased by cooling at different irradiation level

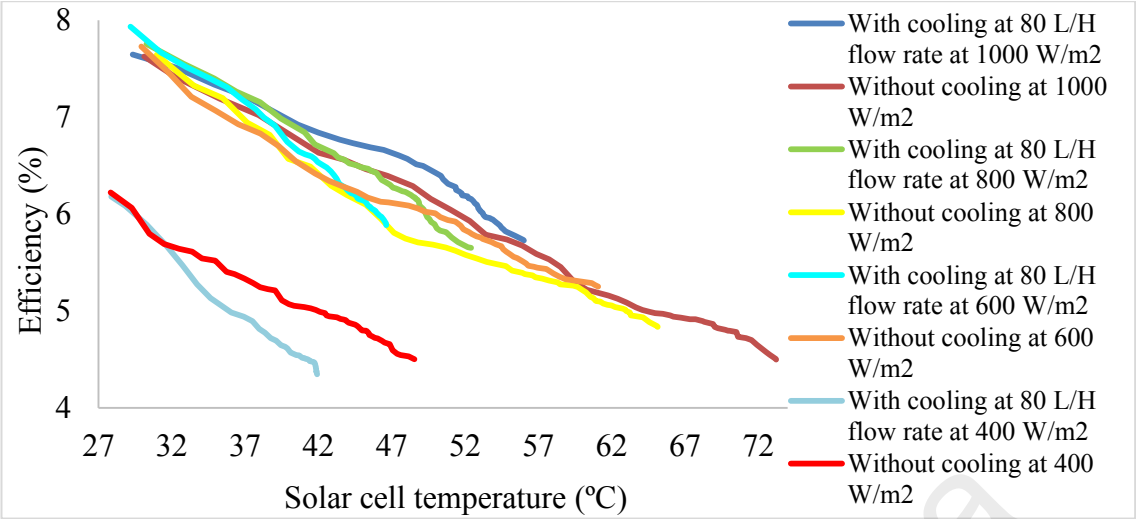

Figure 4.12: Electrical efficiency (%) is increased by cooling at different Irradiation levels

Figure 4.11 and Figure 4.12 show that 80 L/h cooling water flow through the heat exchanger attached to the bottom layer of the solar module can decrease solar cell temperature by 17.21 °C at an irradiation level of 1000 W/m^2. Approximately 8.04 W output power and 1.23% electrical efficiency increases occur because of a decrease in solar cell temperature. The resultant performance of the PV module with a cooling system is 27.33% higher than that without a cooling system.

Table 4.5: Comparison of performance improvements by applying a cooling system in different investigations

Authors, year, time, location, and coordinates		Irradiation levels (W/m^2)		Operating temperature (°C)		Maximum ambient temperature (°C)	Cell temperature (°C) reduction by cooling	Performance (%) improvement by cooling	Comparison with present investigation
		At starting period	At peak period	At starting period	At peak period				
Current experimental results; Solar Thermal Lab, UMPEDAC, University of Malaya; Latitude 26°18'N, Longitude 50°08'E	Without cooling	1000	1000	32.1	88.1	27	22.4	27.33%	Presents better PV module performance than previous experiments
	With cooling	1000	1000	31.8	65.75	27			
Bahaidarah et al. (2013); February 2012; KFUPM, Dhahran, Saudi Arabia; Latitude 26°18'N, Longitude 50°08'E	Without cooling	240	979	25	44	21	15	9%	PV module performance is significantly lower than that in the present investigation.
	With cooling	240	979	21	35	21			
Chandrasekar et al. (2013); April 2013; Anna University, BIT Campus, Tiruchirappalli, India; . Latitude 10°39'N, Longitude 78°44'E	Without cooling	600	1300	37	65	37	20	15.56%	PV module performance is significantly lower than that in the present investigation.
	With cooling	600	1300	40	50	37			

Chandrasekar et al. (2013) decreased PV cell temperature by 20 °C, improved output power by approximately 6.5 W, and increased electrical efficiency by 1.4% under outdoor operating conditions. Bahaidarah et al. (2013) reduced solar cell temperature by 20% by using a water cooling system on the back surface of the PV module and

consequently increased electrical efficiency by approximately 9% (Bahaidarah et al., 2013). Thus, the PV module in the current investigation shows better performance than those in the studies of Chandrasekar et al. (2013) and Bahaidarah et al. (2013).

The use of a water coolant flowing at a rate of 80 L/h through the heat exchanger attached to the bottom layer of the solar module can decrease solar temperature by 12.73 °C at an irradiation level of 800 W/m^2. Approximately 4.27 W output power and 0.81% electrical efficiency increases are attributed to a decrease in solar cell surface temperature. The resultant performance of the PV module is 16.87% higher than that without cooling. In their experiment, Fudholi et al. (2014) reduced solar cell temperature by 5.3 °C and consequently improved the electrical efficiency of the PV module by 0.80% by introducing a water coolant flowing at a rate of 0.014 kg/s through a heat exchanger device at an irradiation level of 800 W/m^2. They also conducted their investigation under indoor operating conditions. Their final results agree well with the current experiment results.

The application of an 80 L/h cooling water through the heat exchanger attached to the bottom layer of the solar module results in a solar cell temperature decrease of 14.45 °C at an irradiation level of 600 W/m^2. Approximately 2.49 W output power and 0.64% electrical efficiency increases occur with a decrease in solar cell surface temperature. The resultant performance of the PV module is 12.08% higher than the performance achieved without cooling.

The use of water flowing through the heat exchanger attached to the bottom layer of the solar module at a rate of 80 L/h decreases solar temperature by 6.65 °C at an irradiation level of 400 W/m^2. This result indicates that cooling water flow has no effect on the performance of the PV module at an irradiation level of 400 W/m^2 or lower.

4.1.4 Heat Transfer by the Heat Exchanger Fins

The rectangular fins fixed on the semi-circular copper tube also enhance the rate of heat removal from the PV module surface and positively influence the performance of the device. Figure 4.13 compares the rates of heat removal from the module surface with fins and without fins attached to the heat exchanger device.

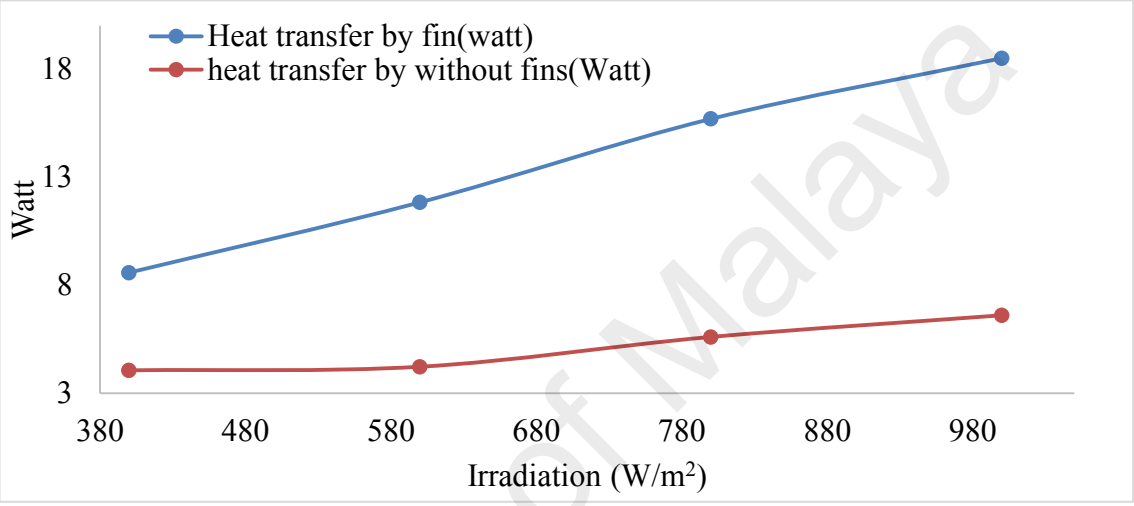

Figure 4.13: Heat transfer with and without fins on the rectangular semi-circular copper sheet (with cooling)

With cooling, the rectangular fins can transfer 11 W more heats from the solar cell surface than without fins. In the current experiment, a continuous water cooling technique is used to maintain module surface temperature within the normal operating range to increase the overall output performance of the PV module.

4.1.5 Effect of Air Cooling on PV Module Performance

For the investigation on the reducing effect of air cooling on solar cell temperature, airflow rate and irradiation level are set to 34 L/min and 800 W/m^2, respectively. However, the possible decrease in solar cell temperature is minimal if this cooling system is used in steady state. Thus, PV output performance exhibits no considerable

enhancement in steady state as a result of air cooling. However, when cell temperature is below 62 °C, air cooling can enhance the performance of the PV module.

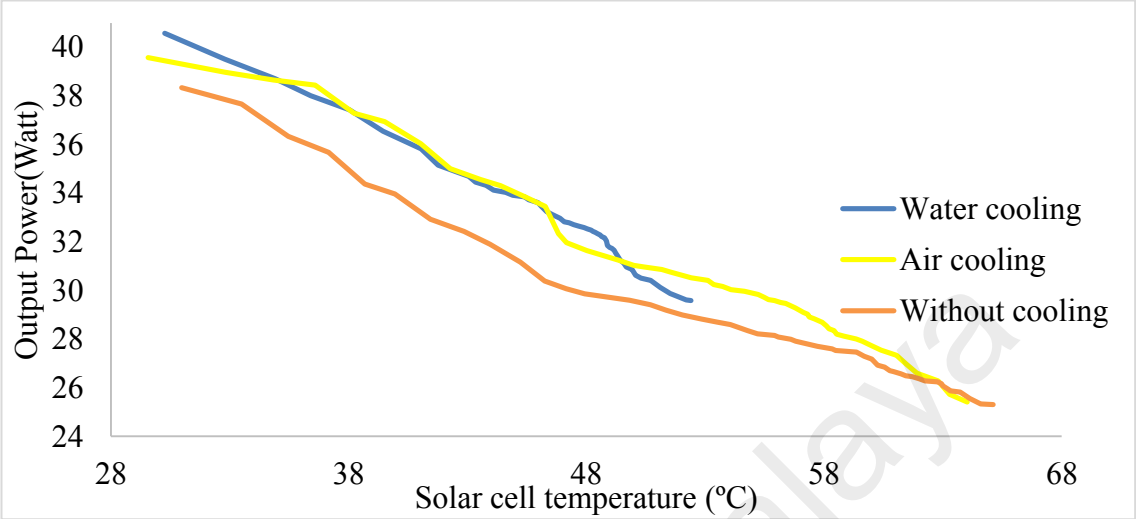

Figure 4.14: Comparison of the effects of water, air, and without cooling on PV module output power (W) at an irradiation level of 800 W/m^2

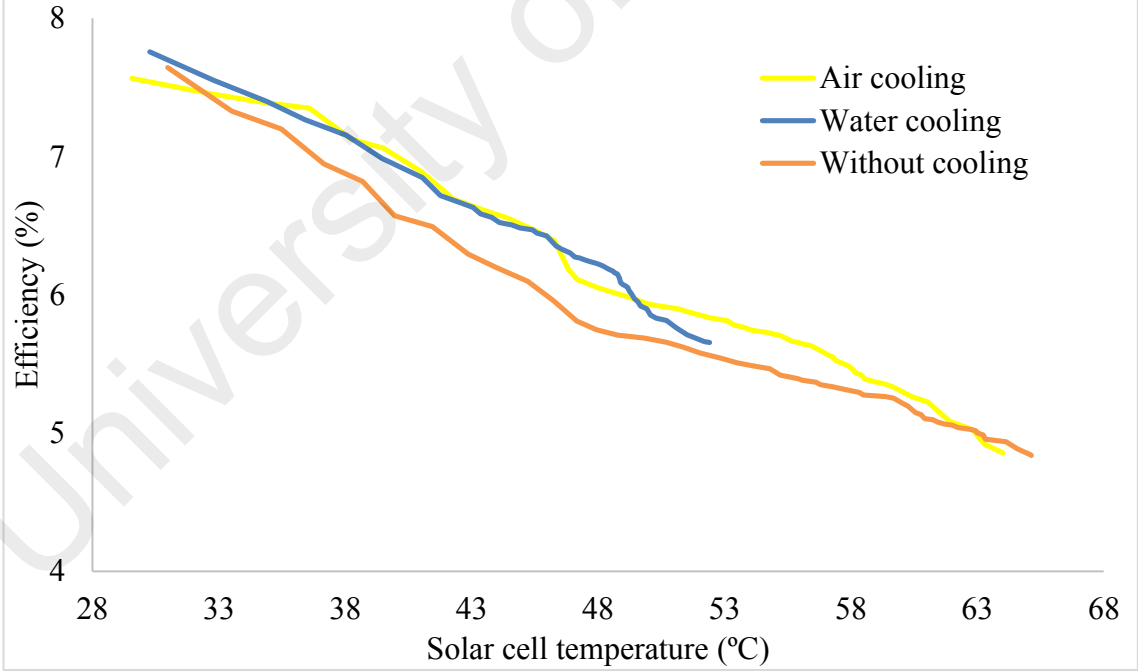

Figure 4.15: Comparison of the effects of water, air, and without cooling on PV module efficiency (%) at an irradiation level of 800 W/m^2

Figure 4.14 and Figure 4.15 show that under cooling operating conditions with 34 L/min cooling air flow rate at an irradiation level of 800 W/m^2, the initial module

temperature is 29.56 °C, electrical efficiency is 7.56%, and output power is 39.57 W. After a stable condition is attained, module temperature increases to 64.02 °C, efficiency decreases to 4.86%, and output power decreases to 25.41 W. Approximately 2.71% electrical efficiency and 14.16 W output power are reduced from the initial values as a result of the 34.46 °C increment in solar module temperature; consequently, output performance under these conditions is 35.79% lower than the preliminary output performance. Under cooling operating conditions with 34 L/min cooling air flow rate at an irradiation level of 800 W/m^2, approximately 0.08% electrical efficiency and 0.41 W output power decreases occur per 1 °C enhancement of module surface temperature.

A 1.12 °C decrease in solar cell temperature is obtained by introducing an air flow at a rate of 34 L/min through the heat exchanger attached to the back surface of the PV module at an irradiation level of 800 W/m^2. Thus, applying air cooling can only minimally increase PV module output performance. Table 4.6 shows a comparison of the effects of water cooling, air cooling, and without cooling on the performance of the PV module in steady state.

Table 4.6: Comparison of the effects of water, air, and without cooling on the performance of the PV module in steady state at an irradiation level of 800 W/m^2

Cooling system	Solar cell temperature (°C)	Output power (W)	Efficiency (%)
Water cooling	52.40	29.58	5.65
Air cooling	64.02	25.41	4.86
Without cooling	65.14	25.31	4.84

Under stable operating conditions and at an irradiation level of 800 W/m^2, water cooling can reduce the temperature of the solar cell layer by 12.73 °C, increase output power by approximately 4.27 W, and enhance electrical efficiency by 0.81%. These results show

that output performance with water cooling is 16.87% higher than that without cooling. By contrast, an air cooling system cannot improve the output performance of the PV module in steady state. However, when solar cell temperature is lower than 60 °C, air cooling can increase output performance to a certain extent, as shown in the results in Table 4.6. The specific heat capacity of water is 4200 J/(kg·K), which is significantly higher than that of air. Thus, water is an effective cooling agent because it does not permit solar cell temperature to exceed 50 °C.

4.1.6 Effect of Humidity on PV Module Performance

The output performance of the PV module is also influenced by the RH of the atmosphere. Initially, the PV module output power is observed in relation to module surface temperature at 40% RH and 800 W/m^2 irradiation level. Subsequently, output power is observed with respect to module surface temperature at 50% and 60% RH under the same irradiation level.

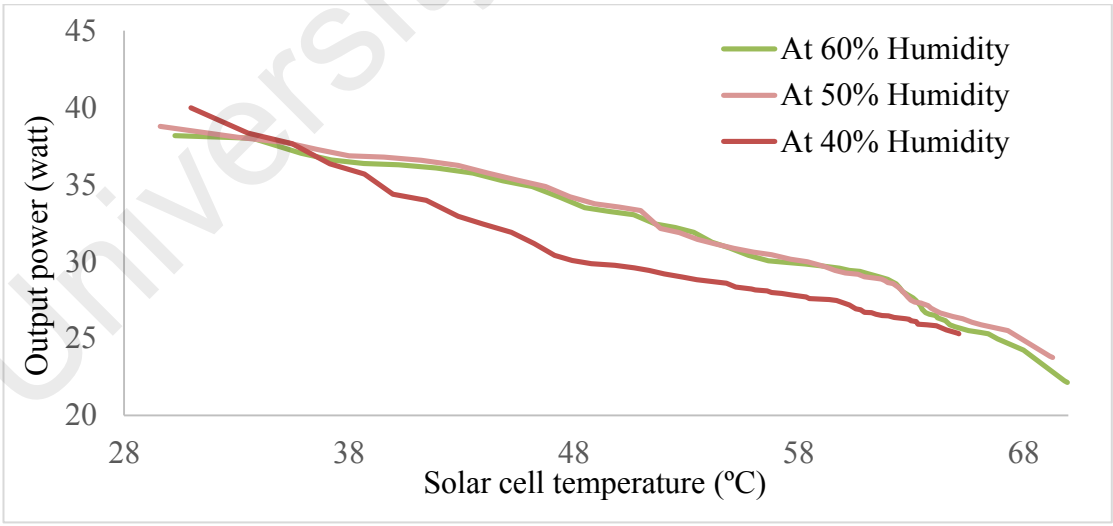

Figure 4.16: Output power vs. solar cell temperature at different RH values at an irradiation level of 800 W/m^2

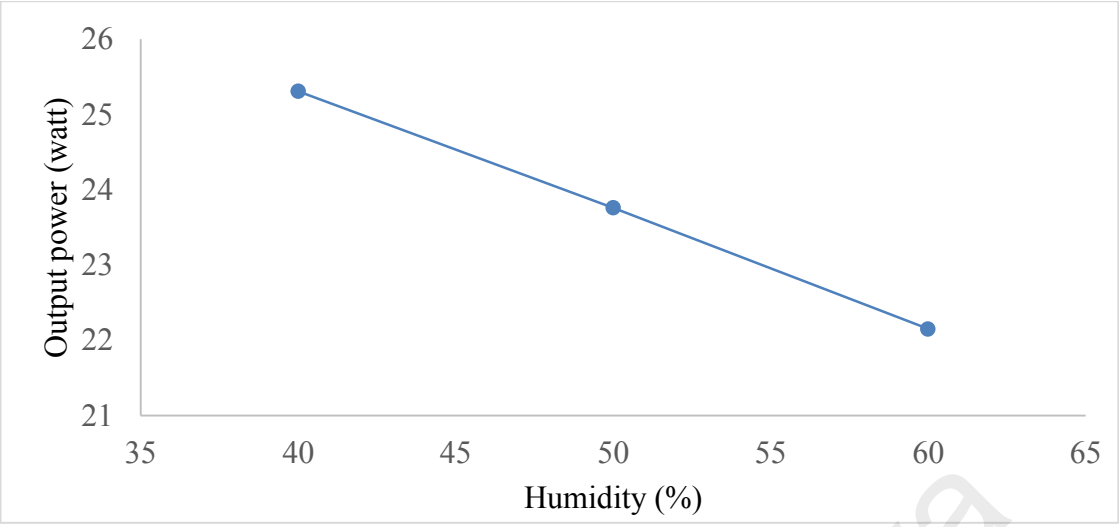

Figure 4.17: Humidity vs. output power in steady state at an irradiation level of 800 W/m^2

Figure 4.16 and Figure 4.17 show that, under indoor operating conditions, the PV module generates 25.31, 23.76, and 22.15 W output power at 40%, 50%, and 60% RH, respectively. Approximately 3.16 W output power is reduced because of the 20% increment in RH in the surrounding area of the PV module. Thus, for every 10% increment in RH, the output power of the PV module declines by 1.58 W.

4.1.7 Effect of Dust on PV Module Performance

Dust deposition on solar cell surface also influences PV module output performance, as observed in the current investigation. Dust particles are spread on the upper glass layer of the PV module at a rate of 0.012 g/cm^2, and the output efficiency and power at 800 W/m^2 irradiation level is observed under indoor operating conditions.

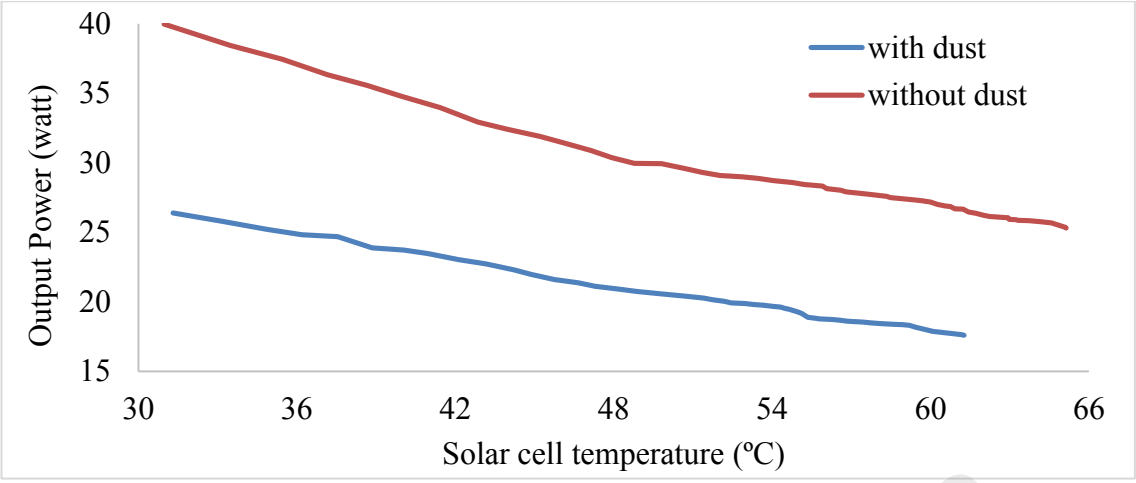

Figure 4.18: Dust effect on solar cell output power at an irradiation level of 800 W/m^2

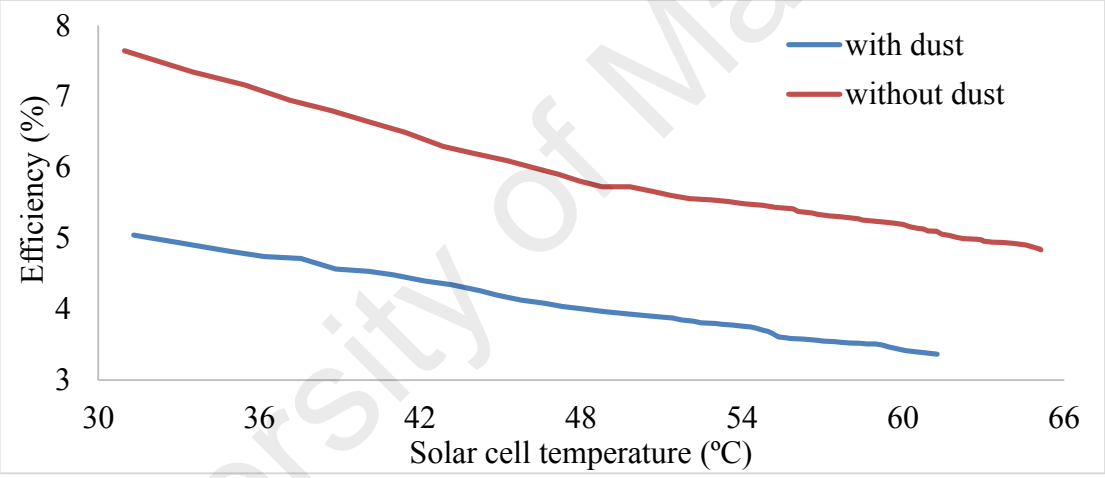

Figure 4.19: Dust effect on solar cell efficiency at an irradiation level of 800 W/m^2

Figure 4.18 and Figure 4.19 show that, without dust at an irradiation level of 800 W/m^2 in steady state, the PV module cell temperature is 65.14 °C, electrical efficiency is 4.84%, and output power is 25.31 W. After dust particles are spread on the glass surface of the module, solar cell temperature decreases to 61.27 °C, electrical efficiency decreases to 3.37%, and output power decreases to 17.61 W. Thus, dust deposition reduces the electrical efficiency of the PV module by 1.47% and its output power by 7.70 W. In the current investigation, the output performance of the PV module with dust is 30.43% than that without dust.

4.2 Outdoor Performance of the PV Module

4.2.1 Effect of Temperature on PV Module Performance

The output power of the PV module is affected by various operating parameters, such as ambient temperature, solar irradiation level, humidity, and wind velocity. Under outdoor operating conditions, solar irradiation level fluctuates continuously.

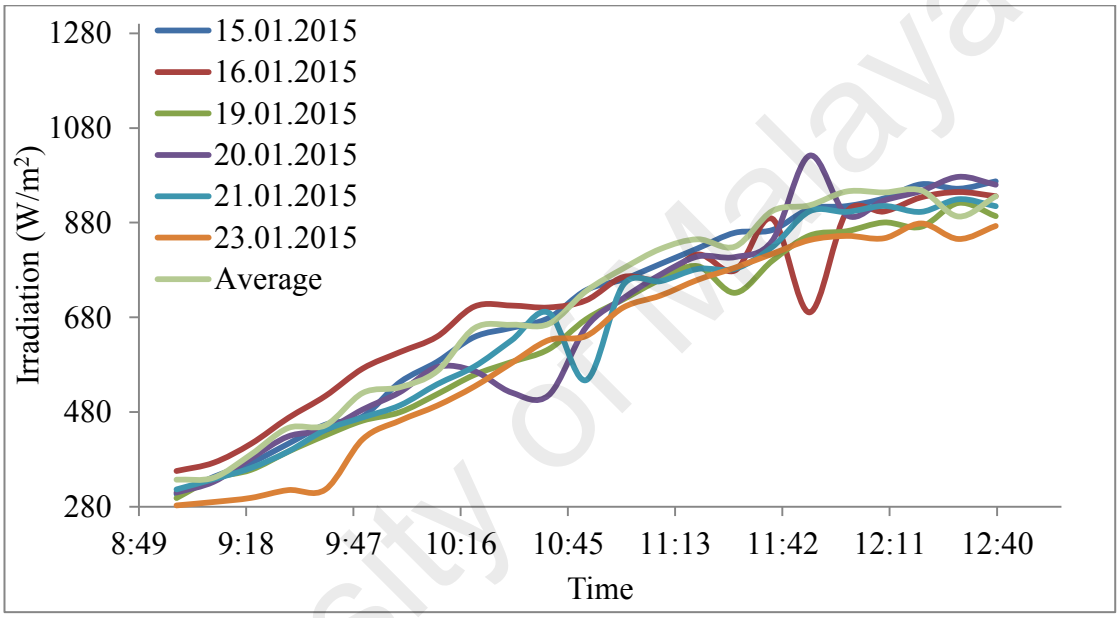

Figure 4.20: Time vs. irradiation level

Figure 4.20 shows that the data used for analysis are collected at similar irradiation levels on different days. An average irradiation value is considered with respect to time throughout the analysis. With an increment in solar irradiation level, solar cell temperature and output power are increased. Solar module efficiency is inversely related to solar cell temperature, as shown in Figure 4.21.

.

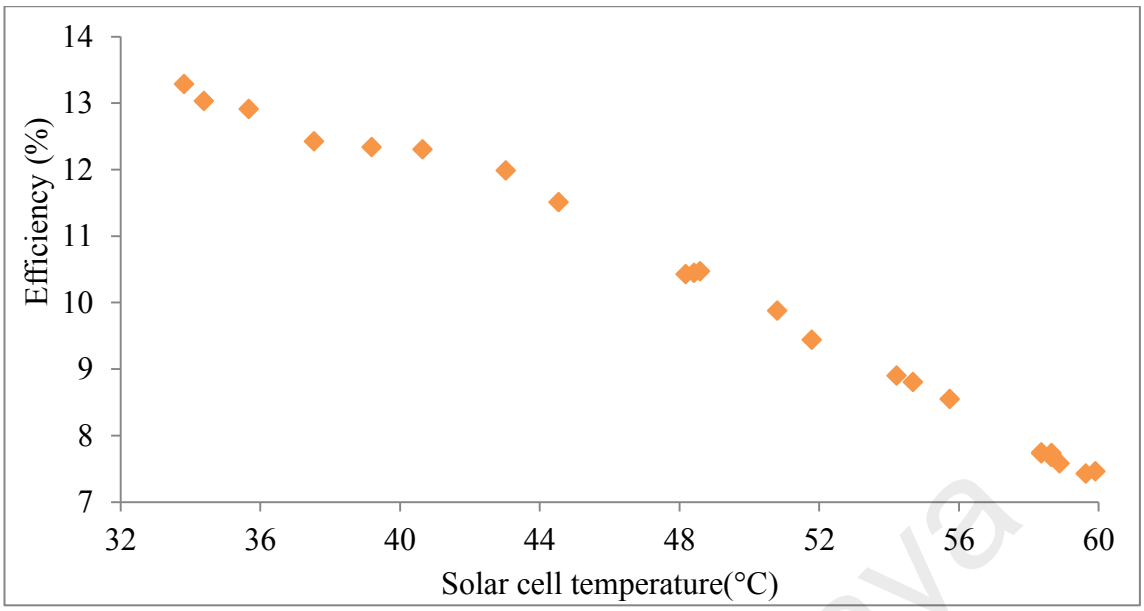

Figure 4.21: Solar cell temperature vs efficiency (without cooling)

Figure 4.21 shows that in the initial state without cooling, the efficiency of the module is 13.29%, and the cell temperature is 33.82 °C. Under peak operating conditions, the efficiency of the module dropped to 7.46%, whereas PV module temperature increased to 59.92 °C. Overall electrical efficiency decreased by 5.82% as a consequence of the 26.10 °C increment in PV module temperature, thereby resulting in an efficiency that is 43.83% lower than the initial efficiency. Approximately 0.22% electrical efficiency is reduced per 1 °C increment in PV module temperature under outdoor operating conditions without cooling.

Figure 4.22 and Figure 4.23 show that the top glass surface, bottom surface, and solar cell temperature increase over time under both water-cooling and non-cooling conditions because irradiation level increases with time.

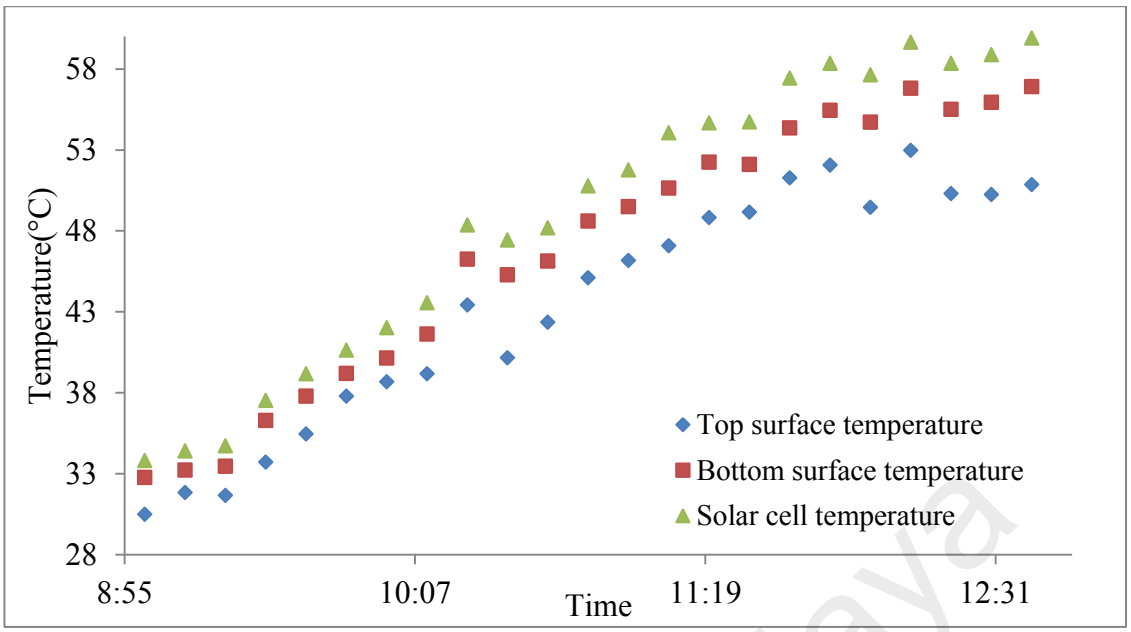

Figure 4.22: Temperatures at different layers of the solar module at various times (without cooling)

In the current investigation, outdoor cell temperature without cooling are 33.82 °C and 59.92 °C during the initial and peak periods, respectively. Chandrasekar et al. (2013) conducted an experiment at Anna University, BIT Campus, Tiruchirappalli, India; they found that solar cell temperatures without cooling conditions were approximately 37 °C at an irradiation level of 600 W/m^2, which corresponded to the initial operating period, and approximately 65 °C at an irradiation level of 1300 W/m^2, which corresponded to the peak operating period. Their experiment was run in April 2012, when the highest ambient temperature was 37 °C (Chandrasekar et al., 2013). Bahaidarah et al. (2013) observed that solar cell temperatures were 25 °C at an irradiation level of 240 W/m^2 and 44 °C at an irradiation level 979 W/m^2 without cooling at KFUPM, Dhahran, Saudi Arabia. The experiment was performed in February 2012 when the maximum ambient temperature was 21 °C (Bahaidarah et al., 2013). The solar cell temperature in the current work agrees with that in the work of Chandrasekar et al. (2013) but differs from that in the work of Bahaidarah et al. (2013). The difference lies in the variation in the incident irradiation level and ambient temperature.

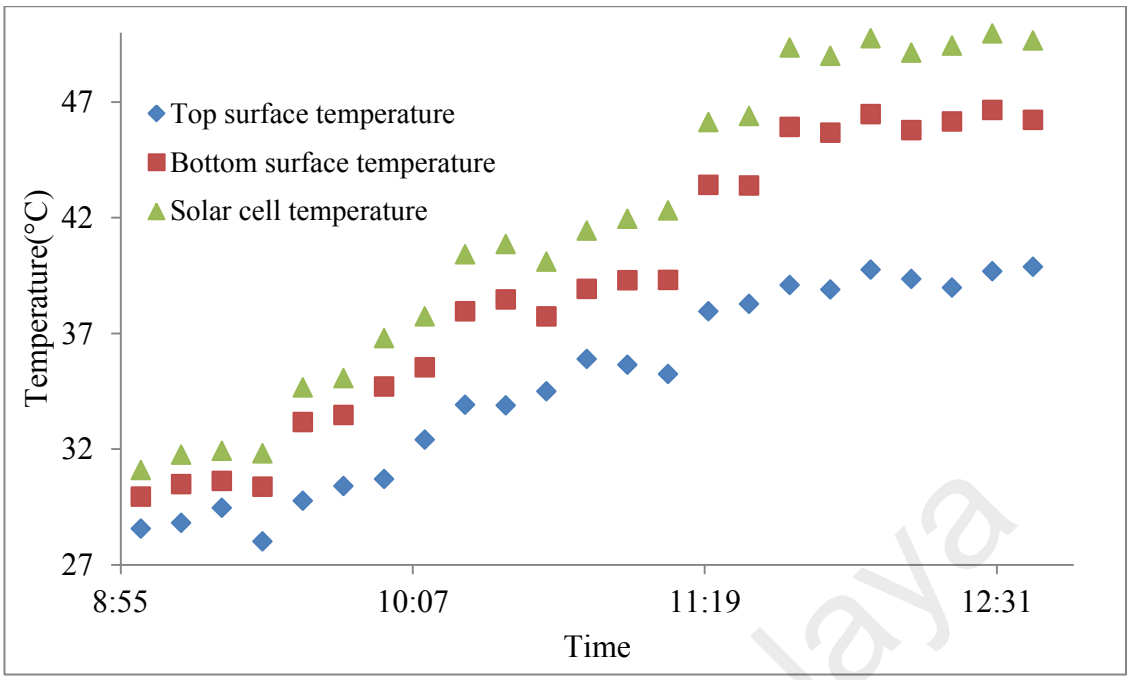

Figure 4.23: Temperatures at different layers of the solar module at various times (with cooling)

In the current investigation, the cell temperatures are 31.09 °C and 49.64 °C with water cooling during the initial and peak operating periods, respectively. Chandrasekar et al. (2013) from Anna University, BIT Campus, Tiruchirappalli, India found that the temperatures of a cooled solar cell was 40 °C at an irradiation level of 600 W/m^2 and 50 °C at an irradiation level of 1300 W/m^2 during the initial and peak operating periods, respectively. Their experiment was performed in April 2012 when the maximum ambient temperature was 37 °C (Chandrasekar et al., 2013). At KFUPM in Dhahran, Saudi Arabia, Bahaidarah et al. (2013) observed that the temperatures of a cooled solar cell were 22°C at an irradiation level of 240 W/m^2 and 35 °C at an irradiation level of 979 W/m^2 in February 2012 and at a maximum ambient temperature of 21 °C. Therefore, the temperatures of a cooled solar cell in the present investigation agree with those recorded by Chandrasekar et al. (2013) but differ from those reported by Bahaidarah et al. (2013). The difference is attributed to the variations in the solar irradiation level, wind velocity, ambient temperature, and the cooling capacities of the coolant and heat exchanger device. Inevitably, differences exist in the operating cell

temperatures among the investigations of Chandrasekar et al. (2013), Bahaidarah et al. (2013), and the present work.

As previously mentioned, approximately 15%–20% of the sunlight hitting a PV module is converted into electricity, whereas the remaining portion produces heat on the solar cell surface (Teo et al., 2012). From the total heat generated on the upper layer of a solar module, a portion is transferred to the surrounding air through convection, whereas the remaining portion is transmitted to the Tedlar bottom surface of the module. Moreover, the Tedlar back surface of the PV module directly absorbs a portion of the heat because of the packing factor (Dubey & Tay 2013). Consequently, the temperature on the top glass surface is lower than that on the Tedlar back layer of the PV module. The solar cell surface of the PV module directly absorbs 96% of the incident solar radiation through the upper glass sheet. The heat transfer coefficient from the solar cell layer to the ambient air through the glass sheet, U_{sca}, is 7.14 W/(m^2·K). However the heat transfer coefficient from the Tedlar bottom layer to the surrounding air, h_{air}, is 5.81 W/(m^2·K). Consequently, the top glass surface of the module loses more heat than the Tedlar back sheet. Therefore, the top glass surface of a PV module has a lower temperature than the Tedlar bottom layer (Dubey & Tay, 2013; Dubey & Tiwari, 2008). The temperature of a solar cell surface directly depends on the incident irradiation level, Tedlar back sheet temperature, and ambient temperature, as shown in Equation (3.6). Table 3.2 shows that the heat capacity of the Tedlar back surface is significantly lower than that of the solar cell layer of the monocrystalline PV module. Therefore, the PV cell heats up rapidly as it absorbs more heat. Consequently, the Tedlar back sheet temperature is lower than the solar cell temperature.

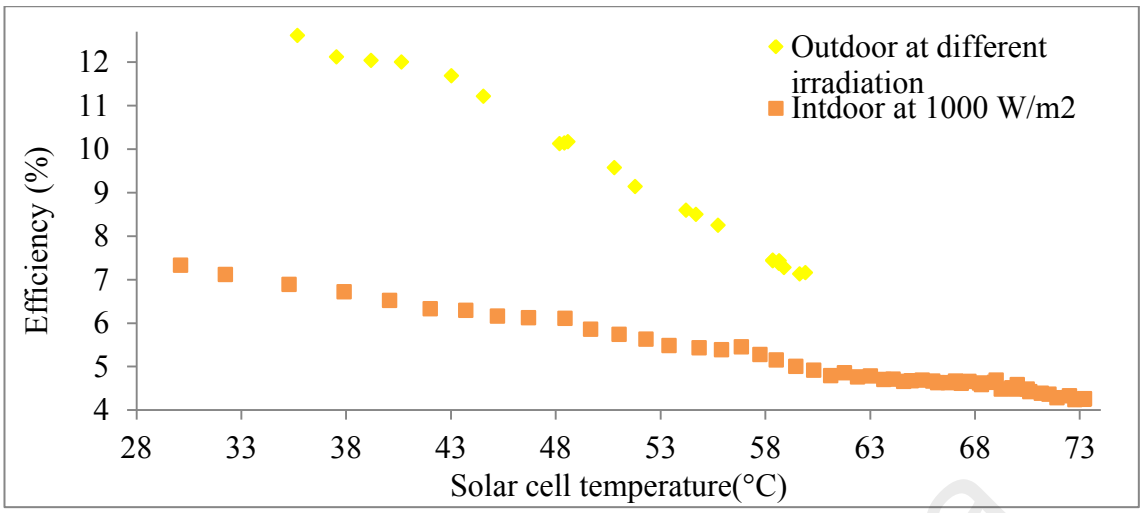

Figure 4.24: Comparison of the temperature-dependent efficiencies of the solar module under indoor and outdoor operating conditions (without cooling)

Figure 4.24 shows that, under indoor operating conditions at an irradiation level of 1000 W/m^2 without cooling, the initial module temperature is 30.11 °C, and the efficiency is 7.63%. After a stable condition is attained, module temperature increases to 73.23 °C and efficiency decreases to 4.50%. Approximately 3.13% electrical efficiency is reduced from the initial efficiency value because of the 43.12 °C increment in the solar module temperature; consequently, the output performance of the PV module under these conditions is 41.03% lower than the preliminary output performance. The total indoor efficiency reduction resulting from an increment in solar cell temperature coincides with the results obtained outdoors. Without cooling at an irradiation level of 1000 W/m^2, electrical efficiency declines by 0.07% per 1 °C enhancement of module surface temperature. The fluctuations in the irradiation level, wind velocity, and ambient temperature affect the output performance of the PV module. The spectral irradiance (W/(m^2·μm)) of solar radiation is also significantly higher than that of artificial halogen lamp radiation. Thus, deviations exist between the indoor and outdoor performance results.

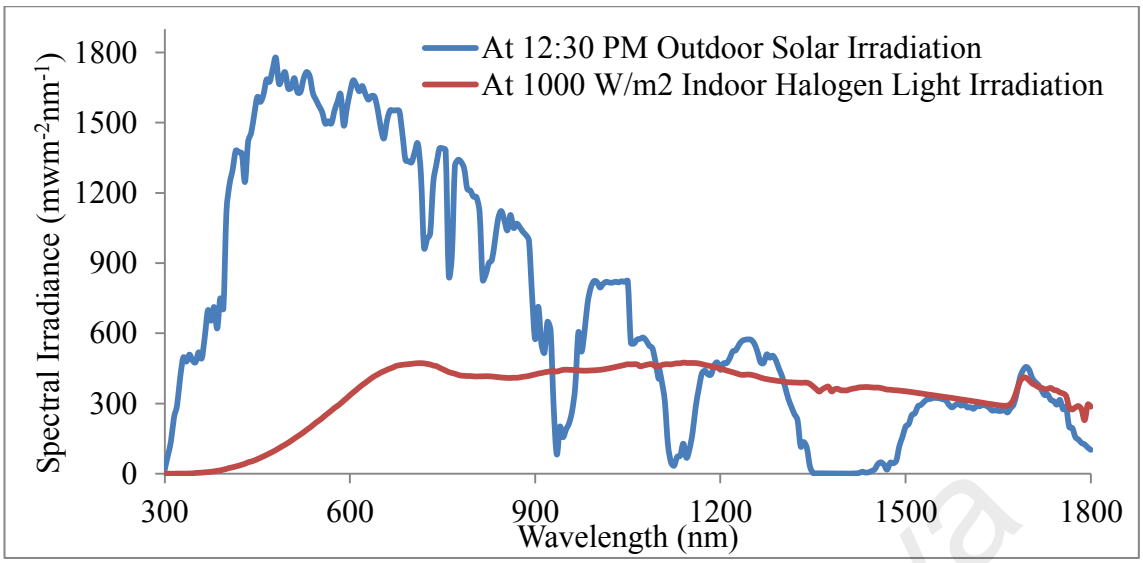

Figure 4.25: Spectral irradiance comparisons between halogen lights and sunlight

Figure 4.25 shows the spectral irradiance comparison between halogen light and sunlight. Compared with sunlight, halogen light generates relatively low efficiency and high heat because it has low photonic energy (education.org, 2015). Thus, the efficiency decline rates with per degree cell temperature increment under indoor and outdoor operating conditions deviate considerably.

4.2.2 Effect of Irradiation Level on PV Module Performance

The effect of incident irradiation on solar cell temperature and its influence on the resultant performance of the PV module are also investigated under outdoor operation conditions, with and without cooling. Figure 4.26 shows that solar cell temperature increases with increasing irradiation intensity. Without cooling during the initial investigation, solar cell temperature is 33.82 °C, and it increases to 59.92 °C during the peak operation period. Solar cell temperature increases by 26.10 °C when irradiation level increases by 683 W/m^2. Thus, solar cell temperature increases by 3.82 °C with each 100 W/m^2 increase in irradiation level without cooling.

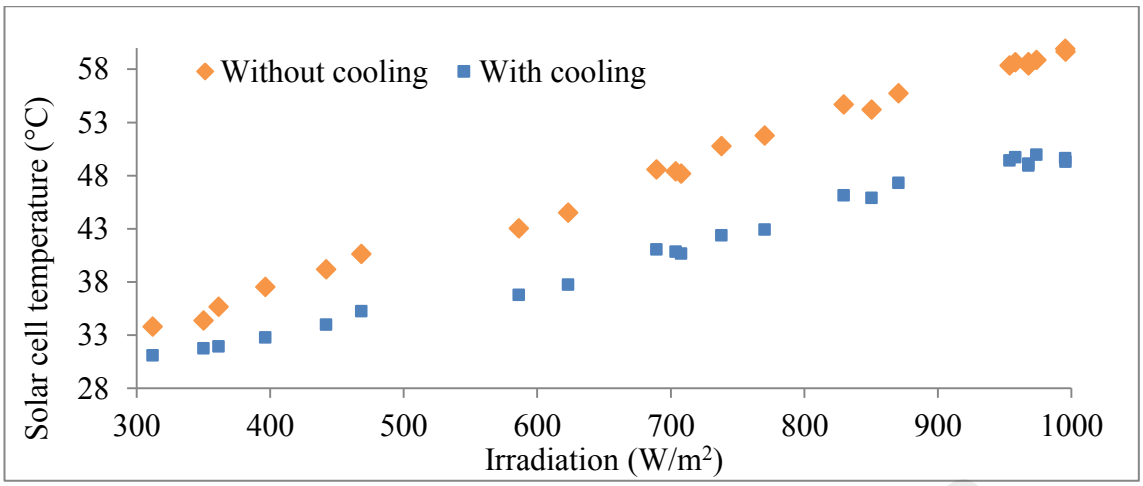

Figure 4.26: Irradiation vs. solar cell temperature

With water cooling during the initial period of investigation, solar cell temperature is 31.09 °C. It then increases to 49.65 °C during the peak operating period. Solar cell temperature increases by 18.56 °C when the irradiation level increases by 683 W/m^2. Thus, for every 100 W/m^2 increase in irradiation level, PV module temperature increases by 2.72 °C with cooling.

Teo et al. (2012) conducted an investigation on the rooftop of the EA Building at the National University of Singapore in September 2009. Without cooling, the range of operating irradiation level was 280–1200 W/m^2, and the module operating temperature range was 47 °C–65 °C. With cooling, the range of irradiation level was 550–1050 W/m^2, and the operating temperatures of the solar ranged from 41 °C to 48 °C. Solar cell temperature increased by 1.8 °C and 1.4 °C with each 100 W/m^2 increase in irradiation level, without and with an air cooling system, respectively (Teo et al., 2012).

Bahaidarah et al. (2013) conducted their experiment at KFUPM, Dhahran, Saudi Arabia in February 2012, and the highest ambient temperature at that time was 21 °C. The irradiation levels ranged from 240 W/m^2 to 979 W/m^2. Without cooling, the module operating temperatures ranged from 25 °C to 44 °C. With cooling, the module operating temperatures ranged from 21 °C to 35 °C. Solar cell temperature increased by 2.6 °C

and 1.9 °C with each 100 W/m^2 increase in irradiation level, without and with a water cooling system, respectively (Bahaidarah et al., 2013).

Table 4.7: Comparison of irradiation levels and solar cell temperatures in different investigations

Authors, year, time, location, and coordinates		Irradiation level (W/m^2)		Operating temperature (°C)		Maximum ambient temperature (°C)	Cell temperature increment per 100 W/m^2 irradiation	Comparison with present investigation
		Starting period	Peak period	Starting period	Peak period			
Current experimental results; Solar Thermal Lab, UMPEDAC, University of Malaya; Latitude 26°18'N, Longitude 50°08'E	Without cooling	312	995	34	60	35	3.82	Agrees with two of the three previous investigations
	With cooling	312	995	31	50	35	2.71	
Teo et al. (2012), September 2009; EA Building, National University of Singapore; Latitude 1° 17′ N, Longitude 103° 46′ E	Without cooling	280	1200	47	65		1.8	Differs from present investigation because of different operating conditions
	With cooling	550	1050	41	48		1.4	
Bahaidarah et al. (2013); February, 2012;KFUPM, Dhahran, Saudi Arabia; Latitude 26°18'N, Longitude 50°08'E	Without cooling	240	979	25	44	21	2.6	Agrees with present investigation
	With cooling	240	979	21	35	21	1.9	
Chandrasekar et al. (2013); April 2013; Anna University, BIT Campus, Tiruchirappalli, India. Latitude 10°39'N, Longitude 78°44'E	Without cooling	600	1300	37	65	37	4	Agrees with present investigation
	With cooling	600	1300	40	50	37	1.4	

Chandrasekar et al. (2013) conducted their experiment at Anna University, BIT Campus, Tiruchirappalli, India in April 2012, and the maximum ambient temperature at that time was 21°C. The operating irradiation levels ranged from 600 W/m^2 to 1300 W/m^2. Without cooling, the module operating temperatures ranged from 37 °C to 65 °C. With cooling, the module operating temperatures ranged from 40 °C to 50 °C. Solar cell temperature increased by 4 °C and 1.4 °C with each 100 W/m^2 increase in irradiation, without and with a water cooling system, respectively (Chandrasekar et al., 2013).

The results of the present investigation vary from those reported by Teo et al. (2012) because of the differences in module operating temperature, incident solar irradiation level, coolant quality, ambient temperature, and wind velocity. By contrast, the current experimental results agree with those obtained by Chandrasekar et al. (2013) and Bahaidarah et al. (2013).

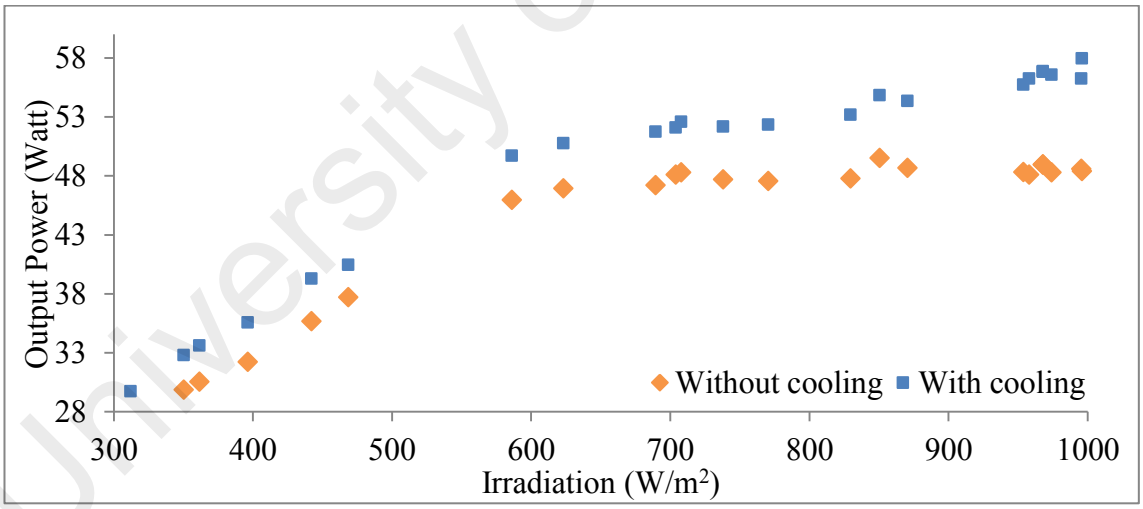

Figure 4.27: Irradiation vs. output power

Figure 4.27 shows that the output power of the PV module increases with increasing irradiation level. Without cooling, the initial incident irradiation level is approximately 312 W/m^2, and the output power is 27.12 W. During peak operation period, incident irradiation level is approximately 995 W/m^2, and output power is 48.59 W. Output power

increases by 21.47 W with an increase in irradiation level of approximately 683 W/m^2. Without cooling, output power increases by 3.14 W per 100 W/m^2 increase in irradiation level. With water cooling, the initial incident irradiation level is approximately 312 W/m^2, and output power is 29.72 W. During peak operation period, incident irradiation level is approximately 995 W/m^2, and output power is 56.23 W. Output power increases by 26.51 W with an increase of approximately 683 W/m^2 in irradiation level. With cooling, output power increases by 3.88 W for every 100 W/m^2 increase in irradiation level.

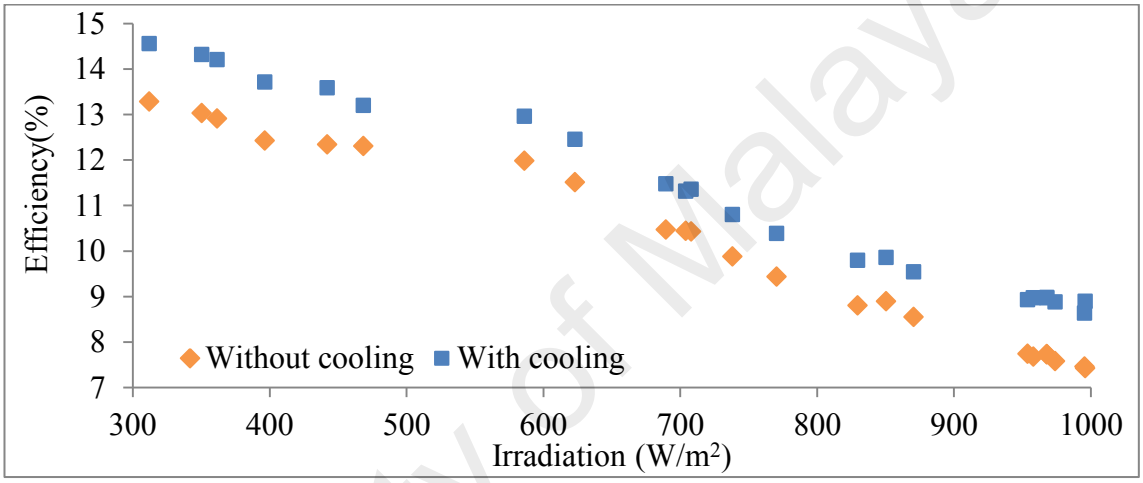

Figure 4.28: Irradiation level vs. efficiency

Figure 4.28 shows that the electrical efficiency of the PV module decreases with an increase in irradiation level. Without cooling, the initial incident irradiation level is approximately 312 W/m^2, and electrical efficiency is 13.29%. During peak operation period, incident irradiation level is approximately 995 W/m^2, and electrical efficiency is 7.46%. The electrical efficiency of the module decreases by 5.82% with a 683 W/m^2 increase in irradiation level. Without cooling, the electrical efficiency of the module decreases by 0.85% with every 100 W/m^2 increase in irradiation level. With water cooling, the initial incident irradiation level is approximately 312 W/m^2, and the electrical efficiency of the module is 14.56%. During peak operation period, the incident irradiation level is approximately 995 W/m^2, and the electrical efficiency of the module is 8.64%. The electrical efficiency of the module decreases by 5.92% with an

increase of 683 W/m^2 in irradiation level. With cooling, the electrical efficiency of the module decreases by 0.87% with every 100 W/m^2 increase in irradiation level.

4.2.3 Effect of Cooling on PV Module Performance

The cooling water flow rate used to investigate the effect of cooling on PV module performance is 90 L/h. Figure 4.29 shows that the efficiency of the module is 14.56% and cell temperature is 31.09 °C in the initial state with water cooling. During peak operating period, the efficiency of the module drops to 8.64%, whereas cell temperature increases to 49.65 °C.

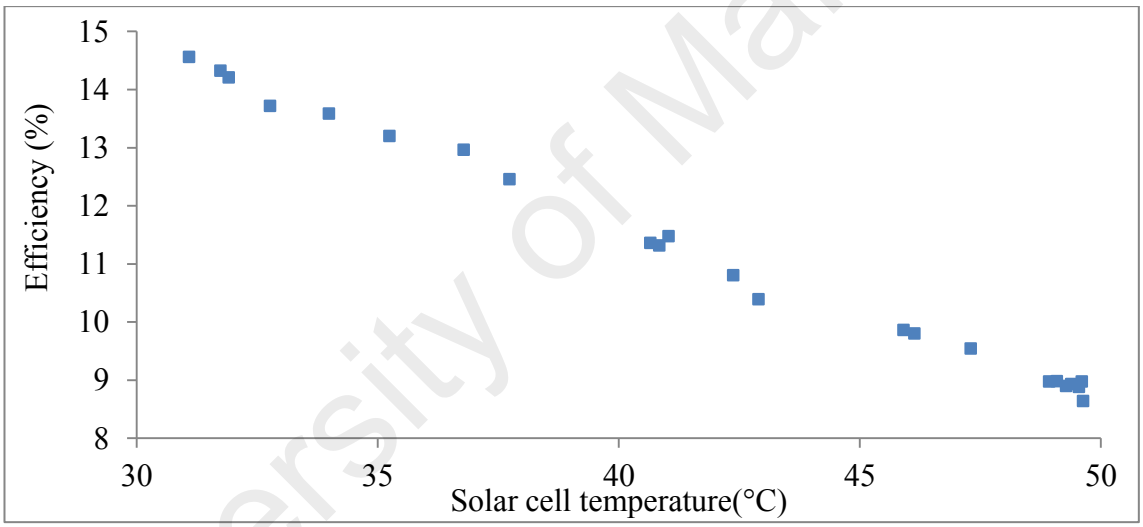

Figure 4.29: Solar cell temperature vs. efficiency (with cooling)

The total electrical efficiency decreases by 5.92% because of an 18.56 °C increase in the solar cell temperature of the PV module, thereby resulting in an efficiency that is 40.68% lower than that achieved under the initial operating conditions. Under outdoor operating conditions with water cooling, electrical efficiency decreases by 0.32% per degree increase in solar cell temperature.

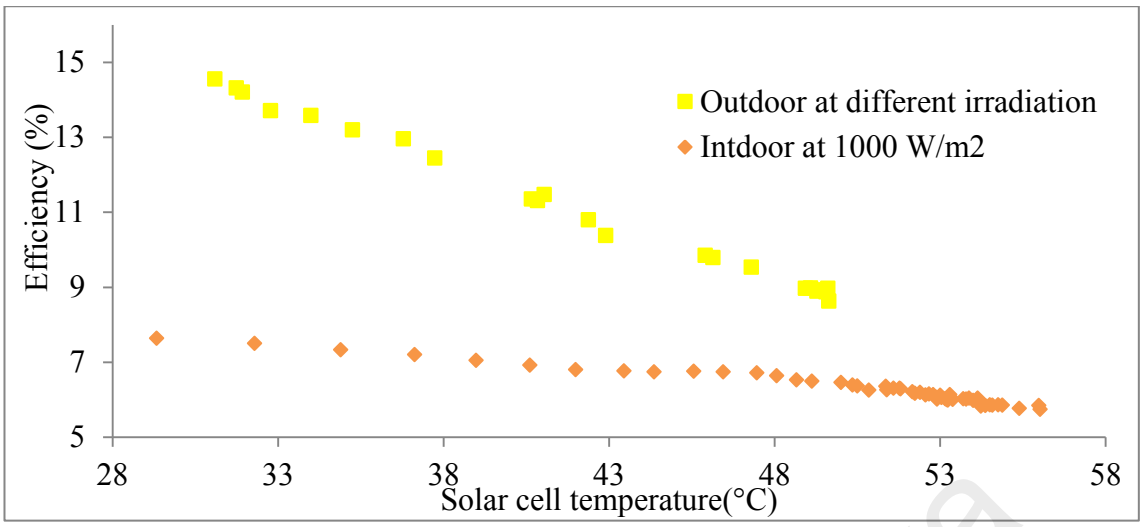

Figure 4.30: Comparison of temperature-dependent efficiencies of the solar module under indoor and outdoor operating conditions (with cooling)

Figure 4.30 shows that, under indoor operating conditions at an irradiation level of 1000 W/m^2, with the same cooling water flow rate, the initial temperature of the PV module is 29.33 °C, and its output electrical efficiency is 7.65%. After a stable operating condition is attained, the PV module temperature increases to 56.02 °C, and the output efficiency drops to 5.73%. Approximately 1.92% electrical efficiency is reduced from the initial value as a result of the 26.69 °C increment in solar module temperature. Consequently, the output performance of the module under these conditions is 25.11% lower than its preliminary output performance. This efficiency decrease attributed to cell temperature increment agrees well with the result of outdoor performance. Under cooling operating conditions with 80 L/h cooling water flow rate at an irradiation level of 1000 W/m^2, approximately 0.07% electrical efficiency is reduced per 1 °C enhancement of module surface temperature.

Fluctuations in incident irradiation levels, surrounding temperatures, and wind velocities influence the resultant performance of the PV module in an outdoor operating environment. The spectral irradiance (W/(m^2·μm)) of solar radiation is also considerably higher than that of artificial halogen lamp radiation. Consequently,

halogen lamp radiation generates more heat and has lower efficiency than sunlight because the former has lower photonic energy (education.org, 2015). Thus, efficiency decline rates per degree cell temperature increment under indoor and outdoor operating conditions deviate considerably.

The effect of cooling water flow rate on the performance of the PV module is also investigated.

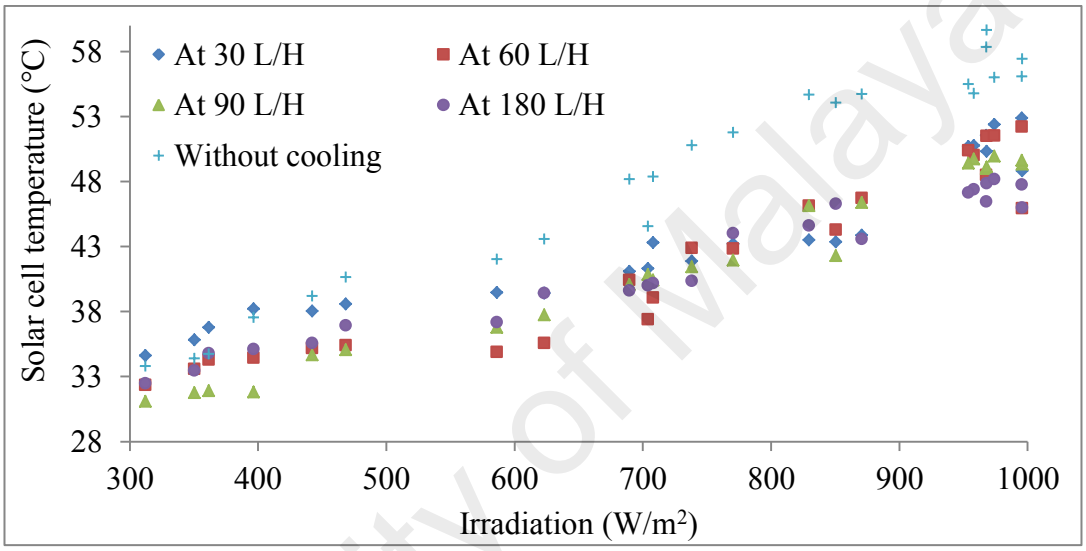

Figure 4.31: Solar cell temperature at different flow rates

Figure 4.31 shows that solar cell temperature is reduced as flow rate increases across different irradiation levels. Therefore, the efficiency of the solar module increases with increased cooling water flow rate. However, the reduction in cell temperature is minimal when cooling water flow rate is increased.

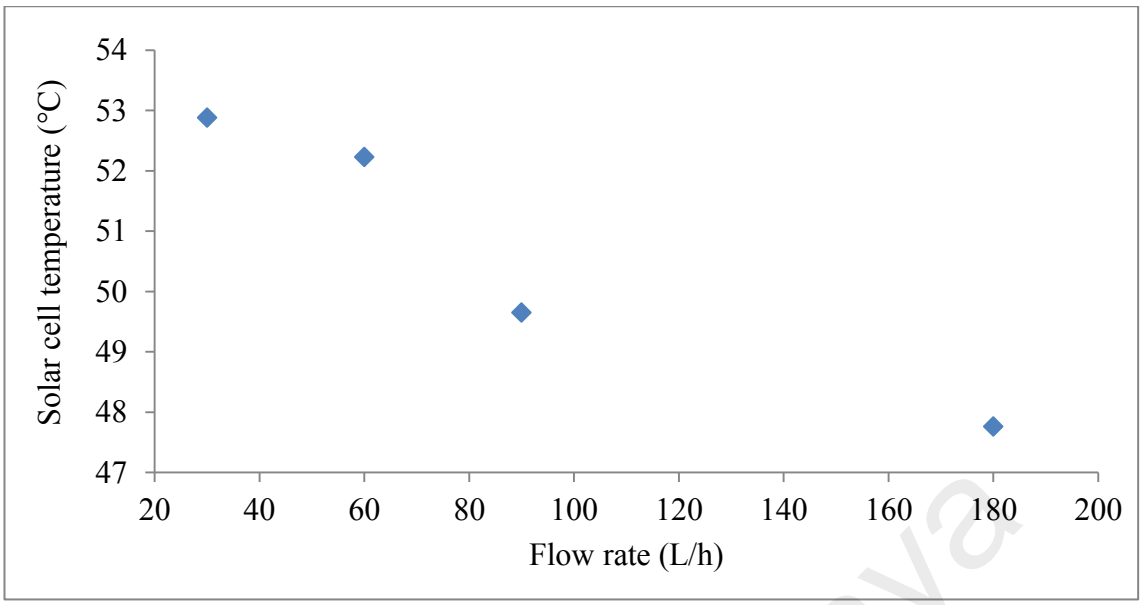

Figure 4.32: Flow rate vs. solar cell temperature

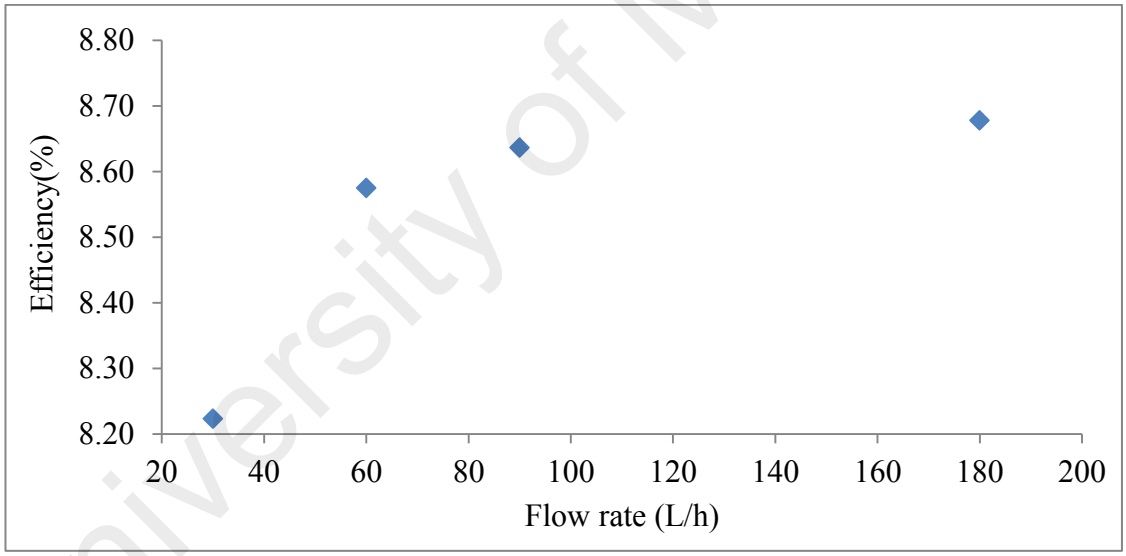

Figure 4.33: Flow rate vs. efficiency

Figure 4.32 and Figure 4.33 respectively show solar cell temperature reduction and efficiency increment at different flow rates under peak operating conditions. Solar cell temperature reduction and solar module efficiency increment are linear up to a cooling water flow rate of 90 L/h. Beyond this rate, however, the reduction in cell temperature is minimal with an increment in flow rate. Hence, the 90 L/h flow rate is the most suitable

for enhancing PV module efficiency. Figure 4.34 shows the enhancement of PV module efficiency with the use of a water cooling system.

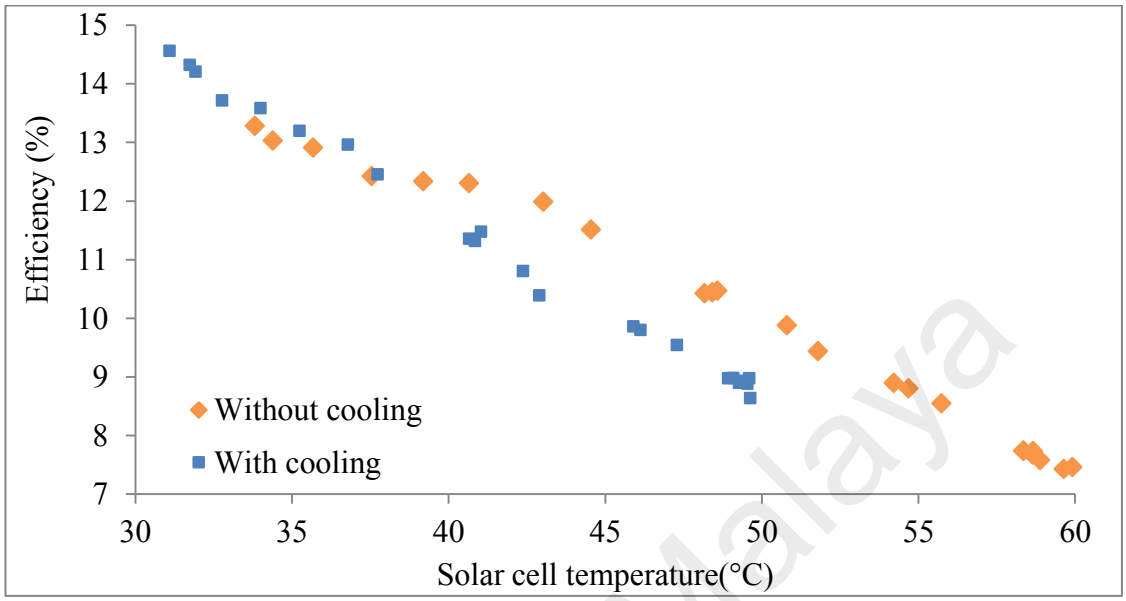

Figure 4.34: Solar cell temperature vs. Efficiency

Figure 4.34 shows that solar cell temperature is reduced by 10.28 °C with water cooling application. A water flow rate of 90 L/h under peak operating conditions increases output power by 7.64 W and electrical efficiency by 1.17%. Outdoors and with cooling condition, module output power or efficiency is increased by 15.72% with respect to output performance without cooling by reducing cell temperature by 17.16%.

Table 4.8: Comparison of performance improvements with a cooling system in different investigations

Authors, year, time, location, and coordinate		Irradiation level (W/m^2)		Operating temperature (°C)		Maximum ambient temperature (°C)	Cell temperature (°C) reduction by applying cooling	Performance (%) improvement by applying cooling	Comparison with present investigation
		Starting period	Peak period	Starting period	Peak period				
Current experimental results; Solar Thermal Lab, UMPEDAC, University of Malaya; Latitude 26°18'N, Longitude 50°08'E	Without cooling	312	995	34	60	35	10.28	15.72%	Shows better performance than previous investigations
	With cooling	312	995	31	50	35			
Bahaidarah et al. (2013); February 2012; KFUPM, Dhahran, Saudi Arabia; Latitude 26°18'N, Longitude 50°08'E	Without cooling	240	979	25	44	21	15	9%	Agrees well with present investigation
	With cooling	240	979	21	35	21			
Chandrasekar et al. (2013); April 2013; Anna University, BIT Campus, Tiruchirappalli, India; Latitude 10°39'N, Longitude 78°44'E	Without cooling	600	1300	37	65	37	20	15.56%	Agrees well with present investigation
	With cooling	600	1300	40	50	37			

Chandrasekar et al. (2013) improved electrical efficiency by 1.4% and output power by 6.5 W under outdoor operating conditions by decreasing the cell temperature of the PV module by 20 °C with an active cooling system (Chandrasekar et al., 2013). Bahaidarah et al. (2013) also decreased the cell temperature of the PV module by 20% with a water cooling system on the back surface and consequently increased electrical efficiency by approximately 9% (Bahaidarah et al., 2013). Therefore, the present investigation

provides better PV module performance than the studies of Chandrasekar et al. (2013) and Bahaidarah et al. (2013).

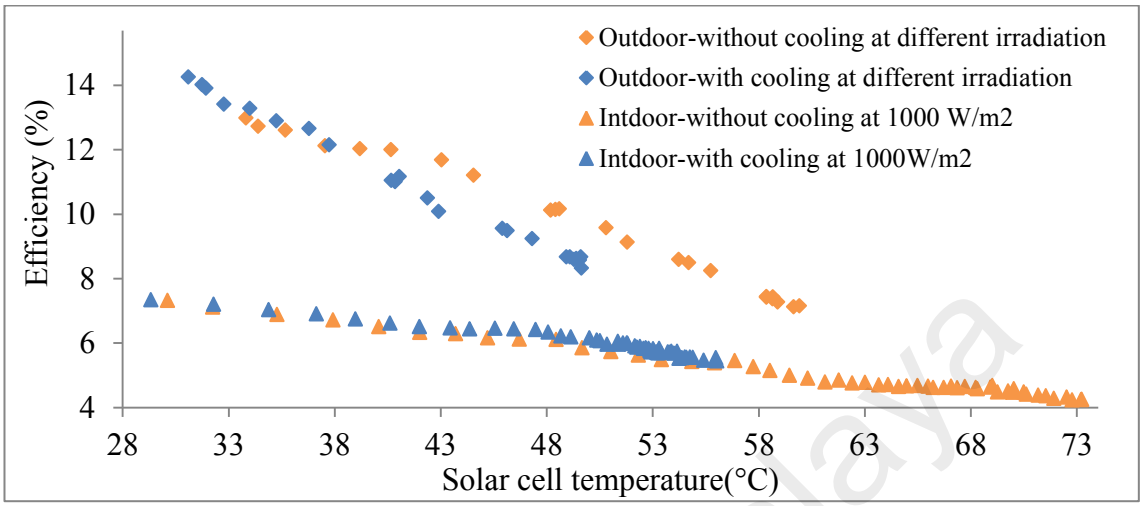

Figure 4.35: Comparison of efficiency enhancement of the PV module with a water cooling system under indoor and outdoor operating conditions

Under indoor operating conditions at an irradiation level of 1000 W/m^2, approximately 17.21 °C is reduced from solar cell temperature by using water coolant flowing at a rate of 80 L/h through a heat exchanger fixed to the bottom Tedlar layer of the PV module. When module temperature is reduced, output power and electrical efficiency can be increased by approximately 8.04 W and 1.23%, respectively. These results agree well with the outdoor performance results. Electrical energy can be increased by 27.33% when a water cooling system is applied under indoor operating conditions. The enhancement of efficiency is greater indoors than outdoors because the outdoor solar module is affected by various ambient operating conditions, such as incident irradiation level, wind velocity, and surrounding temperature fluctuations. The spectral irradiance (W/(m^2·μm)) of solar radiation is also significantly greater than that of artificial halogen radiation. With lower photonic energy, the radiation from the artificial simulator yields lower efficiency and more heat than solar radiation (education.org, 2015). Thus, the efficiency decline rate with per degree increment in solar cell temperature under indoor conditions significantly deviates from that under outdoor operating conditions.

4.2.4 Heat Transfer by Heat Exchanger Fins

The rectangular fins fixed to the semi-circular copper tube also enhance the heat removal rate from the PV module surface and exert a positive influence on the performance of the cooling device. Figure 4.36 compares the heat removal rates from the module surface with fins and without fins attached to the heat exchanger device.

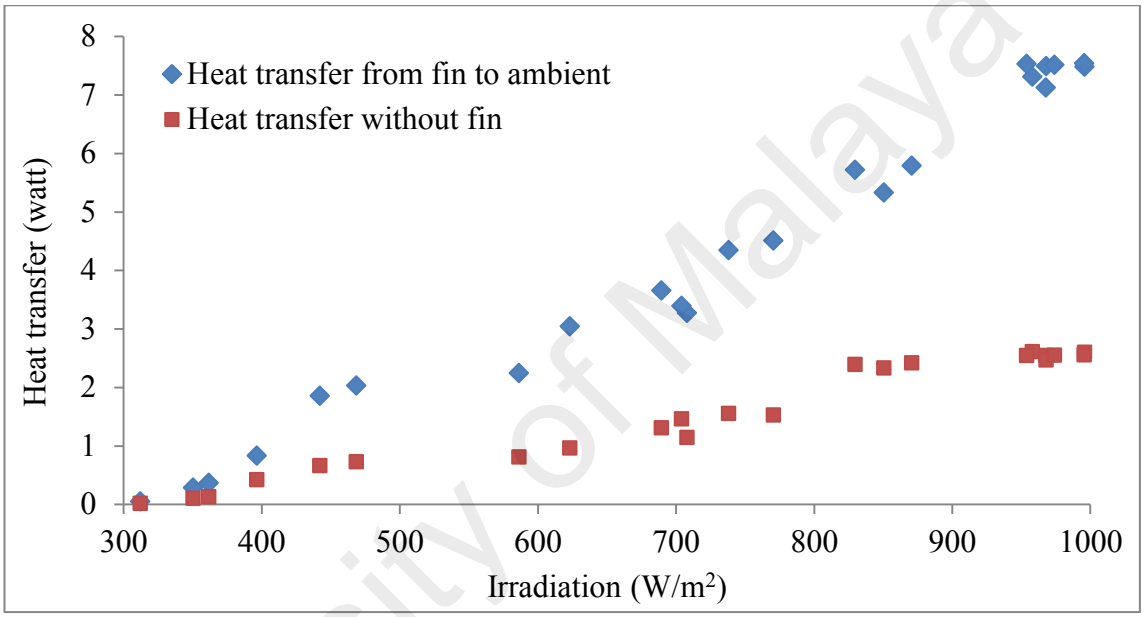

Figure 4.36: Heat transfer with and without fins on the rectangular semi-circular copper sheet (with cooling)

Figure 4.36 shows that, under cooling operating conditions, the rectangular fins can transfer 5 W more heat from the solar cell surface than without fins. Thus, the continuous cooling water flow through the heat exchanger device decreases the temperatures of the bottom surface and solar cell. A portion of heat from the bottom surface is also directly lost to ambient air through convection. Another portion of heat is also transferred to the surroundings from the fins attached to the rectangular half round of the heat exchanger. Additional heat is transferred to flowing water from the back surface.

4.2.5 Effect of Humidity on PV Module Performance

The output performance of the PV module is also affected by the RH in the surrounding environment under outdoor operating conditions. The output efficiency of the PV module during peak operating period is investigated at an irradiation level of approximately 900 W/m^2 and at different RH values for five days in January 2015.

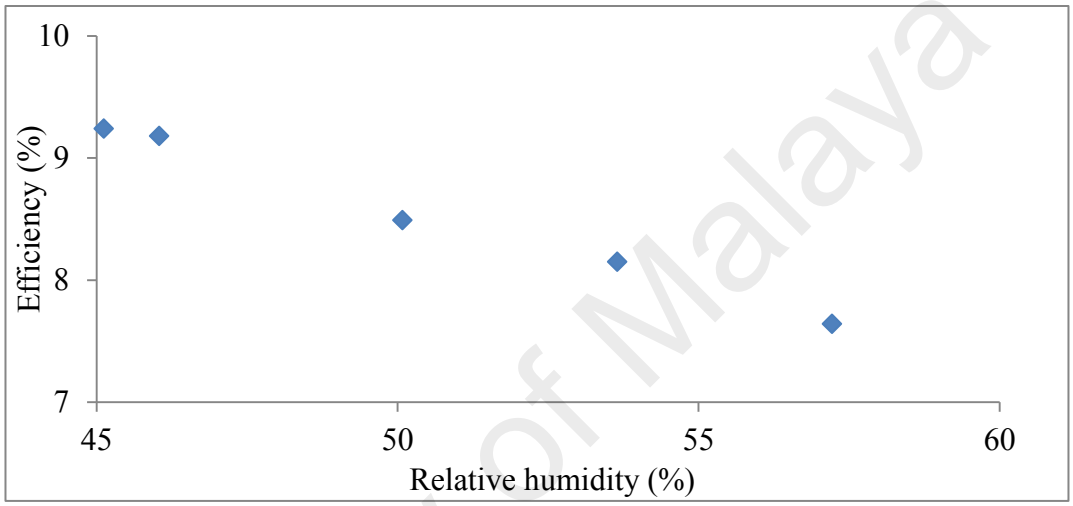

Figure 4.37: Humidity vs. output efficiency during peak operating period

The average RH level on these five days are 57.72%, 53.65%, 46.04%, 50.08%, and 45.12%, and the respective average efficiencies are 7.64%, 8.15% 9.18%, 8.49%, and 9.24%. Thus, output efficiency decreases by 1.6% with a 12.1% increase in RH.

4.2.6 Effect of Dust on PV Module Performance

The effect of dust on the output performance of the PV module is also observed in the current experiment on two different days at similar irradiation levels. This experiment is entirely conducted outdoors. Approximately 0.01 g/cm^2 dust is spread on the top glass surface of the PV module to observe the influence of dust depotions on PV module performance.

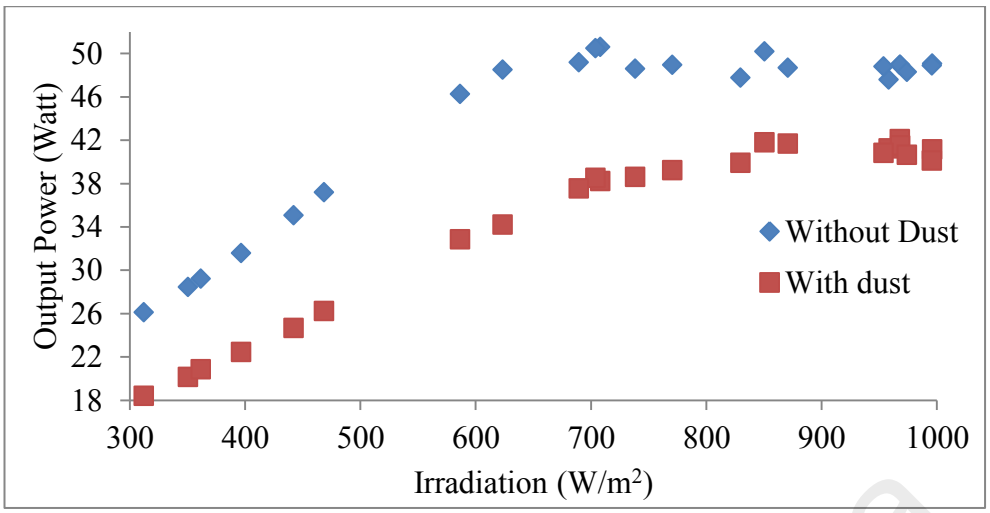

Figure 4.38: Effect of dust on solar cell output power under outdoor operating conditions

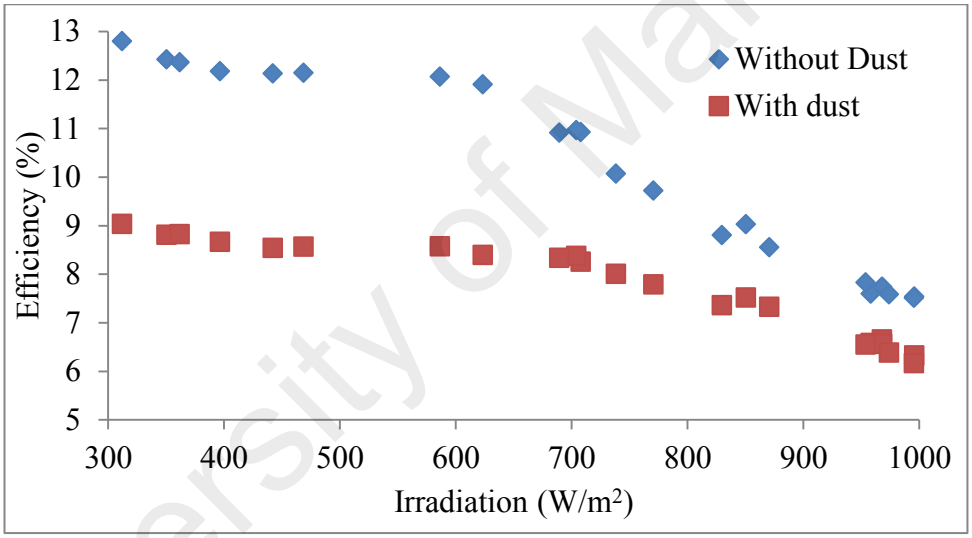

Figure 4.39: Effect of dust on solar cell efficiency under outdoor operating conditions

Figure 4.38 and Figure 4.39 show that solar cell output power and electrical efficiency respectively reach 48.89 W and 7.51% during peak operating period outdoors. Output power drops to 40.14 W and electrical efficiency to 6.16% during peak operating period because of the dust spread on the top glass layer of the PV module. Thus, output power decreases by 8.75 W and efficiency is reduced by 1.34%. Dust deposition on the top glass layer of the PV module causes an output performance that is 17.90% lower than the output performance of the module when it is free of dust.

CHAPTER 5 : CONCLUSIONS AND RECOMMENDATIONS

5.1 Conclusions

Cooling a PV module evidently increases its efficiency under practical operating conditions. The following conclusions can be drawn from the current investigation.

- The output power of the PV module drastically drops because of the increase in solar cell temperature at various irradiation levels. Indoors and without cooling, the total output power decreases by up to 20.47 W and electrical efficiency decreases by up to 3.13% with an increase of 43.12 °C in solar cell temperature; consequently, the output performance of the PV module becomes 41.03% lower than its preliminary output performance. Without cooling and at 1000 W/m^2 irradiation level, output power decreases by 0.47 W and electrical efficiency decreases by 0.07% per 1 °C increment in the cell temperature of the PV module.
- Under outdoor operating conditions without cooling, the total electrical efficiency decreases by up to 5.82% with a 26.10 °C increase in solar cell temperature; consequently, efficiency under these conditions is 43.83% lower than the initial efficiency. Thus, electrical efficiency decreases by 0.22% per 1 °C increase in solar cell temperature.
- Under indoor operating conditions without cooling, solar cell temperature and output power increase by approximately 4.11 °C2.94 W, respectively, for every 100 W/m^2 increase in irradiation level.
- Under outdoor operating conditions without cooling, solar cell temperature and output power increase by approximately 3.82 °C and 3.14 W, respectively, per 100 W/m^2 increase in irradiation level.

- Under indoor operating conditions at an irradiation level of 1000 W/m^2, using a water cooling system reduces PV cell temperature by 17.21 °C and increases output power by 8.04 W and electrical efficiency by 1.23%. The cooling performance of the PV module under these conditions is 27.33% greater than the output of the PV module without a cooling system.
- The output performance of the PV module minimally improves by using an air cooling technique under stable operating conditions.
- Under outdoor conditions, using a water cooling system reduces PV cell temperature by 10.28 °C and increases output power by 7.64 W and electrical efficiency by 1.17%. Consequently, output power under these conditions is 15.72% higher than that without cooling.
- Indoors, output power decreases by 3.16 W with a 20% increase in RH; that is, output decreases by 1.58 W with each 10% increment in humidity in the surrounding area. Outdoors, output efficiency decreases by 1.6% with a 12.1% increase in RH.
- Spreading 0.012 g/cm^2 dust on the module surface results in a 30.43% lower performance indoors and 17.90% lower performance outdoors than the performance of the PV module whose surface is free of dust.

5.2 Recommendations

The proposed water cooling system can considerably increase the output power of a large power plant. In general, most large power stations use demineralized water for cooling to prevent corrosion and erosion inside the cooling tube. Thus, the recommended closed-loop cooling system, which uses a radiator, is more effective when used with demineralized water. The cooling system is also useful for power plants located in regions with a shortage of natural water resources, particularly in hot climate

areas or tropical regions. Further investigation of the closed circulation of the cooling system and its effect on PV output performance may be conducted using different cooling heat exchanger devices and coolants.

The current investigation shows that the output efficiency of the PV module can be considerably increased by applying water cooling through a finned tube-type heat exchanger. However, this heat exchanger device is massive; thus, further study should be conducted to develop a lighter and more convenient heat exchangers for PV modules to increase output performance under practical operations. A more effective coolant, such as a nanofluid, can be used to cool PV modules. Dust and humidity have detrimental effects on PV module efficiency. Thus, further investigation on how to overcome the adverse effects of these parameters on PV module performance should be conducted.

REFFERENCES

Alami, A. H. (2014). Effects of evaporative cooling on efficiency of photovoltaic modules. *Energy Conversion and Management, 77*(0): 668-679.

Alonso-García, M., Ruiz, J., & Chenlo, F. (2006). Experimental study of mismatch and shading effects in the IeV characteristic of a photovoltaic module. *Solar Energy Materials and Solar Cells, 90*: 329-340.

Araki, K., & Yamaguchi, M. (2003). Novel equivalent circuit model and statistical analysis in parameters identification. *Solar Energy Materials and Solar Cells, 75*(3–4): 457-466.

Armstrong, S., & Hurley, W.G. (2010). A thermal model for photovoltaic panels under varying atmospheric conditions. *Applied Thermal Engineering, 30*: 1488-1495.

ASTM. (1992). Standard Tables for Terrestrial Solar Spectral Irradiance at Air Mass 1.5 for a 37 degree Tilted surface *E892-87*.

ASTM. (1999). Standard Solar Constant and Air Mass Zero Solar Spectral Irradiance Tables E490-73a,.

Bahaidarah, H., Subhan, A., Gandhidasan, P., & Rehman, S. (2013). Performance evaluation of a PV (photovoltaic) module by back surface water cooling for hot climatic conditions. *Energy, 59*: 445-453.

Bahaidarah, H., Subhan, A., Gandhidasan, P., & Rehman, S. (2013). Performance evaluation of a PV (photovoltaic) module by back surface water cooling for hot climatic conditions. *Energy, 59*(0): 445-453.

Bauwens, P. D., J. (2014). Reducing partial shading power loss with an integrated Smart Bypass. *Solar Energy, 103*: 134–142.

Beattie, N. S., Moir, R. S., Chacko, C., Buffoni, G., Roberts, S. H., & Pearsall, N. M. (2012). Understanding the effects of sand and dust accumulation on photovoltaic modules. *Renewable Energy, 48*(0): 448-452.

Biggs, A. (2012). A short history of photovoltaic solar power. Retrieved from http://www.evwind.es/2012/2008/2005/a-short-history-of-photovoltaic-solar-power/21013.

Bose, B. K. (2010). Global Warming: Energy, Environmental Pollution, and the Impact of Power Electronics *Industrial Electronics Magazine, IEEE, 4*(1): 6-17.

BP Statistical Review of World Energy (2008). Retrieved from *http://www.bp.com/liveassets/bp_internet/china/bpchina_english/STAGING/local_assets/downloads_pdfs/statistical_review_of_world_energy_full_review_2008.pdf*.

Breitenstein, O., Bauer, J., Lotnyk, A., & Wagner, J. M. (2009). Defect induced non-ideal dark I-V characteristics of solar cells,. *Superlattices and Microstrutures, 45*: 182-189.

Breitenstein, O., Rakotoniaina, J. P., Al Rifai, M. H., & Werner, M. (2004). Shunt types in crystalline silicon solar cells. *Progress in Photovoltaics: Research and Applications, 12*(7): 529-538.

Breitenstein, O., Rakotoniaina, J. P., & Schmidt J. (2002). Comparison of shunt imaging by liquid crystal sheets and lock-in thermography. *Presented at the 12th Workshop on Crystalline Silicon Solar cells Material and Processing, Colorado*.

Cengel, Y. A. (2006). Heat and Mass Transfer: A practical Approach. *Mc Graw Hill, Third edition*.

center for solar energy research and application, T. (2013). How does PV Cells Work. *GÜNAM*, Retrieved from http://gunam.metu.edu.tr/index.php/solar-technology/pv-working-principles.

Ceylan, İ., Gürel, A. E., Demircan, H., & Aksu, B. (2014). Cooling of a photovoltaic module with temperature controlled solar collector. *Energy and Buildings, 72*(0): 96-101.

Chandrasekar, M., Suresh, S., Senthilkumar, T. & Karthikeyan, M. G. (2013). Passive cooling of standalone flat PV module with cotton wick structures. *Energy Conversion and Management, 71*: 43-50.

Dallas, W., Polupan,O., & Ostapenko, S. (2007). Resonance ultrasonic vibrations for crack detection in photovoltaic silicon wafers. *Meas. Sci. Technol., 18*: 852–858.

Davis, G. R. (1990). Energy for Planet Earth. *Scientific American, 263*(3): 54-60.

Dinçer, F., & Meral, M. E. (2010). Critical Factors that Affecting Efficiency of Solar Cells. *Smart Grid and Renewable Energy, 1*: 47-50.

Dolara, A., Lazaroiu, G. C., Leva, S., & Manzolini, G. (2013). Experimental investigation of partial shading scenarios on PV(photovoltaic) modules. *Energy, 55*: 466-475.

Dubey, S., & Tay, A. A. O. (2013). Testing of two different types of photovoltaic–thermal (PVT) modules with heat flow pattern under tropical climatic conditions. *Energy for Sustainable Development, 17*: 1-12.

Dubey, S., & Tiwari, G. N. (2008). Thermal modeling of a combined system of photovoltaic thermal (PV/T) solar water heater. *Solar Energy, 82*(7): 602-612.

Dubey, S., Sandhu, G. S., & Tiwari, G. N. (2009). Analytical expression for electrical efficiency of PV/T hybrid air collector. *Applied Energy, 86*(5): 697-705.

Duffie, J. A., & Beckman, W.A. (1991). Solar Engineering and Thermal Processes,. *John Wiley & Sons Inc., New York.*

Education.org, p. (2015). spectral-irradiance. Retrieved from *http://www.PVEO/pvcdrom/properties-of-sunlight/spectral-irradiance*.

Ettah, E. B., Udoimuk, A. B. , Obiefuna J. N. & Opara, F. E. (2012.). The Effect of Relative Humidity on the Efficiency of Solar Panels in Calabar, Nigeria. *Universal Journal of Management and Social Sciences, 2*(3): 8-11.

Fei, L., Siyu, G., Walsh, T. M., & Aberle, A. G. (2013). Improved PV Module Performance Under Partial Shading Conditions *PV Asia Pacific Conference, 33*: 248 – 255.

Fertig, F., Rein, S., Schubert, M., & Warta, W. (2011). Impact of junction breakdown in multi-crystalline silicon solar cells on hot spot formation and module performance. *26th European PV solar energy conference and exhibition, Humburg, Germany.*

Floyd Associates, I. (2010). Solar Power: Photovoltaic Technologies. . *Beverly Hills: Floyd Associates, Inc.*

Fluga, S., & Eigenbrod, H. (2009). Inline-Thermografie-System pruft Solarzellen—den Mikrorissen auf der Spur. *QZ, 54*, 9.

Fudholi, A., Sopian, K., Yazdi, M. H., Ruslan, M. H., Ibrahim, A. & Kazem, H. A. (2014). Performance analysis of photovoltaic thermal (PVT) water collectors. *Energy Conversion and Management, 78*(0): 641-651.

Fuyuky, T., Kondo, H., Yamazaki, T., Takahaschi, Y., & Uraoka, Y. (2005). Photographic surveying of minority carrier diffusion length in polycrystalline silicon solar cells by electroluminescence. *Appl. Phys. Lett., 86*, 262108.

Gabor, A. M., Ralli, M.M., Alegria,L., Brodonaro, C. Woods, J., & Felton, L. (2006). Soldering induced damage to thin Si solar cells and detection of cracked cells in modules. *Proceedings of the 21st EUPVSEC, WIP, Dresden, Germany*, 2042–2047.

Goetzberger, A., & Hoffmann, V. U. (2005). Photovoltaic Solar Energy Generation. .*Springer-Verlag Berlin Heidelberg*(ISBN 3-540-23676-7).

Goetzberger, A., Hebling, C., & Schock, H.-W. (2003). Photovoltaic materials, history, status and outlook. *Materials Science and Engineering: R: Reports, 40*(1): 1-46.

Gwandu, B. A. L., & Creasey, D. J. (1995). Humidity: A factor in the appropriate positioning of a photovoltaic power station. *Renewable Energy, 6*(3): 313-316.

Hai, J., Lin, L. & Ke, S. (2011). Experimental investigation of the impact of airborne dust deposition on the performance of solar photovoltaic (PV) modules. *Atmospheric Environment, 45*: 4299-4304.

Hanif, M., Ramzan, M., Rahman, M., Khan, M., Amin, M. & Aamir, M. (2012). Studying Power Output of PV Solar Panels at Different Temperatures and Tilt Angles. *ISESCO JOURNAL of Science and Technology, 8*(14): 9-12.

Hasnain, S. M., Alawaji, S. H. & Elani, U. A. (1998). Solar energy education - a viable pathway for sustainable development. *Renewable Energy, 14*(1-4): 387-392.

Hatch, J. E. (1984). Aluminum. *Properties and Physical Metallurgy, second ed. ASM International,*.

Herrmann, W., Wiesner, W., & Vaassen, W. (1997, 29 Sep-3 Oct 1997). *Hot spot investigations on PV modules-new concepts for a test standard and consequences for module design with respect to bypass diodes.* Paper presented at the Photovoltaic Specialists Conference, 1997., Conference Record of the Twenty-Sixth IEEE.

Hettelsater, D. (2002). Solar Cell Lab. *University of California, Santa Cruz*.

Hosseini, R., Hosseini, N., & Khorasanizadeh, H. (2011). An experimental study of combining a photovoltaic system with a heating system. . *World renewable energy congress 2011 Sweden*.

How solar cells work. (2013). *Solar Energy, Retrieved from http://energybible.com/solar_energy/solar_cells.html*.

Hurng-Liahng, J., Yi-Hao, C., Jinn-Chang, W., & Kuen-Der, W. (2015). Operation strategy for a lab-scale grid-connected photovoltaic generation system integrated with battery energy storage. *Energy Conversion and Management, 89*(0): 197-204.

Ikegami, T., Maezono, T., Nakanishi, F., Yamagata, Y., & Ebihara, K. (2001). Estimation of equivalent circuit parameters of PV module and its application to optimal operation of PV system. *Solar Energy Materials and Solar Cells, 67*(1–4): 389-395.

Jie, J., Jian-Ping, L., Tin-Tai, C., Wei, H., & Gang, P. (2007). A sensitivity study of a hybrid photovoltaic/thermal water-heating system with natural circulation. *Applied Energy, 84*: 222–237.

Jones, A. D., & Underwood, C. P. (2001). A Thermal Model for Photovoltaic Systems. *Pergamon, 70*(4): 349–359.

Jong, P. K., Ho, L., Ju, H. S., Young, J. C., & Chung, H. J. (2011). Numerical analysis on the thermal characteristics of photovoltaic module with ambient temperature variation. *Solar Energy Materials & Solar Cells, 95*: 404-407.

Jooss, W. (2002). Multicrystalline and back contact buried contact silicon solar cells. *PhD dissertation, Universitat Konstanz Fachbereich Physik.*

Kajari-Schröder, S., Kunze, I., & Köntges, M. . (2012). Criticality of cracks in PV modules. *Energy Procedia, 27*, 658 – 663.

Kalogirou, S. A. (2009). Solar Energy Engineering, Processes and Systems, Chapter nine – Photovoltaic Systems. *Academic Press*, 469–519.

Karatepe, E., Boztepe, M., & Çolak, M. (2007). Development of a suitable model for characterizing photovoltaic arrays with shaded solar cells. *Solar Energy, 81*(8): 977-992.

Kasap, S. O. (2002). Principles of Electrical Engineering Materials and Devices, Second Edition. *Mc Graw Hill*.

Katkar, A. A., Shinde, N.N. & Patil P.S. . (2011). Performance & Evaluation of Industrial Solar Cell w.r.t. Temperature and Humidity. *International Journal of research In Mechanical engineering and technology, 1*(1): 69-73.

Kawamura, H., Naka, K., Yonekura, N., Yamanaka, S., Kawamura, H., Ohno, H., & Naito, K. (2003). Simulation of I–V characteristics of a PV module with shaded PV cells. *Solar Energy Materials and Solar Cells, 75*(3–4): 613-621.

King, D. L., Kratochvil, J. A., Quintana, M. A., & McMahon, T. J. (2000, 2000). *Applications for infrared imaging equipment in photovoltaic cell, module, and system testing.* Paper presented at the Photovoltaic Specialists Conference, 2000. Conference Record of the Twenty-Eighth IEEE.

Kontges, M., & Bothe., K. . (2008). Elektrolumineszensmessung an photovoltaik-modulen, . *Photovoltaik Aktuell supplement in Elektro Praktiker, 7/8*: 36–40.

Kontges, M., Kunze, I., Kajari-Schroder, S., Breitenmoser, X., & Bjørneklett, B. (2011). The risk of power loss in crystalline silicon based photovoltaic modules due to micro-cracks. *Solar Energy Materials & Solar Cells, 95*: 1131-1137.

Ksenya. (2011). History of solar energy. *Solar turbine*, Retrieved from http://solartribune.com/history-of-photovoltaics/.

Kumar, R., & Rosen, M. A. (2011). A critical review of photovoltaic–thermal solar collectors for air heating. *Applied Energy, 88*(11): 3603-3614.

Lai, J., Perazzo, T., Shi, Z., & Majumdar, A. (1997). Optimisation and performance of high resolution micro-optomechanical thermal sensors. *Sensors and Actuators, 58*: 113-119.

Lalaguna, B., Sa nchez-Friera, P., Mackel, H., Sanchez, D., & Alonso, J. (2008). Evaluation of stress on cells during different interconnection processes. *Proceedings of the 23rd EUPVSEC, WIP, Valencia, Spain,*, 2705–2708.

Lam, K. H., Lai, T. M., Lo, W. C., & To, W. M. (2012). The application of dynamic modelling techniques to the grid-connected PV (photovoltaic) systems. *Energy, 46*, 264 -274.

Limbra, M., & Poulek, V. (2006). Solarni energie (Solar energy). *Praha: CZU xxx s ISBN 80 - 223 - 1488 - 5*.

Liserre, M., Sauter, T. & Hung, J. Y. (2010). Future Energy Systems: Integrating Renewable Energy Sources into the Smart Power Grid Through Industrial Electronics. *Industrial Electronics Magazine, IEEE, 4*(1): 18-37.

Lu, Z. H., & Yao, Q. (2007). Energy analysis of si solar cell modules based on an optical model for arbitrary layers. *Solar Energy, 81*: 636-647.

Macdonald, D., Cuevas, A., Kinomura, A., & Nakano, Y. (2002, 19-24 May 2002). *Phosphorus gettering in multicrystalline silicon studied by neutron activation analysis.* Paper presented at the Photovoltaic Specialists Conference, 2002. Conference Record of the Twenty-Ninth IEEE.

Macdonald, D., Cuevas, A., Kinomura, A., Nakano, Y., & Geerligs, L. J. (2005). Transition-metal profiles in a multicrystalline silicon ingot. *Journal of Applied Physics, 97*(3).

Machacek, J., Prochazka, Z. & Drapela, J. (2009). The temperature dependant efficiency of photovoltaic module - a long term evaluatiobn of experimental measurements. *Renewable Energy, T J Hammons (Ed.), ISBN: 978-953-7619-52-7, InTech,* Retrieved from *http://www.intechopen.com/books/renewable-energy/the-temperature-dependant-efficiency-of-photovoltaicmodules-a-long-term-evaluation-of-experimental*.

Malik, A. Q., Lim, C. M., Tan, K. S., & Blundell, M. (2010). Influence of Temperature on the Performance of Photovoltaic Polycrystalline Silicon Module in the Bruneian Climate. *AJSTD, 26*(2): 61-72.

Panjwani, M. K., & Narejo, G. B. (2014). Effect of Humidity on the Efficiency of Solar Cell (photovoltaic). *International Journal of Engineering Research and General Science, 2*(4): 499-503.

Mekhilef, S., Saidur R., & Kamalisarvestani, M. (2012.). Effect of dust, humidity and air velocity on efficiency of photovoltaic cells. *Renewable and Sustainable Energy Reviews, 16:* 2920–2925.

Meral, M. E., & Dinçer, F. (2011). A review of the factors affecting operation and efficiency of photovoltaic based electricity generation systems. *Renewable and Sustainable Energy Reviews, 15*(5): 2176-2184.

Meyer, E. L., Dyk, E.E.V.,. (2004). Assessing the reliability and degradation of photovoltaic module performance parameters. *IEEE Transactions on Reliability, 53*(1): 83–92.

Miles, R. W., Hynes, K. M. & Forbes I. (2005). Photovoltaic solar cells: An overview of state-of-the-art cell development and environmental issues. *Progress in Crystal Growth and Characterization of Materials, 51*: 1-42.

Minemoto, T., Nagae, S. & Takakura, H. (2007). Impact of spectral irradiance distribution and temperature on the outdoor performance of amorphous Si photovoltaic modules. *Solar Energy Materials and Solar Cells, 91*(10): 919-923.

Moharram, K. A., Abd-Elhady, M. S., Kandil, H. A., & El-Sherif, H. (2013). Enhancing the performance of photovoltaic panels by water cooling. *Ain Shams Engineering Journal, 4*(4): 869-877.

Mukhopadhyay, S., Goswami, R., & Ray, S. (2009). Light induced degradation in nanocrystalline Si films and related solar cells: Role of crystalline fraction. *Solar Energy Materials & Solar Cells, 93*: 674– 679.

Muneer, T., Asif, M. & Munawar, S. (2005). Sustainable Production of Solar Electricity with Particular Reference to the India Economy. *Renewable Sustainable Energy Review, 9*: 444-473.

Murtinger, K., Beranovsky, J. & Tomes, M. (2007). Fotovoltaika. Elektrina ze slunce (Photovoltaics. Electricity from sun). *Brno: ERA Publishers 100PP. ISBN 978-80 - 7366 - 100 - 7*.

Nahar, N., & Gupta, J. . (1990). Effect of dust on transmittance of glazing materials for solar collectors under arid zone conditions of India. *Solar & Wind Technology, 7*(2-3): 237–243.

Notton, G., Cristofari, C., Mattei, M., & Poggi, P. . (2005). Modelling of a double-glass photovoltaic module usingfinite differences. *Applied Thermal Engineering, 25*: 2854-2877.

Odeh, S., & Behnia,M. (2009). Improving Photovoltaic Module Efficiency Using Water Cooling. *Heat Transfer Engineering, 30*(6): 499-505

Olchowik, J. M., Gulkowski, S., Cieślak, K. J., Banaś, J., Jóźwik, I., Szymczuk, D., ... Tomaszewski, R. (2006). Influence of temperature on the efficiency of monocrystalline silicon solar cells in the South-eastern Poland conditions. *Materials Science - Poland, 24*(4): 1127-1132.

Omubo-Pepple, V. B., Israel-Cookey, C. & Alaminokuma, G. I. (2009). Effects of Temperature, Solar Flux and Relative Humidity on the Efficient Conversion of Solar Energy to Electricity. *European Journal of Scientific Research, 35*(2): 173-180.

Oozeki, T., Izawa, T., Otani, K., & Kurokawa, K. (2003). An evaluation method of PV systems. *Solar Energy Materials and Solar Cells, 75*(3–4): 687-695

Otanicar, T., Taylor, R. A. & Phelan, P. E. (2012). Prospects for solar cooling – An economic and environmental assessment. *Solar Energy, 86*(5): 1287-1299.

Othman, A. K., Jakhrani, A. Q., Abidin, W. A. W. Z., Zen, H. & Burhan, A. (2010). A Malaysian Govetrnment Policy. In: Renewable Energy: Solar PV System, . *in world engineering Congress 2010, 2nd-5th August 2010, C.o.N.R.a.G. Technology, Editor 2010, The Federation of Engineering Institutions of Islamic Countries: Kuching, Sarawak, Malayasia.*

Ouma, C. (2013). Monocrystalline vs Polycrystalline Solar Panels. *Exploring Green Technology.com, Retrieved from: http://exploringgreentechnology.com/solar-energy/technology/monocrystalline-solar-cells/*.

Panjwani, M. K., &, Narejo, G. B. (2014). Effect of Humidity on the Efficiency of Solar Cell (photovoltaic). *International Journal of Engineering Research and General Science, 2*(4): 499-503.

Paraskevadaki, E. V., & Papathanassiou, S. A. (2011). Evaluation of MPP voltage and power of mc-Si PV modules in partial shading conditions. *IEEE Transactions on Energy Conversion, 26*(3): 923-932.

Park, K. E., Kang, G. H., Kim, H. I., Yu, G. J.,& Kim, J. T. (2010). Analysis of thermal and electrical performance of semi-transparent photovoltaic (PV) module. *Energy, 35*(6): 2681-2687.

Phylipsen, G. J. M., & Alsema, E. A. (1995). Environmental Life-Cycle Assessment of Multicrystalline Silicon Solar Cell Modules. *Report No. 95057. Netherlands Agency for Energy and the Environment.*

Pingel, S., Zemen, Y., Frank, O., Geipel, T., & Berghold, J. (2009). Mechanical stability of solar cells within solar panels,. *Proceedings of the 24th EUPVSEC, WIP, Dresden, Germany,*, 3459–3464.

PVEO. (2013). Manufacturing Si cells. Retrieved from: *http://PVEO/pvcdrom/manufacturing/multi-crystalline-silicon*.

PVEO. (2015). Properties of sunlight. Retrieved from: *http://PVEO/pvcdrom/properties-of-sunlight/spectral-irradiance*.

Qi, Z., & Qun, L. (2011). Temperature and Reverse Voltage across a Partially Shaded Si PV Cell under Hot Spot Test Condition,. *Solaria Corp, Fremont, CA 94555, USA*.

Qunzhi, Z., & Leilei, S. (2012). Electrical Outputs and Thermal Outputs of Water/Air Cooled Amorphous-Silicon Photovoltaic Modules. *2012 International Conference on Environmental Engineering and Technology, 8*: 83-88.

Radziemska, E. (2003). The effect of temperature on the power drop in crystalline silicon solar cells. *Renewable Energy, 28*(1): 1-12.

Radziemska, E. (2006). Effect of temperature on dark current characteristics of silicon solar cells and diodes. *International Journal of Energy Research, 30*(2): 127-134.

Radziemska, E., & Klugmann, E. (2002). Thermally affected parameters of the current–voltage characteristics of silicon photocell. *Energy Conversion and Management, 43*(14): 1889-1900.

Radziemska, E. K., E. (2002). Thermally Affected Parameters of the Current-Voltage Characteristics of Silicon Photocell. . *Energy Conversion and Management, 43*: 1889-1900.

Rahman, S., & de Castro, A. (1995). Environmental impacts of electricity generation: a global perspective. *Energy Conversion, IEEE Transactions, 10*(2): 307-314.

Ramabadran, R., & Mathur, B. (2009). Effect of shading on series and parallel connected solar PV modules. *Modern Applied Science, 3*: 32- 42.

Ramaprabha, R., & Mathur, B. L. (2009). Impact of partial shading on solar PV module containing series connected cells. *International Journal of Recent Trends in Engineering, 2*(7): 56-60.

Rath, J. K., Brinza, M., Liu, Y., Borreman, A. & Schropp, R. E. I. (2010). Fabrication of thin film silicon solar cells on plastic substrate by very high frequency PECVD. *Solar Energy Materials and Solar Cells, 94*(9): 1534-1541.

Ray, K. L. (2010). Photovoltaic cell efficiency at elevated temperatures. *Massachusetts Institute of Technology,* Retrieved from: *http://dspace.mit.edu/bitstream/handle/1721.1/59937/676836192.pdf?...1*.

Reil, F., Strohkendl, K., Althaus, J., & Vaassen, W. (2009). Mechanische Beanspruchungen für PV Module –Transportbelastungen. *Workshop – Photovoltaik-Modultechnik, (TÜV Rheinland, Köln, Germany)*.

Renewables, H. (2010). PV Technology, The different types of modules & cells. Retrieved from: *http://www.horizonrenewables.co.uk/solar-photovoltaics/solar-pv-technology.html*.

Roth, J. R. (1995). Long term global energy issues,. *Industrial Plasma Engineering, 1*: 21-25.

Sahay, A. S., V. K., Tiwari, A. C., & Pandey, M. (2015). A review of solar photovoltaic panel cooling systems with special reference to Ground coupled central panel cooling system (GC-CPCS). *Renewable and Sustainable Energy Reviews, 42*(0): 306-312.

Sahu, B. K. (2015). A study on global solar PV energy developments and policies with special focus on the top ten solar PV power producing countries. *Renewable and Sustainable Energy Reviews, 43*(0): 621-634.

Said, S. A. M., & Walwil, H. M. (2014). Fundamental studies on dust fouling effects on PV module performance. *Solar Energy, 107*(0): 328-337.

Sanusi, Y. K., Fajinmi, G. R. & Babatunde, E. B. (2011). Effects of Ambient Temperature on the Performance of a Photovoltaic Solar System in a Tropical Area. *The Pacific Journal of Science and Technology, 12*(2): 177-180.

Sardarabadi, M., Passandideh-Fard, M. & Heris, S. Z. (2014). Experimental investigation of the effects of silica/water nanofluid on PV/T (photovoltaic thermal units). *Energy, 66*(0): 264-272.

Schmidt, J., Bothe, K., Macdonald D., Adey J., Jones R., & Palmer D.W. (2005). Mechanisms of light-induced degradation in mono- and multicrystalline silicon solar cells. *Presented at 20th European Photovoltaic Solar Energy Conference, Barcelona, Spain,*, 761–764.

Shan, F., Tang, F., Cao, L. & Fang, G. (2014). Comparative simulation analyses on dynamic performances of photovoltaic–thermal solar collectors with different configurations. *Energy Conversion and Management, 87*(0): 778-786.

Shenck, N. S. (2010). Alternative energy systems. *U.S. Naval Academy Lecture Readings*.

Shimaa, M., Isomurab, M., Wakisakaa, K., Murataa, K., & Tanaka, M. . (2005). The influence of operation temperature on the output properties of amorphous silicon-related solar cells. *Solar Energy Materials & Solar Cells 85*, 167–175.

Sidawi, J., Habchi, R., Abboud, N., Jaafar, A., Allouch, F. A., Moussa, G. E. H., Aillerie, M., Petit, P., Zegaoui, A., & Salame, C. (2011). The effect of reverse current on the dark properties of photovoltaic solar modules *Energy Procedia, 6*: 743–749.

Silvestre, S., Boronat, A., & Chouder, A. (2009). Study of bypass diodes configuration on PV modules. *Applied Energy, 86*(9): 1632-1640.

Simon, M., & Meyer, E. L. (2010). Detection and analysis of hot-spot formation in solar cells. *Solar Energy Materials and Solar Cells, 94*(2): 106-113.

Singh, G. K. (2013). Solar power generation by PV (photovoltaic) technology: A review. *Energy, 53*(0): 1-13.

Singh, P., & Ravindra, N. M. (2012). Temperature dependence of solar cell performance—an analysis. *Solar Energy Materials and Solar Cells, 101*(0): 36-45.

Solar - Help, S. e. f. h. b. (2010). Types of Solar PV Cells. Retrieved from: *http://www.solar-help.co.uk/solar-panel-technology/solar-pv-cells-types.htm*.

Solar cells. (2013). *SOALRWIKI,* Retrieved from*: http://solarwiki.co.uk/index.php?option=com_content&view=article&id=3&Itemid=4*.

Solar photovoltaic electricity empowering the world. (2011). *Solar Generation 6,* Retrieved from*: http://www.greenpeace.org/international/en/publications/reports/Solar-Generation-6/*.

Spertino, F., & Graditi, G. (2014). Power conditioning units in grid-connected photovoltaic systems: A comparison with different technologies and wide range of power ratings. *Solar Energy, 108*: 219-229.

Sulaiman, S. A., Hussain, H. H., Leh, N. S. H. N., & Mohd Razali, M. S. I. . (2011). Effects of Dust on the Performance of PV Panels. *World Academy of Science, Engineering and Technology, 58*: 588-593.

Swaaij, R. A. C. M. M. V., & Klaver, A. (2008). Comparison of amorphous silicon solar cell performance following light and highenergy electron-beam induced degradation. *Journal of Non-Crystalline Solids, 354*: 2464–2467

Teo, H. G., Lee, P. S., & Hawlader, M. N. A. (2012). An active cooling system for photovoltaic modules. *Applied Energy, 90*(1): 309-315.

Tiwari, A., Sodha, M.S., Chandra, A., & Joshi J.C. (2006). Performance evaluation of photovoltaic thermal solar air collector for composite climate of India. *Solar Energy Materials and Solar Cells, 90*(2): 175–189.

Tobías, I., del Cañizo, C. & Alonso, J. (2011). Crystalline Silicon Solar Cells and Modules *Handbook of Photovoltaic Science and Engineering* (pp. 265-313): John Wiley & Sons, Ltd.

Tomabechi, K. (2010). Energy Resources in the Future. *Energies, 3*: 686-695.

Tonui, J. K., & Tripanagnostopoulos, Y. (2007). Improved PV/T solar collectors with heat extraction by forced or natural air circulation. *Renewable Energy, 32*: 623–637.

Touati, F. A., Al-Hitmi, M. A., & Bouchech, H. J. (2012). Study of the Effects of Dust, Relative Humidity, and Temperature on Solar PV Performance in Doha: Comparison Between Monocrystalline and Amorphous PVS. *International Journal of Green Energy, 10*(7): 680-689.

Tyagi, V. V., Rahim, N. A. A., Rahim, N. A. & Selvaraj, J. A. L. (2013). Progress in solar PV technology: Research and achievement. *Renewable and Sustainable Energy Reviews, 20*(0): 443-461.

Ugwuoke, P. E., & Okeke, C. E. (2012). Performance Assessment of Three Different PV Modules as a Function of Solar Insolation in South Eastern Nigeria *International Journal of Applied Science and Technology, 2*(3): 319-327.

Umbach, F. (2010). Global energy security and the implications for the EU. *Energy Policy, 38*(3): 1229-1240.

Valeh-e-Sheyda, P., Rahimi, M., Karimi, E., & Asadi, M. (2013). Application of two-phase flow for cooling of hybrid microchannel PV cells: A comparative study. *Energy Conversion and Management, 69*(0): 122-130.

van Dyk, E. E., & Meyer, E. L. (2004). Analysis of the effect of parasitic resistances on the performance of photovoltaic modules. *Renewable Energy, 29*(3): 333-344.

Weinreich, B., Schauer, B., Zehner, M., & Becker, G. (2012). Validierung der Vermessung gebrochener Zellen im Feld mittels Leistungs PV-Thermographie. *im Tagungsband 27. Symposium Photovoltaische Solarenergie (Bad Staffelstein, Deutschland, OTTI)*, 190.

Wendt, J., Träger, M., Mette, M., Pfennig, A., & Jäckel, B. (2009). The Link Between Mechanical Stress Induced by Soldering and Micro Damages in Silicon Solar Cells. *Proc. Of 24th EUPVSEC (WIP, Hambrug, Germany)*, 3420-3423.

Wendt, J., Trager, M., Mette,M., Pfennig, A., & Jackel, B. . (2009). The link between mechanical stress induced by soldering and micro damages in silicon solar cells. *Proceedings of the 24th EUPVSEC, WIP, Hamburg, Germany*, 3420–3423.

Wohlgemuth J. and Herrmann, W. (1994). Reliability testing for PV modules,. *Proceedings of the 29th IEEE Photovoltaic Specialist Conference*, 889–892.

World Energy Outlook 2007. (2007). *International Energy Agency (IEA)*.

Woyte, V., Nijs, J., & Belmans, R. (2003). Partial shadowing of photovoltaic arrays with different system configurations: literature survey and field results. *Solar Energy, 74*(3): 217-233.

WSPI. World Solar Power Introduction. (2010). Retrieved from: *http://www.mbendi.com/indy/ener/sola/p0005.htm*.

Yoshioka, H., Nishikawa, S., Nakajima, S., Asai, M., Takeoka, S., Matsutani, T., & Suzuki, A. (1996, 13-17 May 1996). *Non hot-spot PV module using solar cells with bypass diode function.* Paper presented at the Photovoltaic Specialists Conference, 1996., Conference Record of the Twenty Fifth IEEE.

Zegaoui, A., Petit, P., Aillerie, M., Sawicki, J., & Charles, J. (2012). Experimental Validation of Photovoltaic Direct and Reverse Mode Model. Influence of Partial Shading. *Energy Procedia, 18*: 1247 – 1253.

LIST OF PUBLICATIONS

Journal paper

Rahman, M. M., Hasanuzzaman, M., & Rahim, N. A. (2015). Effects of various parameters on PV-module power and efficiency. Energy Conversion and Management, 103, 348-358. (Q1, IF: 4.380).

Rahman, M. M., Hasanuzzaman, M., & Rahim N. A. Effects of atmospheric conditions on energy efficiency of photovoltaic modules operating in Malaysia. Journal of Cleaner Production (Under Review).

Conference paper

Rahman, M. M., Hasanuzzaman, M., & Rahim N. A. Temperature effect of photovoltaic module under partial shading operation condition, 2014 IEEE Conference on Clean Energy and Technology (CEAT), Sarawak, Malaysia.